Materials exploration and device optimization for tandem solar cells

Jiang Tang

Wuhan National Laboratory for Optoelectronics (WNLO),

School of Optical and Electronic Information (SOEI),

Huazhong University of Science and Technology (HUST)

Email: jtang@mail.hust.edu.cn

華中科技大學
HUAZHONG UNIVERSITY OF SCIENCE AND TECHNOLOGY

2025/05/23，Sydney

Monolitihcally integrated optoelectronic devices

microelectronics-transistors

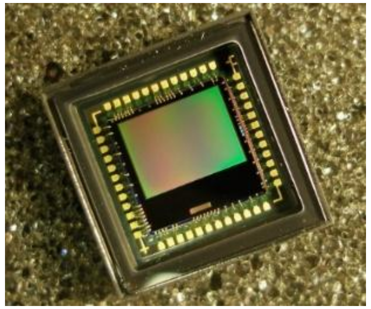

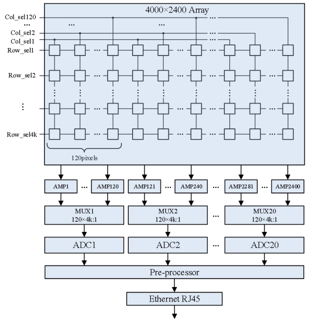

optoelectronics-diodes

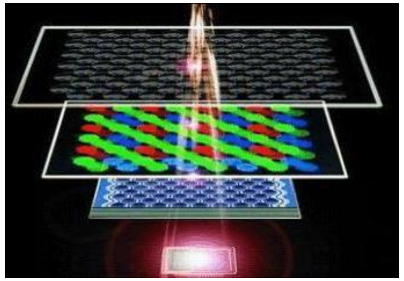

Monolithical integration: transistor+diodes

detection: ROIC+IR/X-ray detector

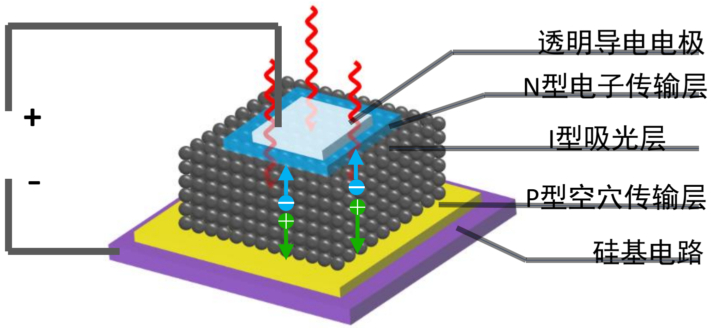

display: TFT+LED

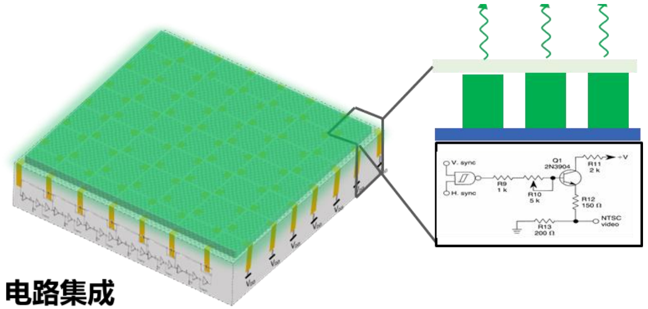

solar cell: pero/pero tandem

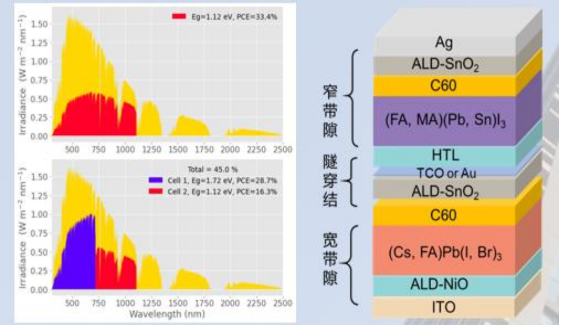

SWIR imaging

Seeing is believing, 83% of information from visual

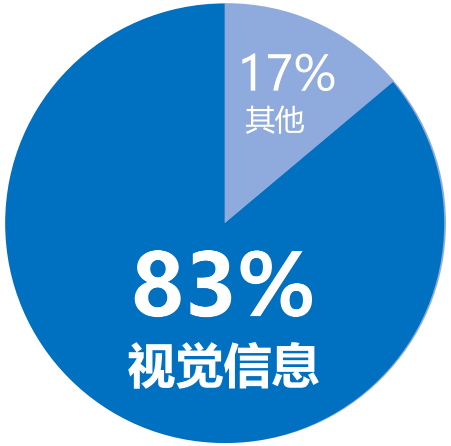

km ⟷ **nm**

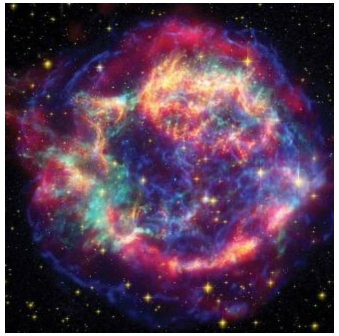

universe

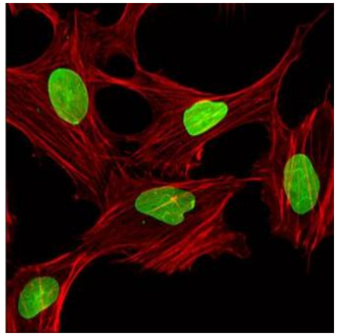

cells

SWIR (0.7-3 μm) has better penetration through wafer、water、mist and so on, and hence find wide applications

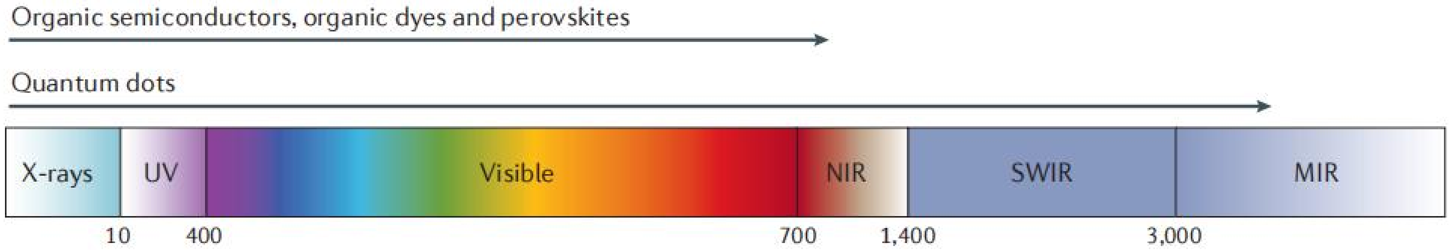

remote sensing

infrared detection

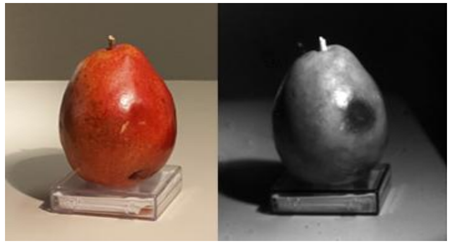

food checking

cell phone

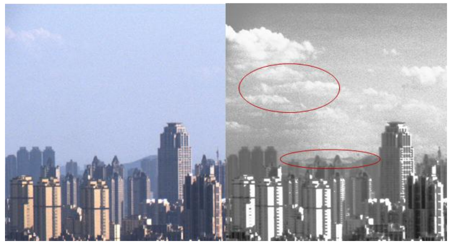

see through frog

autonomous driving

Fabrication procedure for CQD image sensors

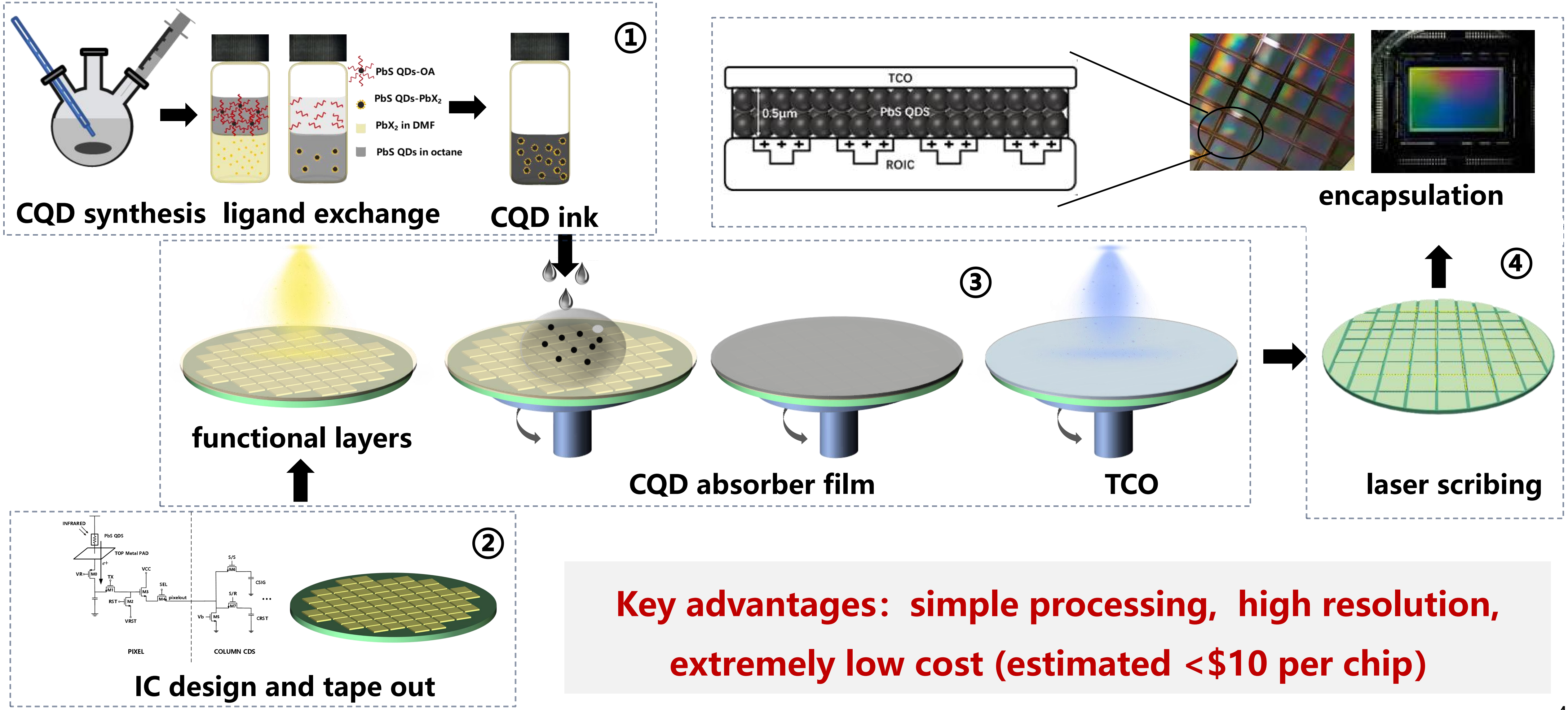

Key advantages: simple processing, high resolution, extremely low cost (estimated <$10 per chip)

From materials to final modules

ROIC

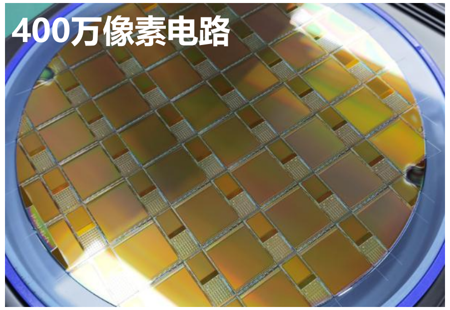

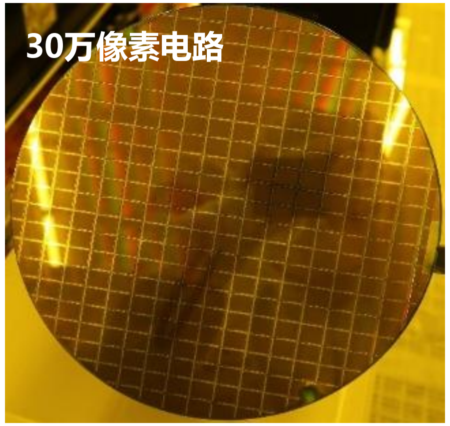

Chips

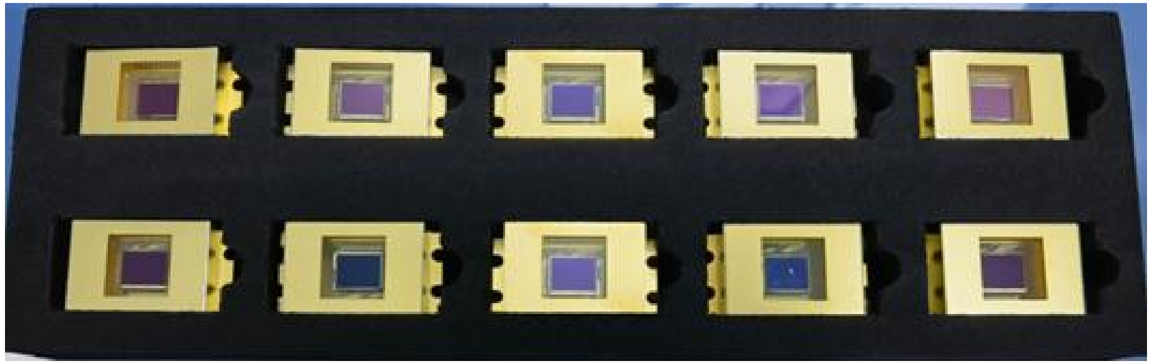

modules

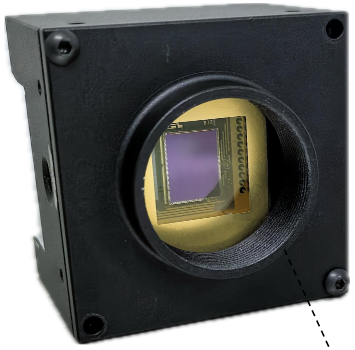

PGA encapsulation

mass production is on-going, but quite challenging with yield and stability

CQDs vs InGaAs imagers

InGaAs

InP single crystal, MOCVD

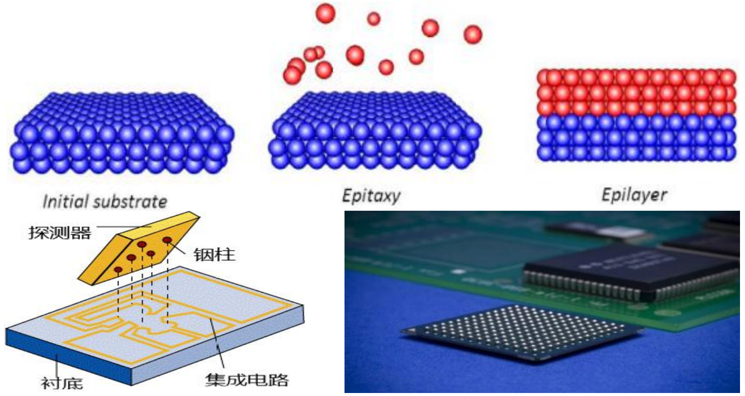

bonding process, 4 inch wafer

military only

VS

CQD

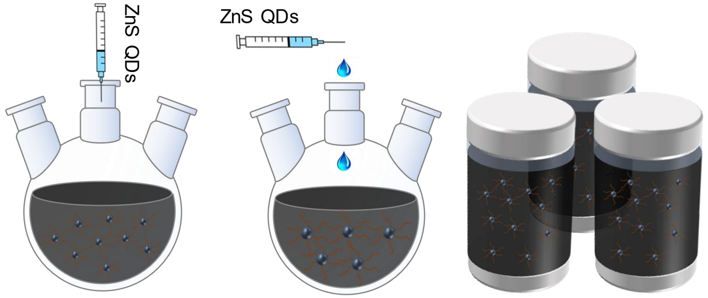

solution synthesis

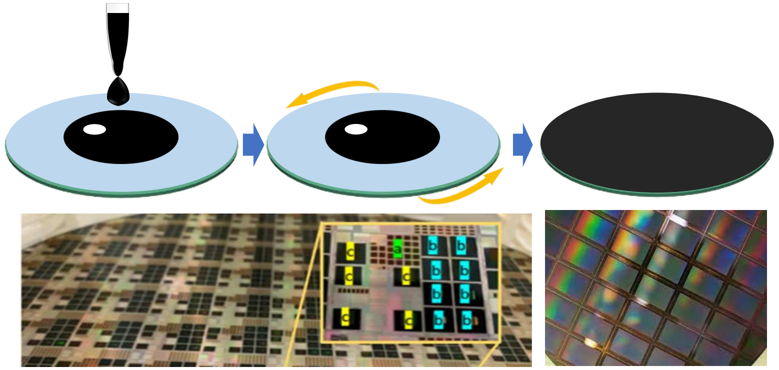

monlithic integration, 12 inch wafer

civil application

cost down by 100 fold, enable their large-scale deployment!

Photos taken by our SWIR camera

frog | SWIR | visible

-5 dB

-8 dB

-11 dB

videos at a raining morning

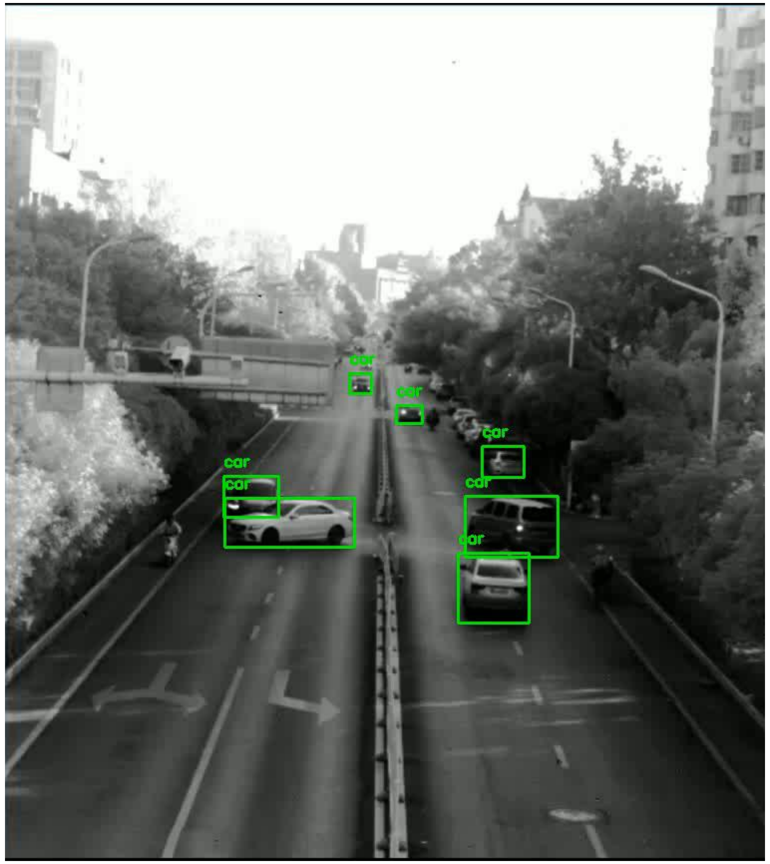

> 5kms imaging

Thermally evaporated perovskite LEDs

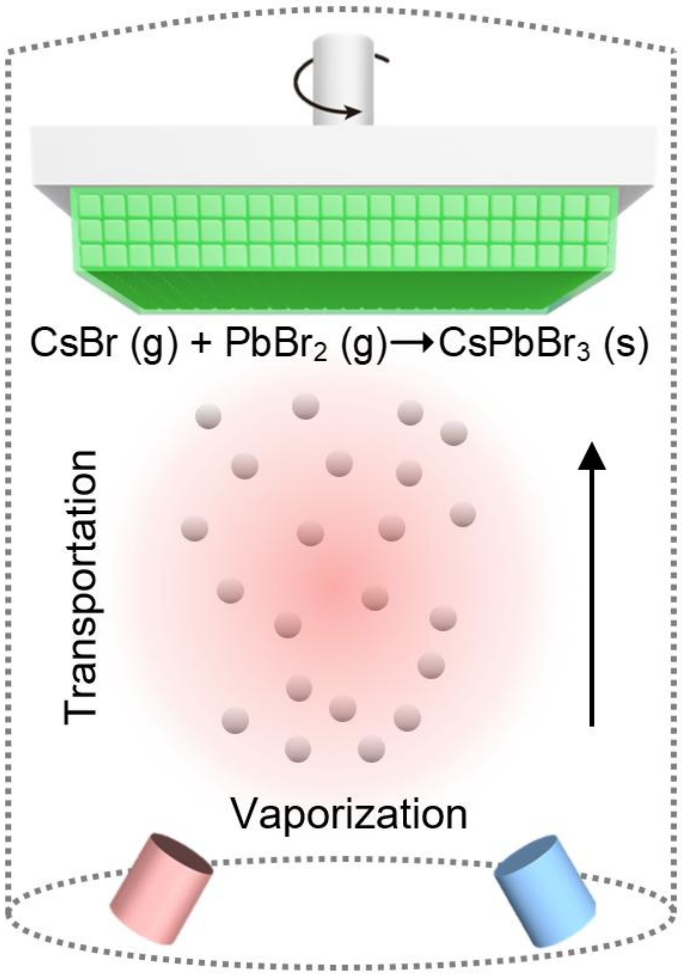

CVD from solid precursors

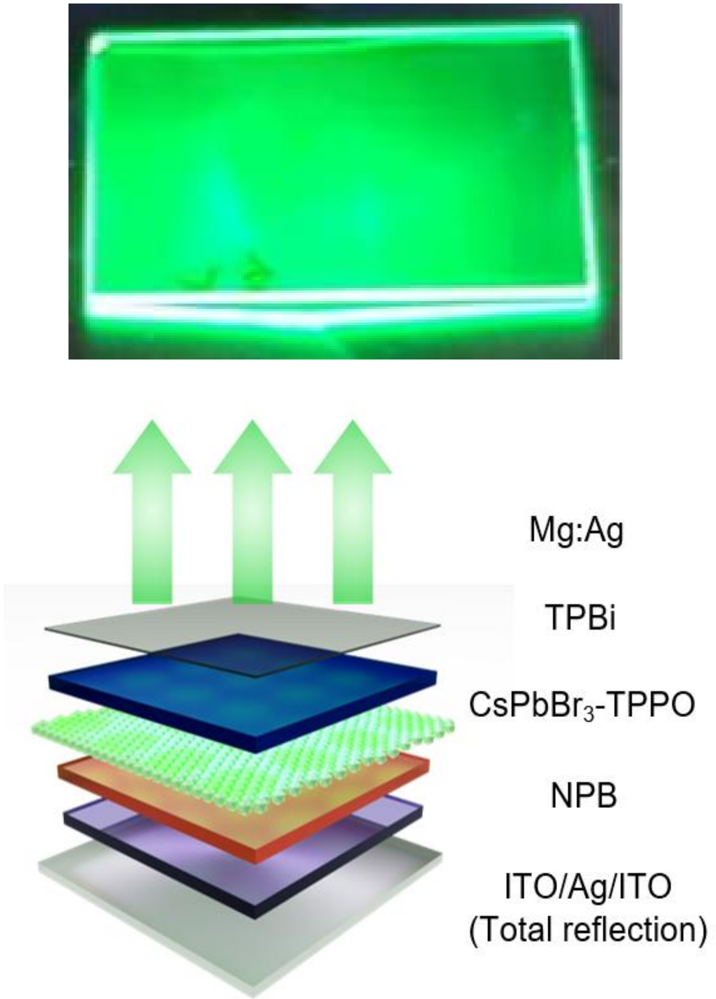

Device configuration

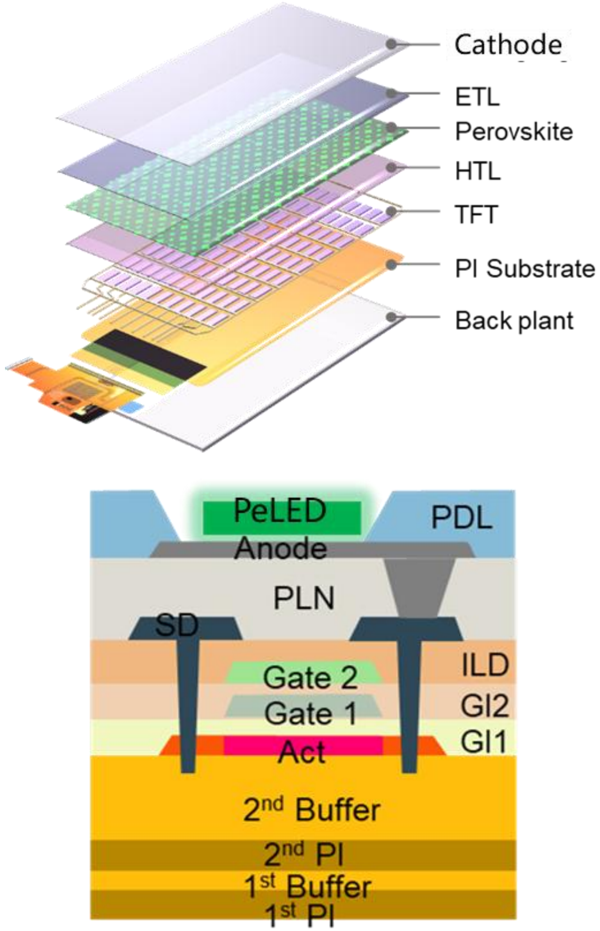

TFT integration

Perovksite green displays and micro-displays

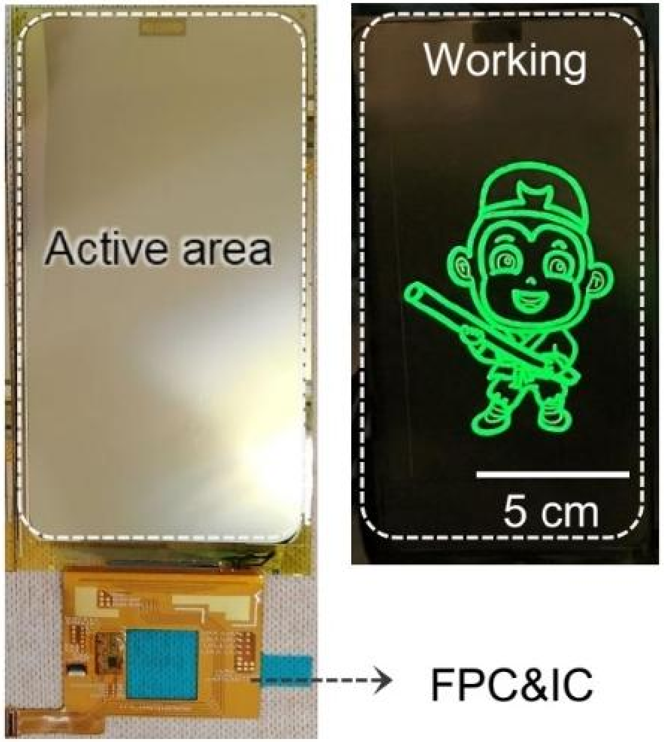

Static images

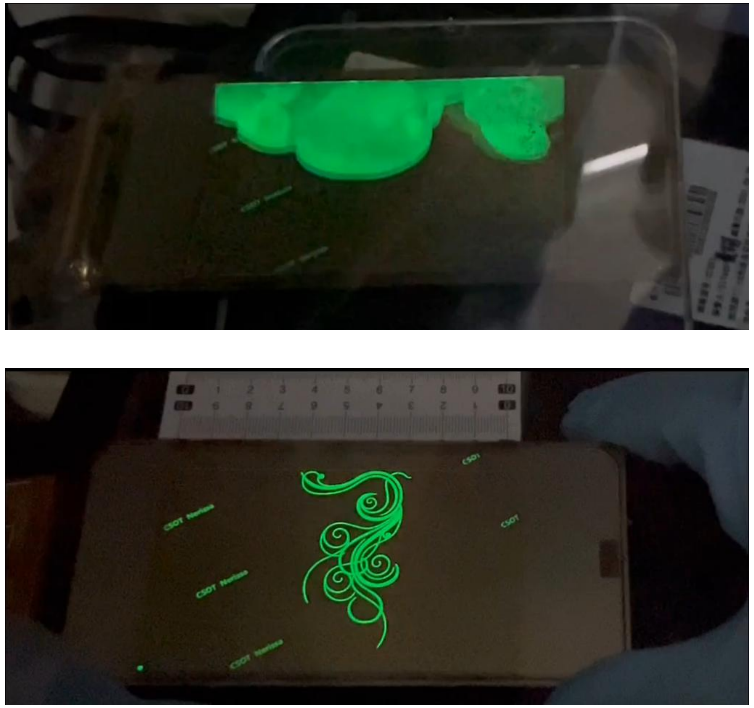

Videos with grayscale information

monolithic intergation with TFT/CMOS, world-first perovskite display

J. Li, J. Luo*, Jiang Tang* et al. *Nat. Photonics* 2023 17, 435-441

electroluminescence from rare earth compounds

monolithic integration

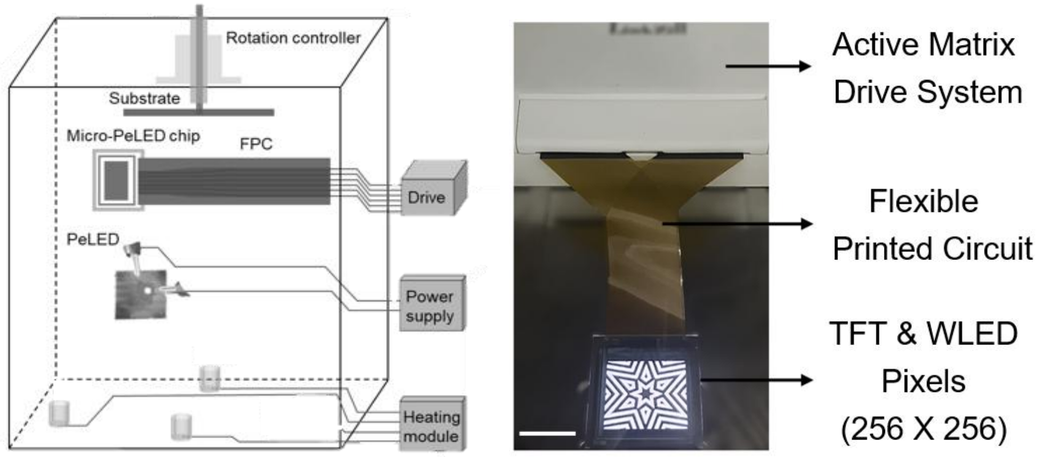

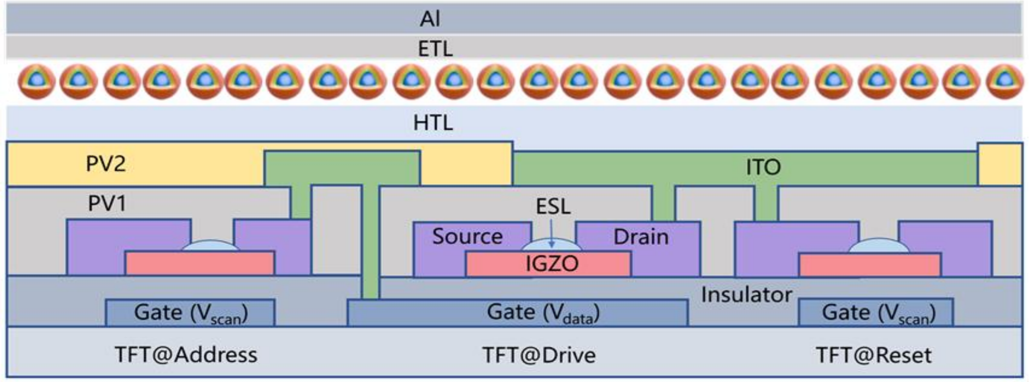

displays

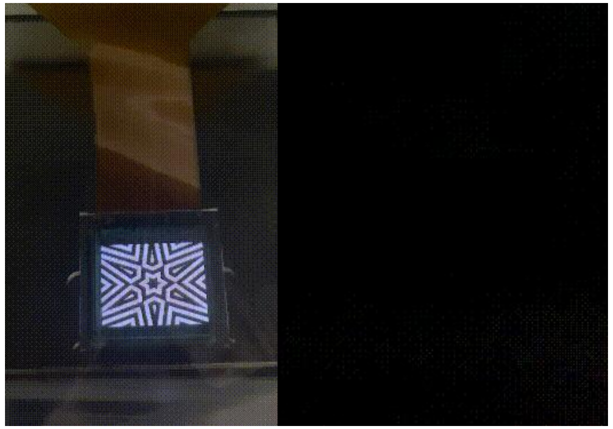

Unpublished results

Using $CsEuI_3$/mcp emitter layer , we first demonstrate electroluminescence and white displays by directly injection into 4f obitals of Eu^{2+}

Outline

Traditional carbon energy VS clean energy

Traditional carbon energy
coal, petroleum, natural gas, etc.

Carbon emission **VS** **Carbon neutral**

Clean energy
Solar cells, wind energy, etc.

Photovoltaics is one of the effective ways to achieve carbon neutral.

Pictures from Internet

Single-junction photovoltaics status and future

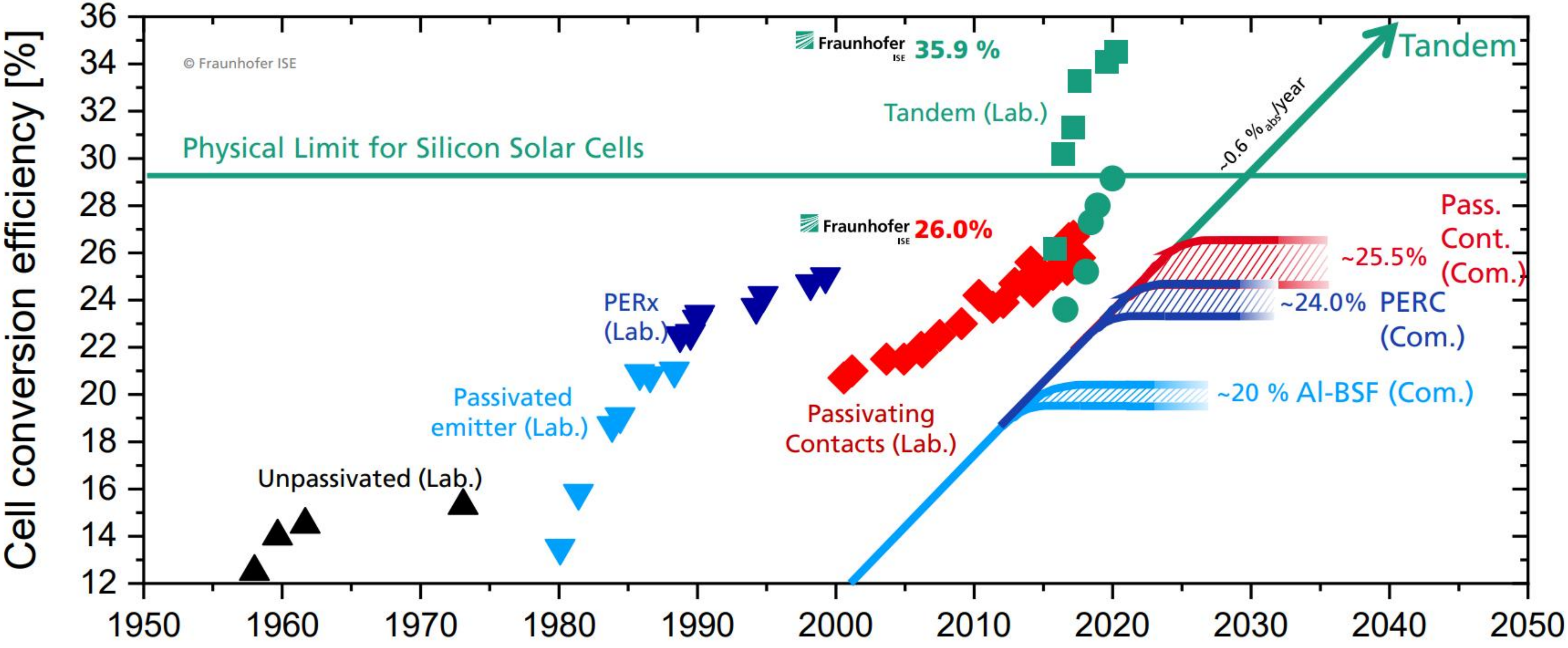

Single-junction PV efficiency is approaching their theoretical limit.

Graph: Fraunhofer ISE 2021

Tandem PV: improving efficiency and reducing cost

Absolute PCE increases by **1%**

Cost per kW·h decrease by **7%**

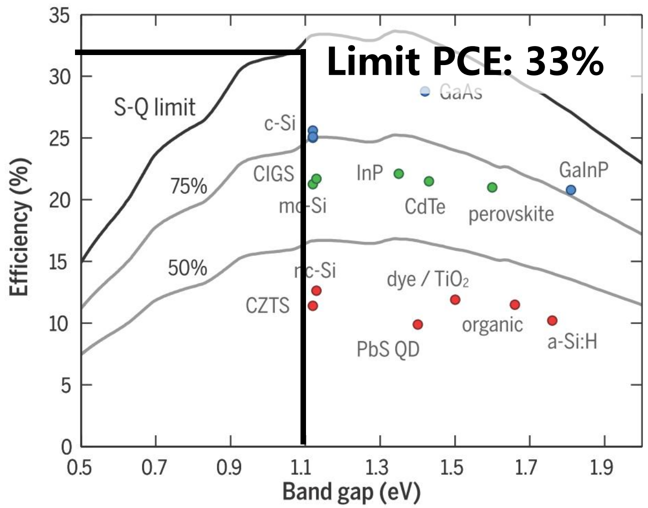

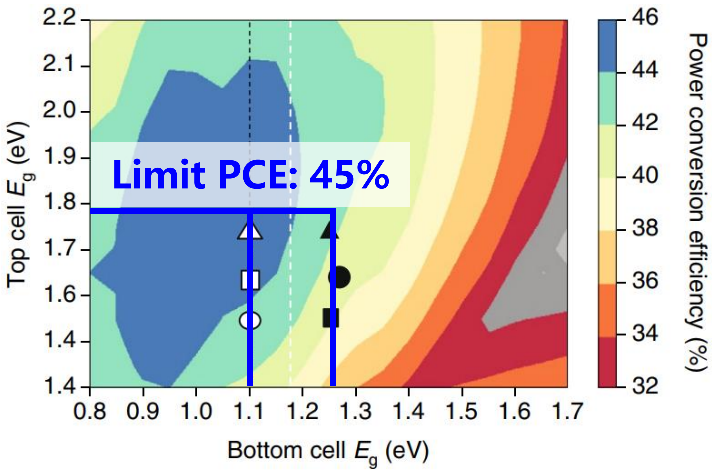

Single-junction PV (<33%):

Low spectral range

High thermal relax loss

Tandem PV (~45%):

High spectral range

Low thermal relax loss

Tandem solar cells are considered as the next-generation low-cost PV technology.

Working principle of tandem solar cell

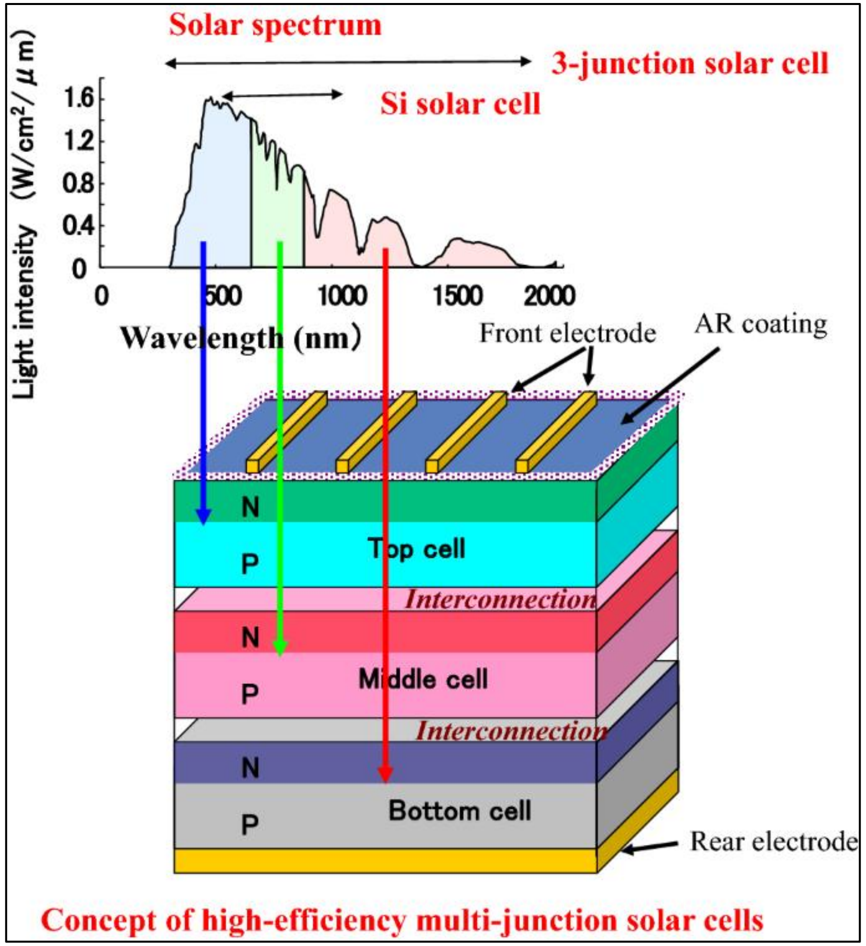

Concept of high-efficiency multi-junction solar cells

sunlight absorption

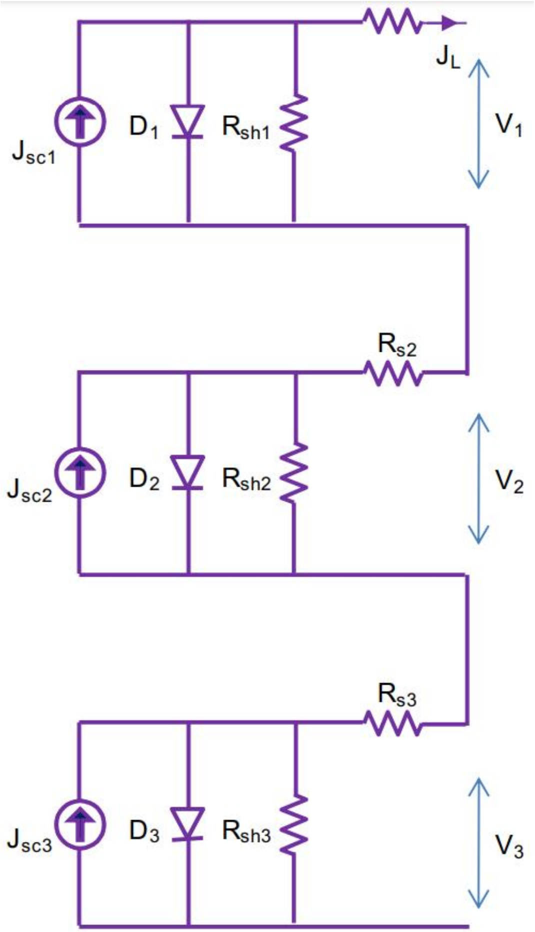

equivalent circuit

$$I_T = A_{top} q \int_{E_{gT}}^{\infty} F(E) QE(E) dE,$$

$$I_M = A_{top} q \int_{E_{gM}}^{E_{gT}} F(E) QE(E) dE,$$

$$I_B = A_{top} q \int_{E_{gB}}^{\min(E_{gT}, E_{gM})} F(E) QE(E) dE + A_{step} q \int_{E_{gB}}^{\infty} F(E) QE(E) dE,$$

$$V(I) = \frac{kT}{q} \ln \prod_{i=1}^{2,3} \left(\frac{I_{SCi} - I}{I_{0i}} + 1 \right)$$

$$V_{oc} = \frac{kT}{q} \ln \prod_{i=1}^{2,3} \left(\frac{I_{SCi}}{I_{0i}} + 1 \right)$$

J-V equation

Theoretical efficiency of tandem solar cells

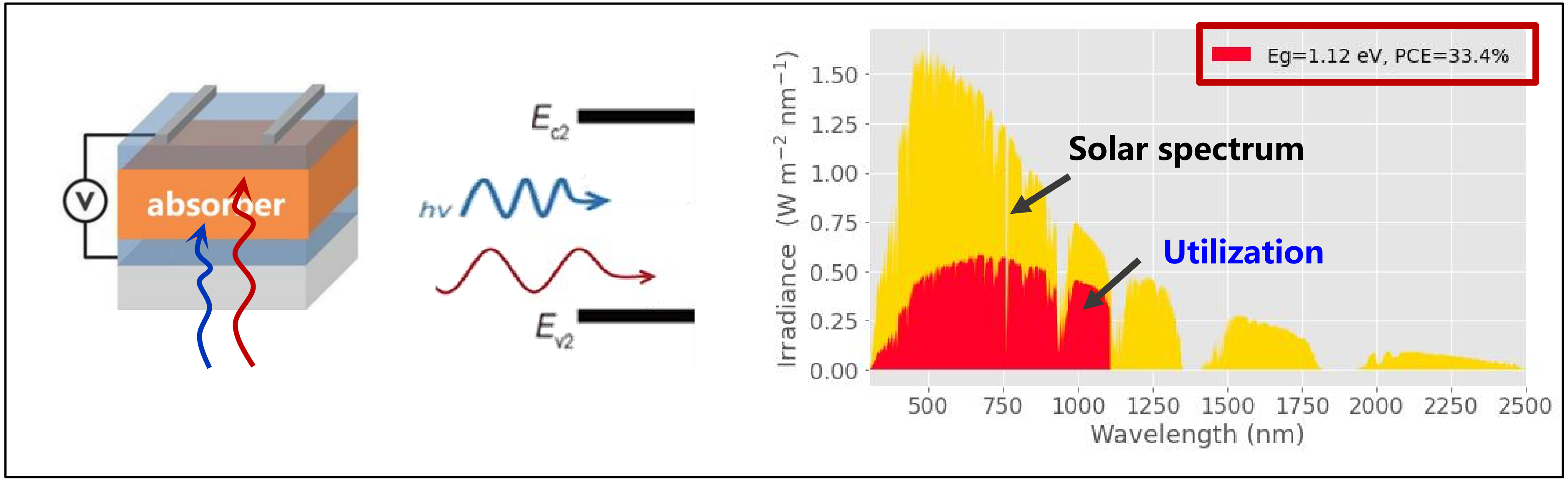

Single-junction PV

~33%

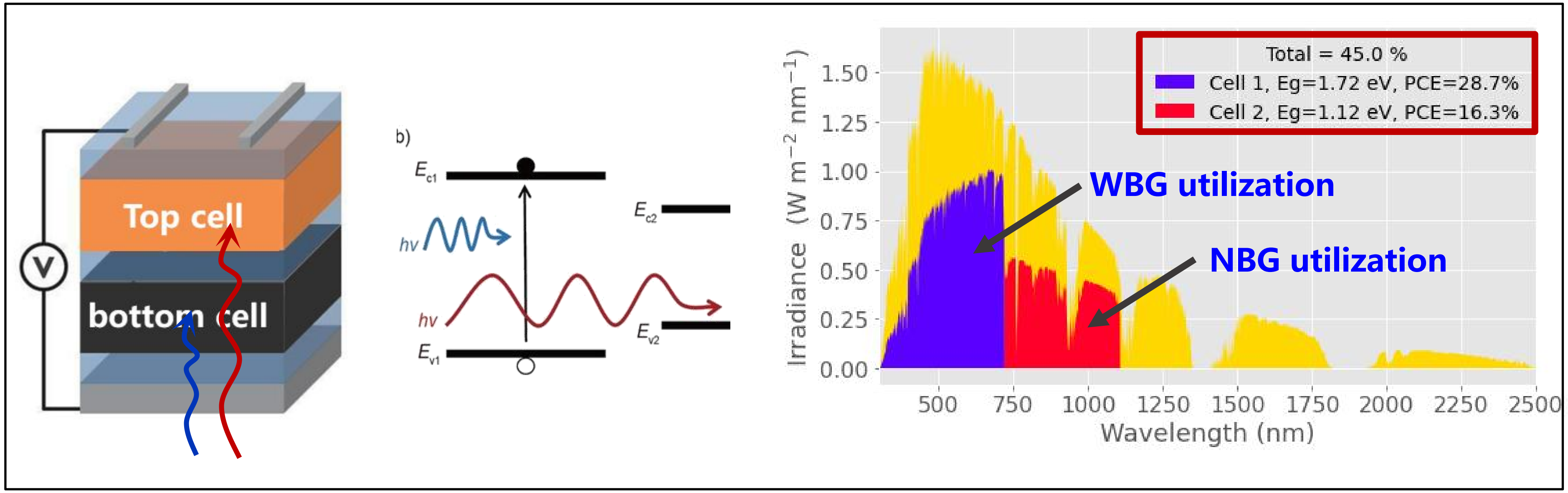

Two-junction tandem PV

~45%

Types and development trend of tandem solar cells

Tandem solar cells

III-V-based	Si-based		Perovskite-based	
2J-32.9%	Si/a-Si	2T-15.04%	Si/PVSK	2T-34.6%
3J 37.9%	Si/III-V	2T-32.8%	III-V/PVSK	2T-24.3%
5J 38.8%	Si/II-VI	2T-16.8%	PVSK/PVSK	2T-30.1%
6J-39.2%	Si/OPV	2T-25.2%	CIGS/PVSK	2T-24.2%
	Si/DSSC	2T-17.2%	OPV/PVSK	2T-25.6%

Candidate materials for tandem solar cells

NBG materials (1.1~1.2 eV)

	PCE	Stability	Cost
Si	✓	✓	✓
III-V	✓	✓	×
CIGS	×	✓	✓
Sn-Pb PVSK	✓	×	✓
organic	×	×	✓

Target NBG materials:

Si, CIGS, Sn-Pb PVSK

WBG materials (1.65-1.8 eV)

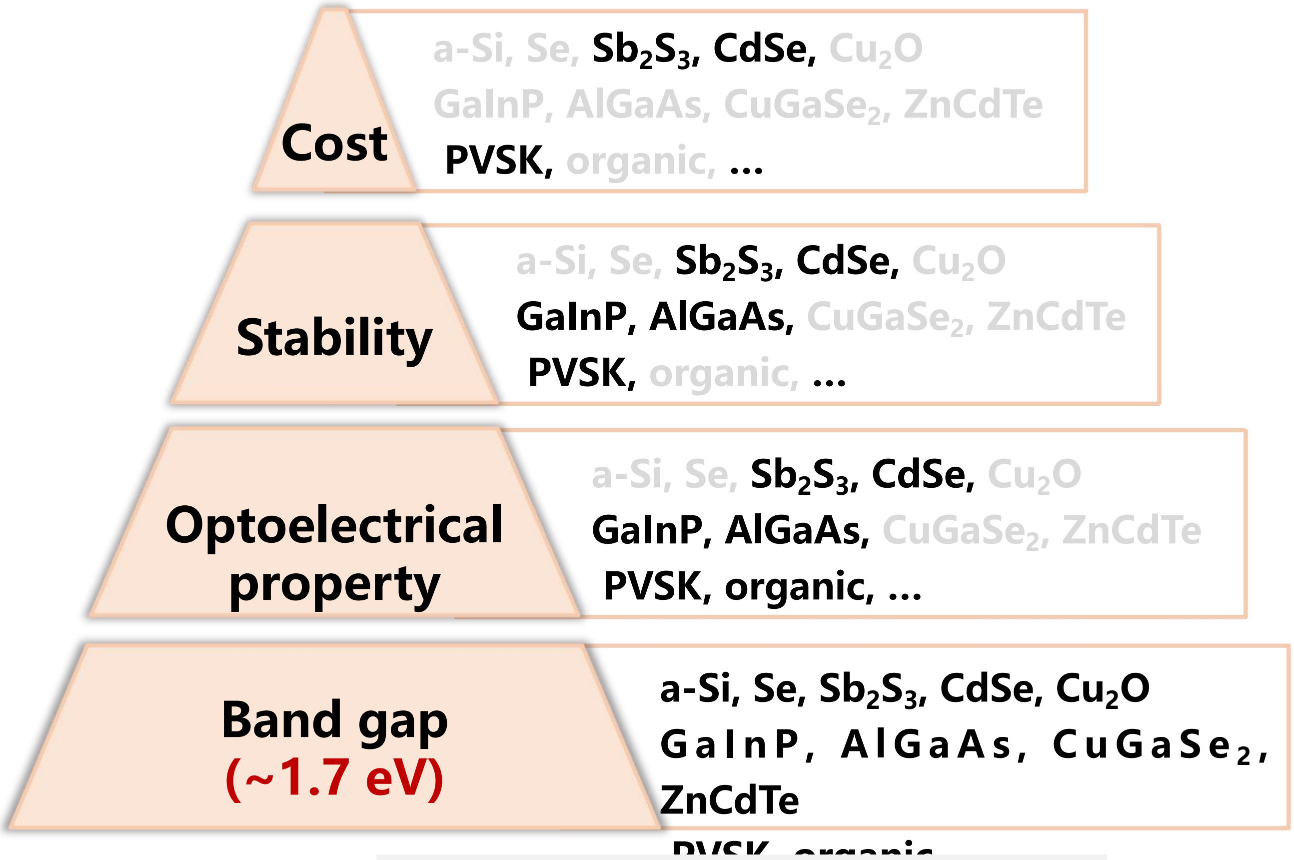

Target WBG materials:

Sb_2S_3, CdSe, $CsPbI_3$, PVSK

Outline

1. Background of tandem solar cells

2. Exploration for Si-based tandem solar cells

   ◆ 1.72 eV CdSe solar cells

   ◆ 1.68 eV Sb_2S_3 solar cells

   ◆ 1.72 eV $CsPbI_3$ solar cell

3. Exploration for all-perovskite tandem solar cells

4. Summary and acknowledgment

Why is CdSe?

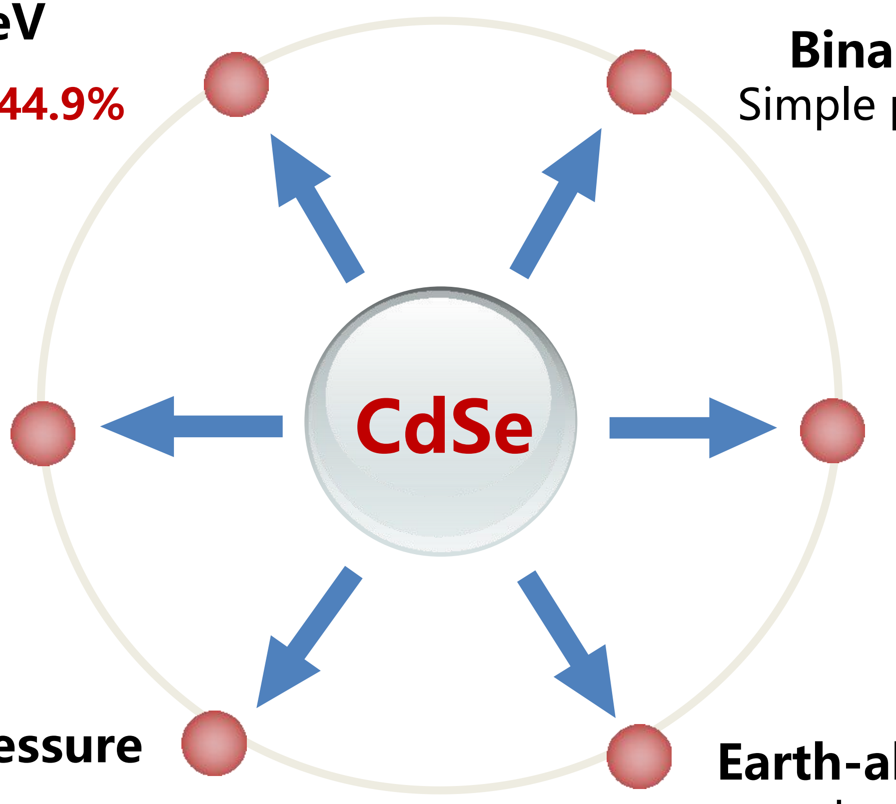

Suitable E_g ~1.7 eV
A theoretical efficiency **44.9%**

Binary compound
Simple phase, less defects

α ~10^5 cm^{-1}
Thickness: 1-2 μm

High melting point
Hight stability

High saturation vapor pressure
Compatible with CdTe

Earth-abundance
Low cost

CdSe: promising top-cell material for Si-based tandem devices

Photoelectric properties of CdSe

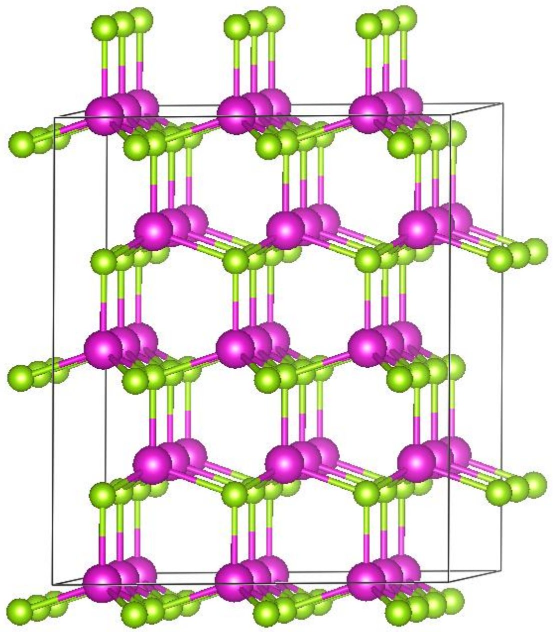

Hexagonal symmetry

	a-Si	Se	Sb_2S_3	CdSe	Cu_2O
E_g (eV)	1.7	~1.9	1.68	1.72	2.1
α (cm^{-1})	10^5	10^4-10^5	10^5	10^4-10^5	10^4-10^5
μ ($cm^2\ V^{-1}\ s^{-1}$)	0.5	1-20	6.4	500	70
Conduction type	p	p	p	n	p

CdSe enjoys high absorption coefficient and high mobility

Semiconductor Data Handbook;
S. Lu, C. Chen*, J. Tang, Frontier. Optoelectron., 2020, 13, 246.

Develop RTE technique to fabrication CdSe film

Simple phase

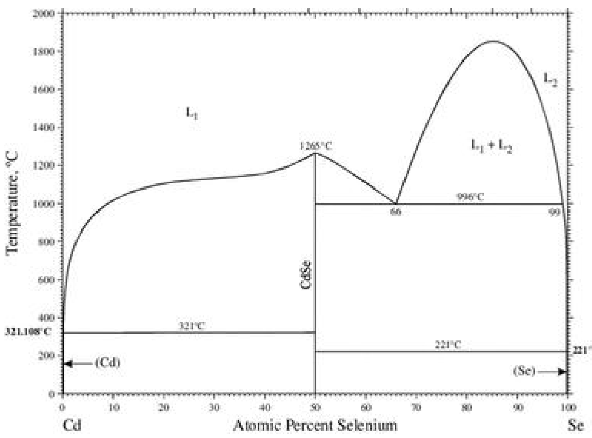

High P_{sat}

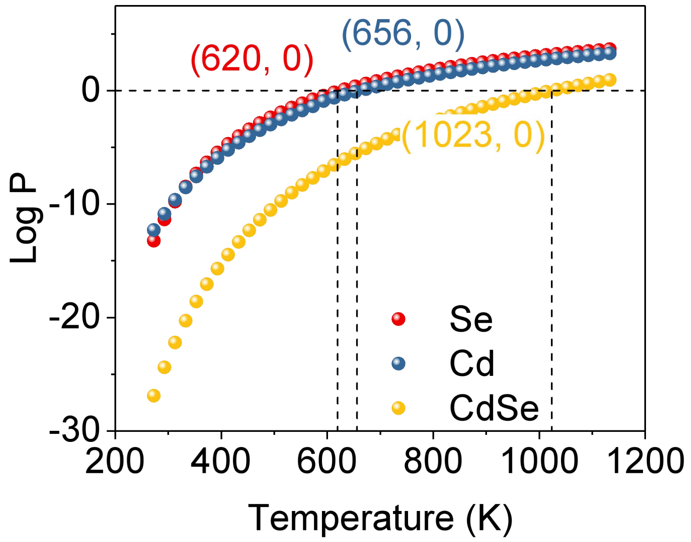

Tube furnace

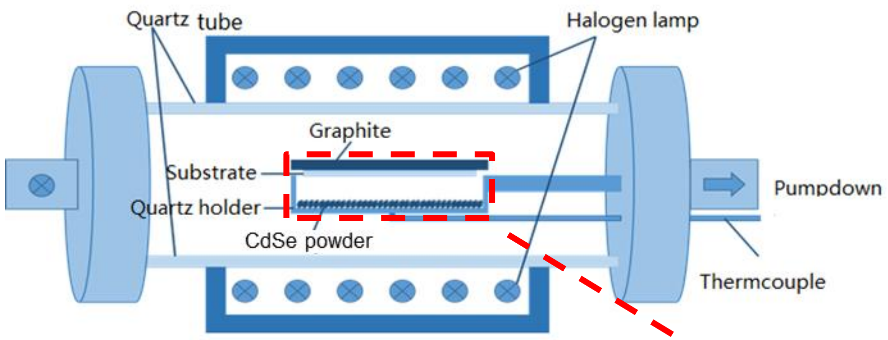

Rapid thermal evaporation

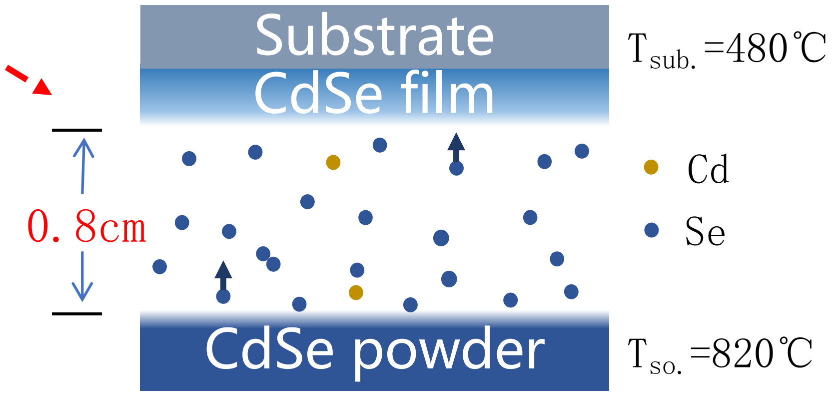

Easy fabrication: 10 Pa vacuum, 35s deposition, simple instrument

Characterization of CdSe film

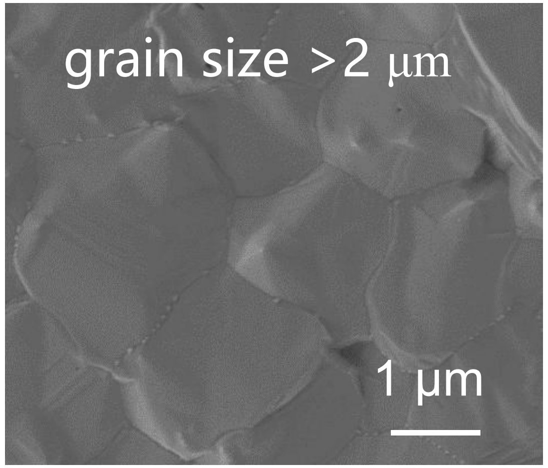

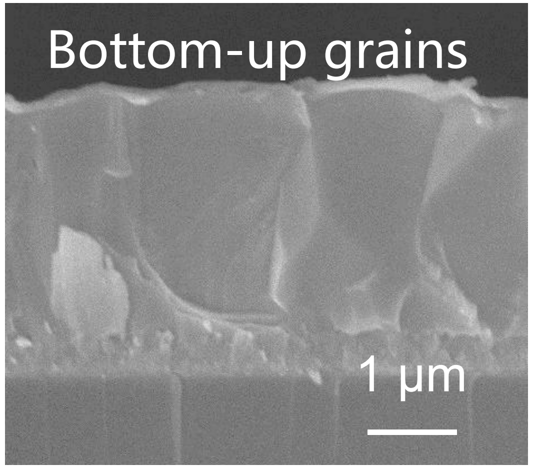

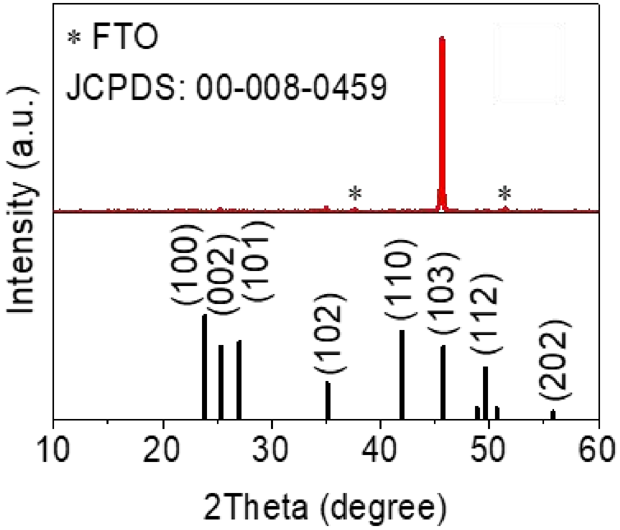

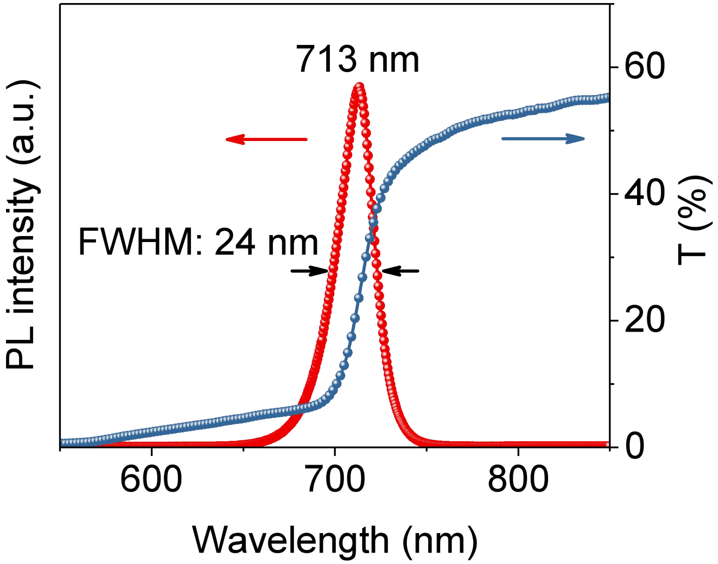

High-quality CdSe thin film is deposited by vacuum method

C. Chen*, **J. Tang***, et al. Advanced Energy Materials 2022, 12, 2200725.

Design and fabrication of CdSe solar cells

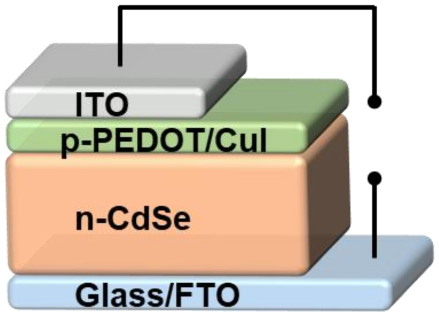

np-type device structure

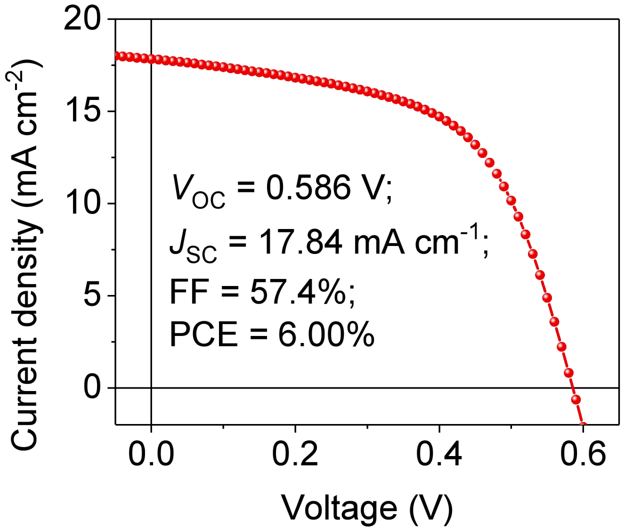

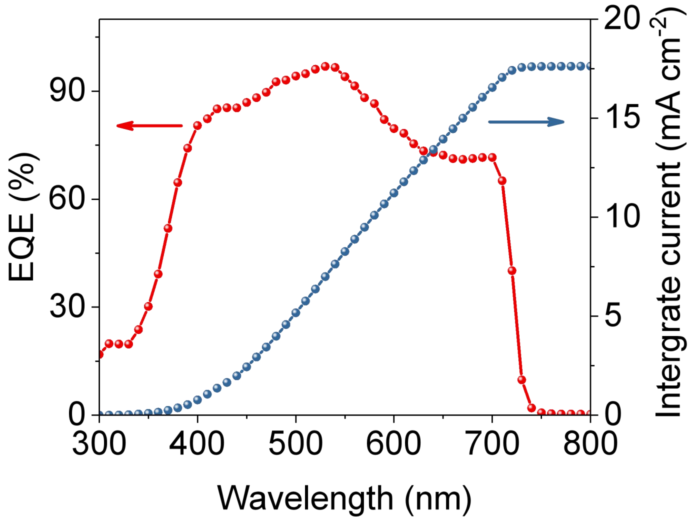

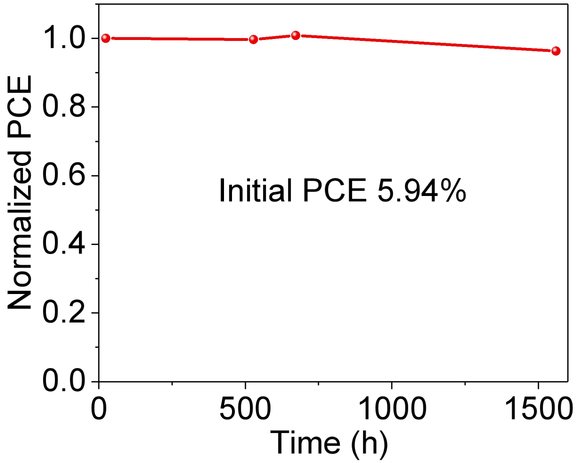

V_{OC} (V)	J_{SC} (mA cm^{-2})	FF (%)	PCE (%)	Note
1.453	**21.40**	**91.1**	**28.3%**	S-Q
0.586	17.84	57.4	6.0%	Our work

A champion PCE of 6%; storage stability >1500 h

C. Chen*, **J. Tang*,** et al. Advanced Energy Materials 2022, 12, 2200725.

V_{OC} loss analysis of CdSe solar cells

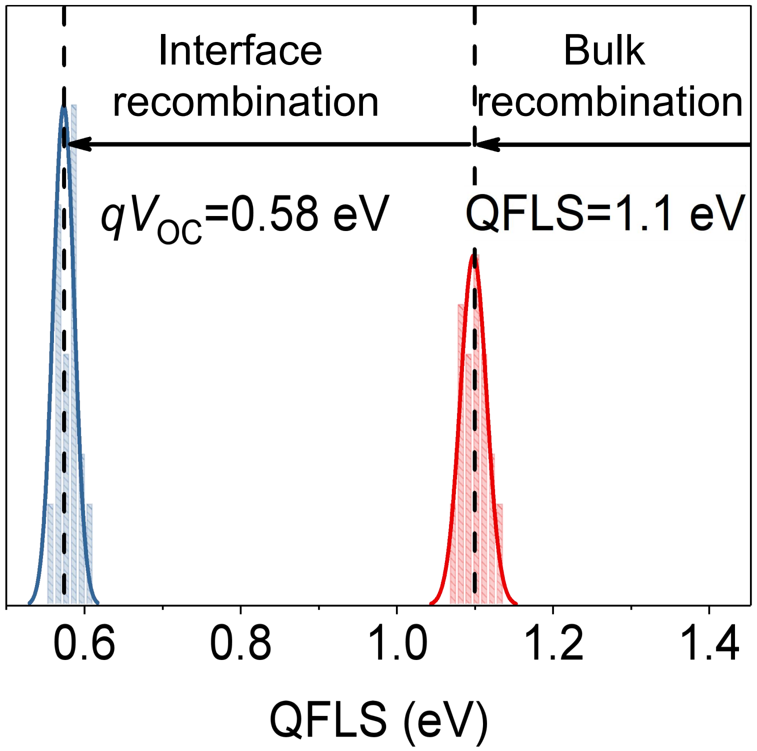

Würfel generalized Planck law

$$I_{\mathrm{PL}}(E)=\frac{2\pi E^2 a(E)}{h^3c^2}\frac{1}{\exp\left(\frac{E-\Delta E_F}{k_BT}-1\right)}$$

$$ln\left(\frac{I_{\mathrm{PL}}(E)h^3c^2}{2\pi E^2}\right)=-\frac{E}{k_BT}+\frac{\Delta E_F}{k_BT}$$

- **Bulk recombination loss: 0.353 V**
- **Interface recombination loss: 0.58 V**

Bulk and interface defects result in large V_{OC} loss

C. Chen*, **J. Tang*,** et al. Advanced Energy Materials 2022, 12, 2200725.

Defects analysis of CdSe solar cells

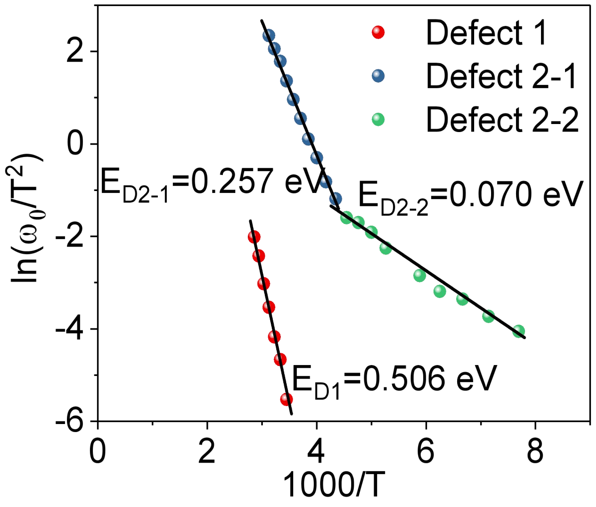

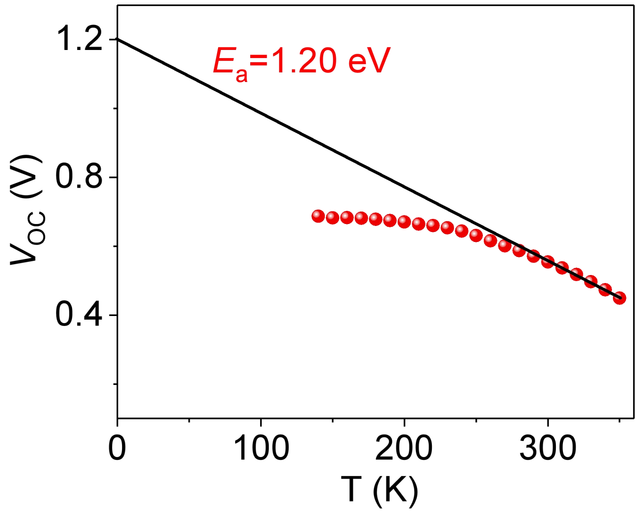

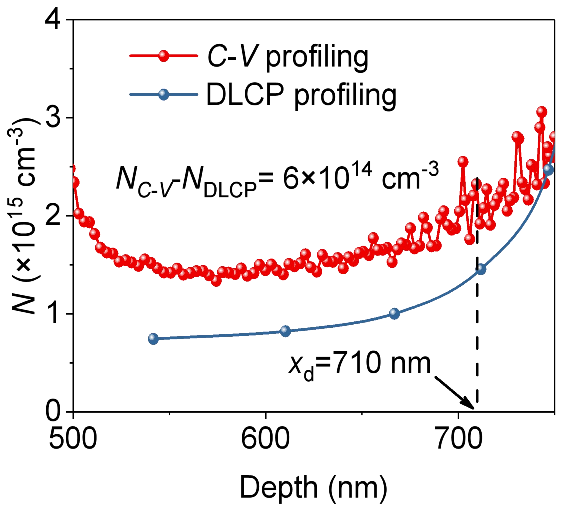

Defect type	E_a (eV)	σ (cm²)	N_t (cm⁻³)
V_{Se}	0.506	4.73×10^{-13}	8.18×10^{14}
Cd_i	0.257	3.39×10^{-13}	2.84×10^{14}
	0.070	1.46×10^{-13}	6.58×10^{14}

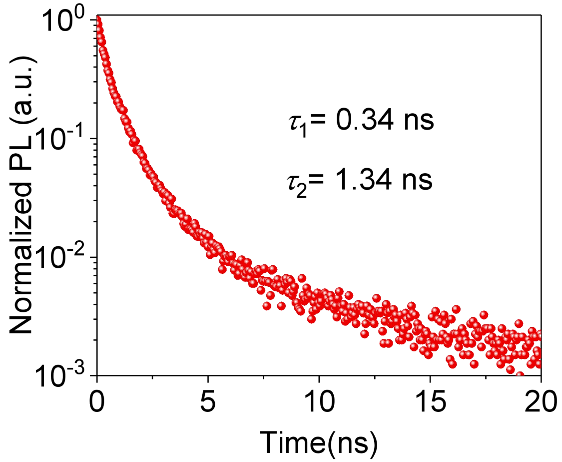

Bulk and interface defects limit V_{OC} and PCE

J. Tang, et al. ACS App. Mater. Inter. 2023, 15, 17858

Stacking faults in CdSe solar cells

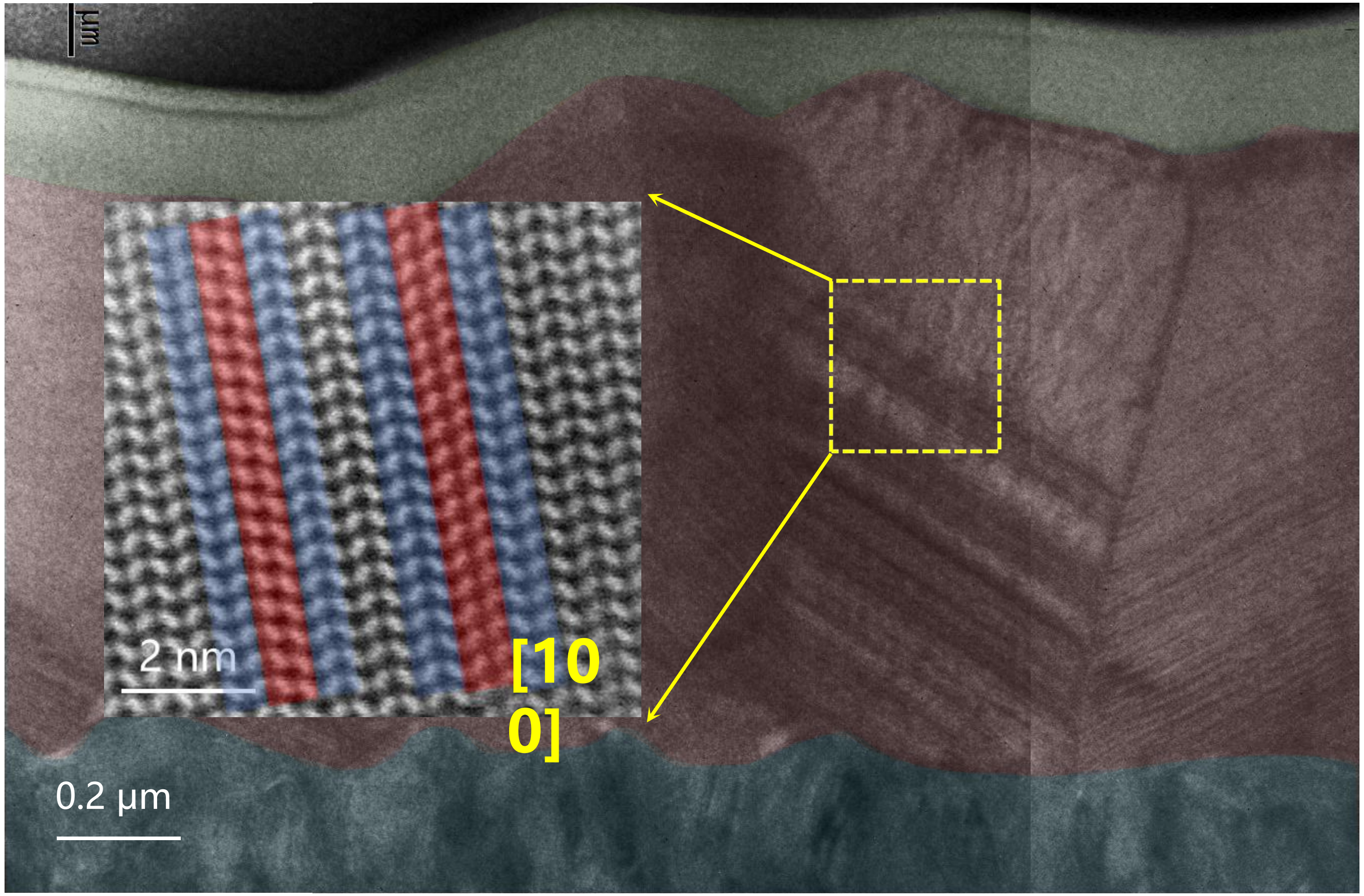

A large number of stacking faults (density ~5 nm^{-1}) exist in the CdSe film

Stacking faults in CdSe solar cells

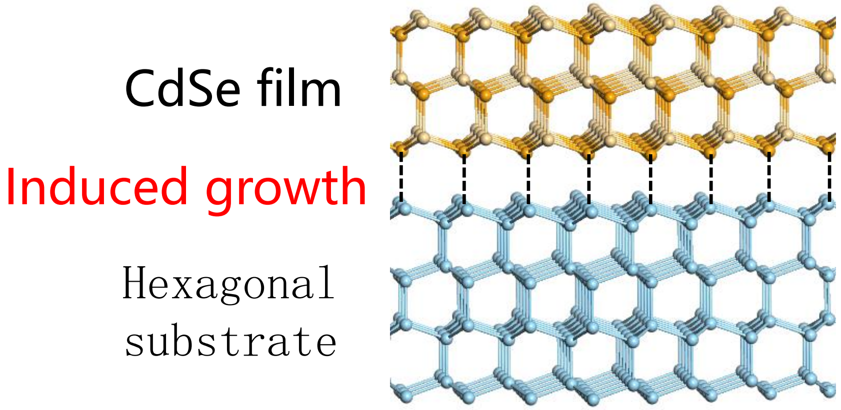

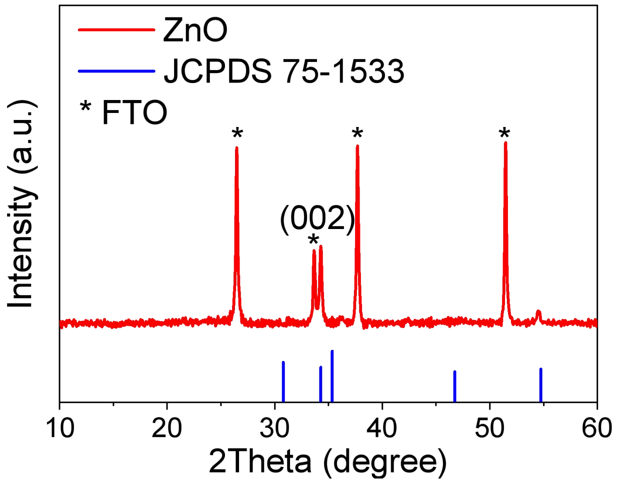

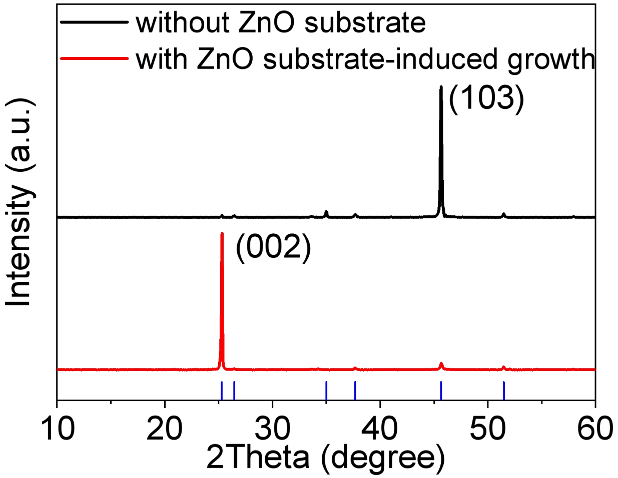

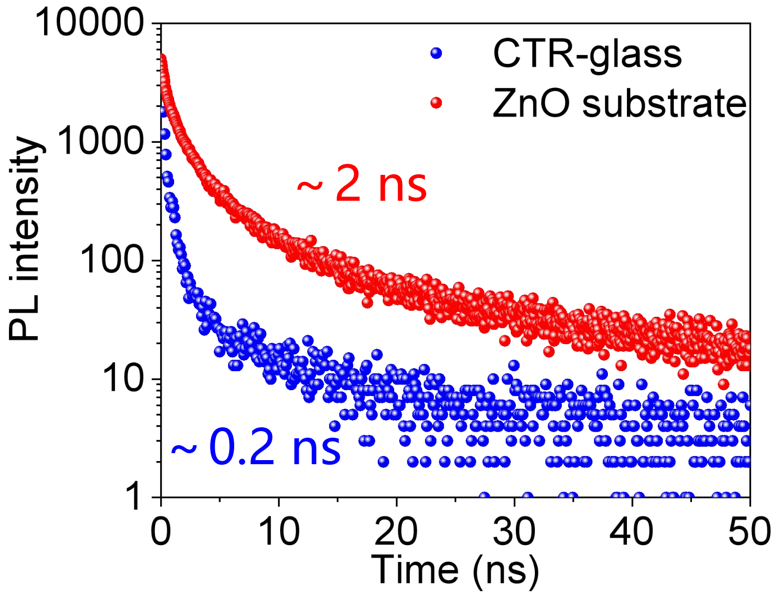

- ZnO layer induces (002)-oriented CdSe film
- The stacking faults are eliminated
- Carrier lifetime is improved by 10 times

Future research direction

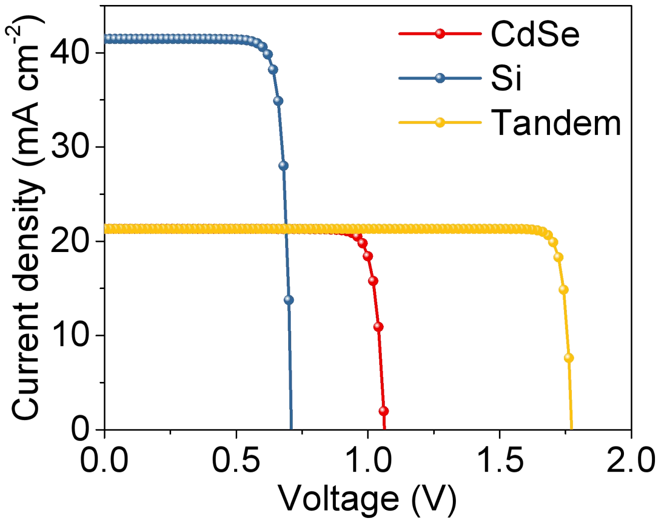

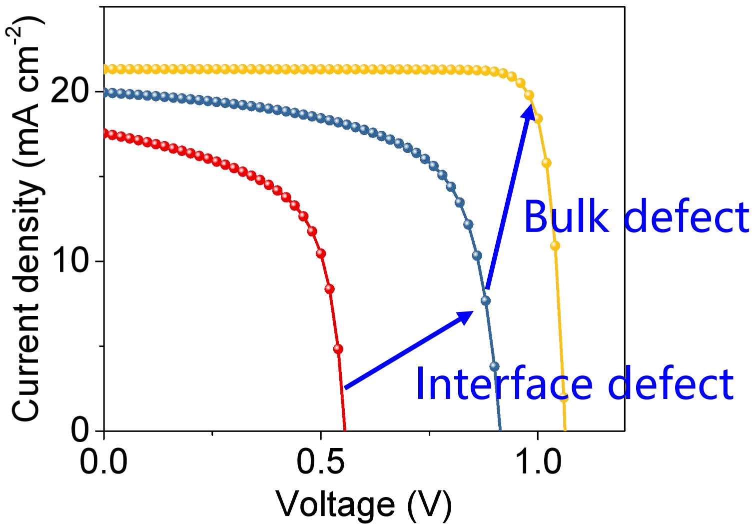

- ☐ **Passivate bulk defects via in-situ or post-treatment**
- ☐ **Suitable HTL (ZnSe or ZnTe) and passivation of interface defects**
- ☐ **Exploration of CdSe/Si tandem solar cell**

Outline

1. Background of tandem solar cells
2. Exploration for Si-based tandem solar cells
   - ◆ 1.72 eV CdSe solar cells
   - ◆ 1.68 eV Sb_2S_3 solar cells
   - ◆ 1.72 eV $CsPbI_3$ solar cell
3. Exploration for all-perovskite tandem solar cells
4. Summary and acknowledgment

Why is Sb_2S_3?

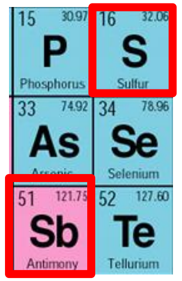

Binary components, single phase

$$2Sb + 3S \longrightarrow Sb_2S_3$$

Non-toxic, stable, high abundance, cheap

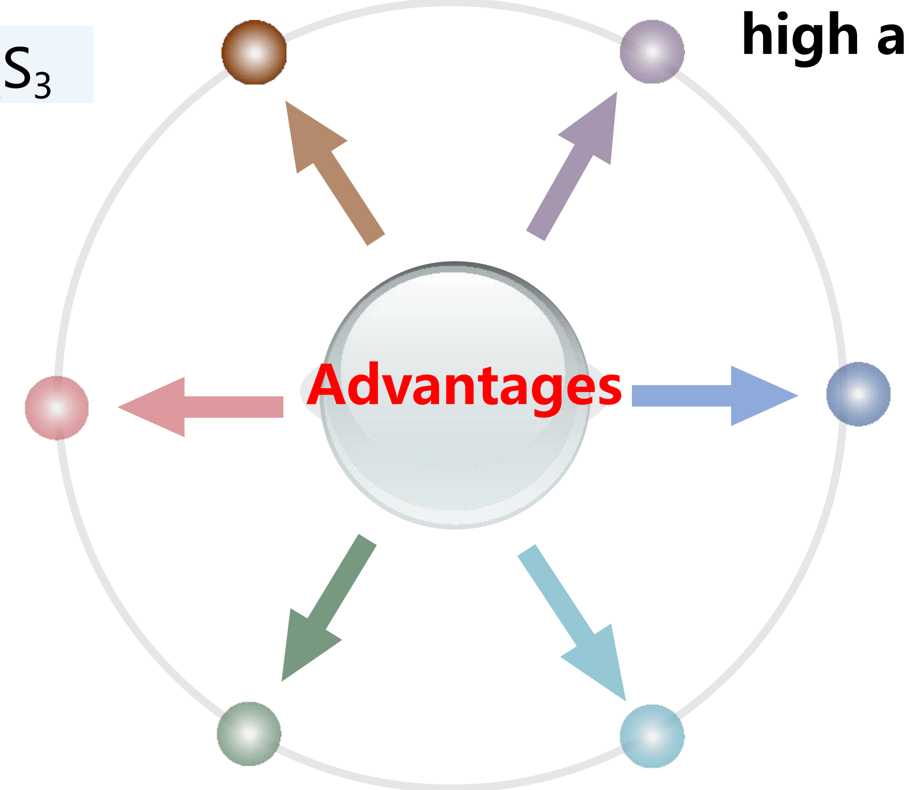

1D crystal structure

Benign GB

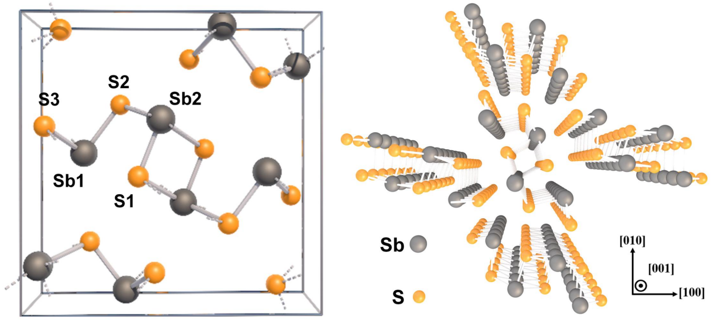

Low melting Tem. (550℃)

Low crystallization Tem.

Suitable E_g ~1.73 eV

A theoretical tandem efficiency **44%**

α ~10^5 cm^{-1}

thickness<1 μm

Challenge of Sb_2S_3 solar cells

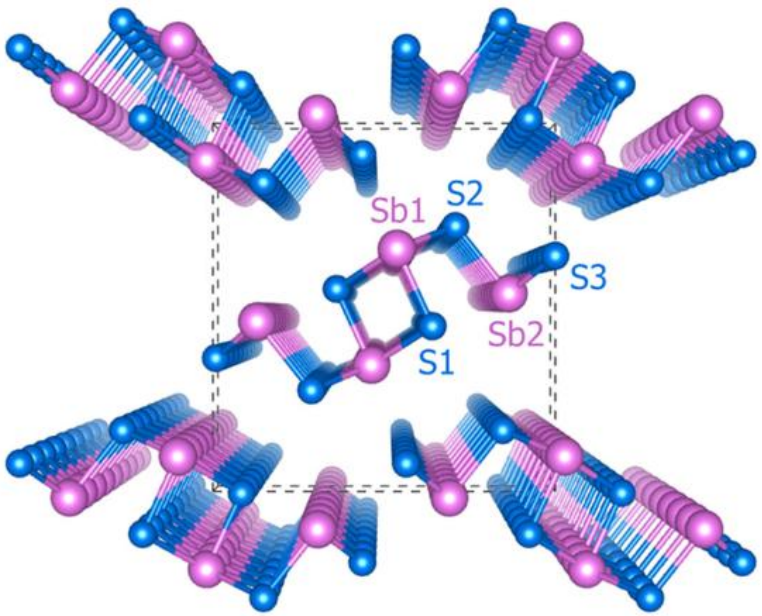

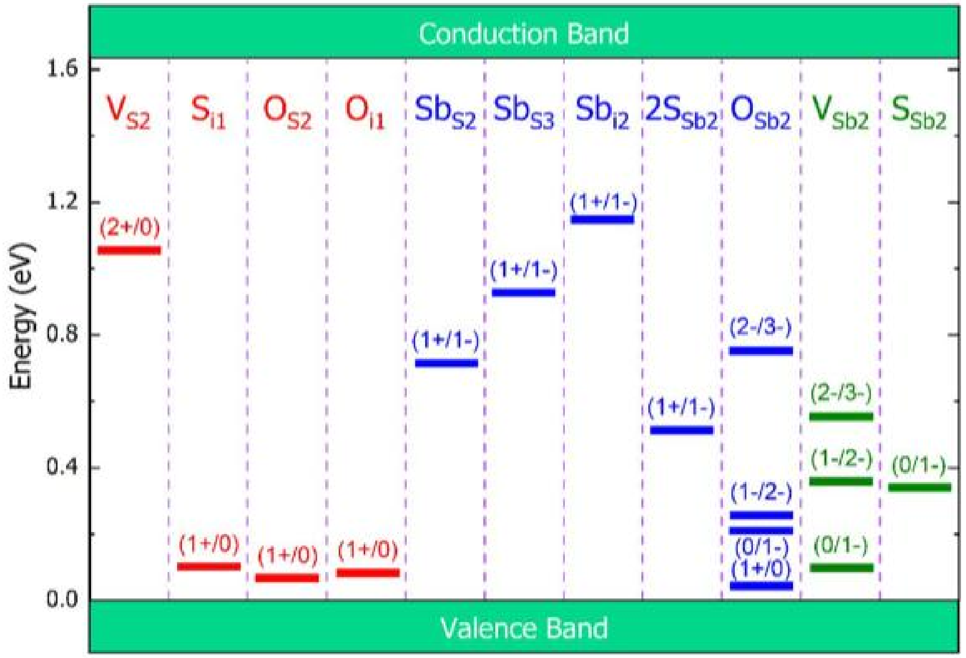

Figure 6. Calculated transition energy levels of intrinsic defects and O dopants on different sites, in the bandgap of Sb_2S_3.

V_S defect: deep defect level and low formation energy

Ref. Shiyou Chen*, et al. Solar RRL 2020, 4, 1900503

Codoping strategy for improving film quality

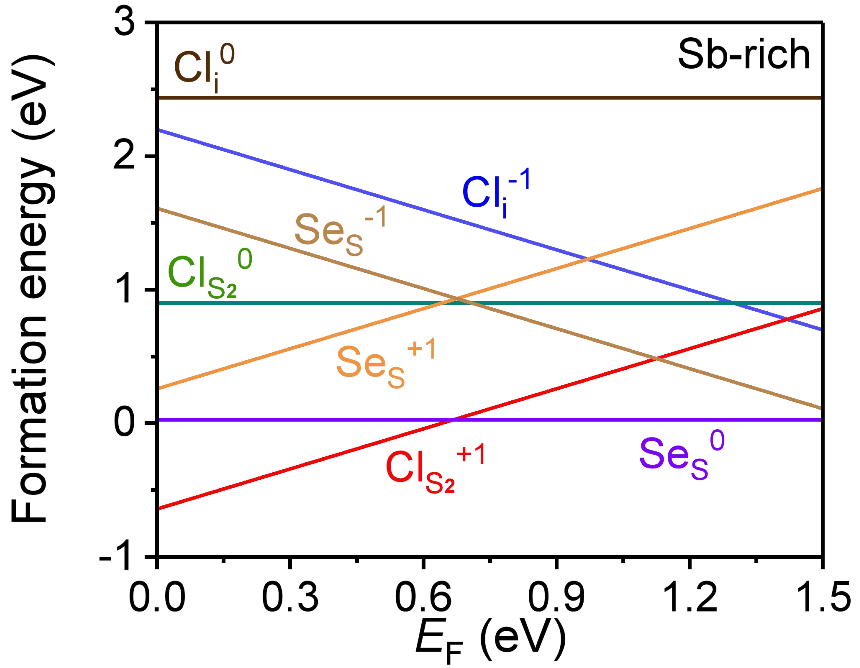

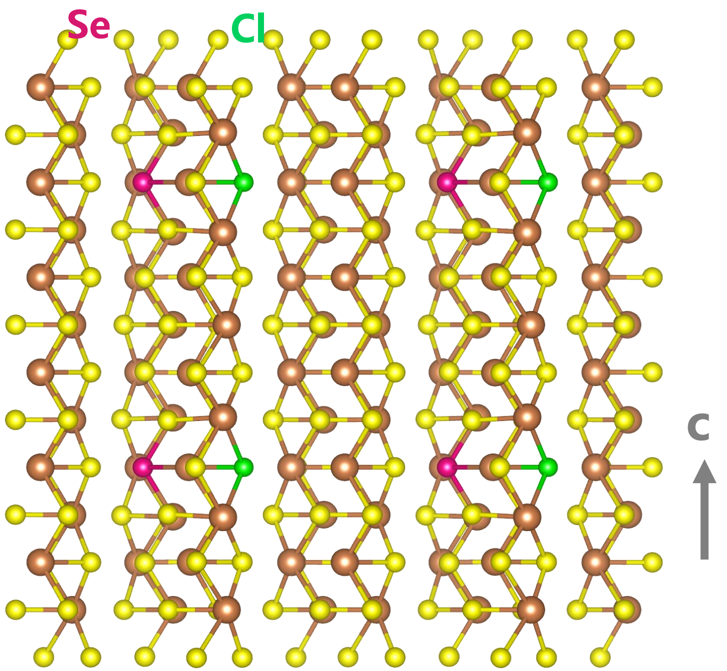

- ✓ Hydrothermal method compatible with various ions
- ✓ Cl and Se codoping has not introduced additional defect
- ✓ Under Sb rich state, both Cl_{S2}^{+} and Se_{S}^{0} could passivate V_S

J. Tang, H. Song*, et al. Adv. Energy Mater. 2022, 12, 2202897

Codoping strategy for improving film quality

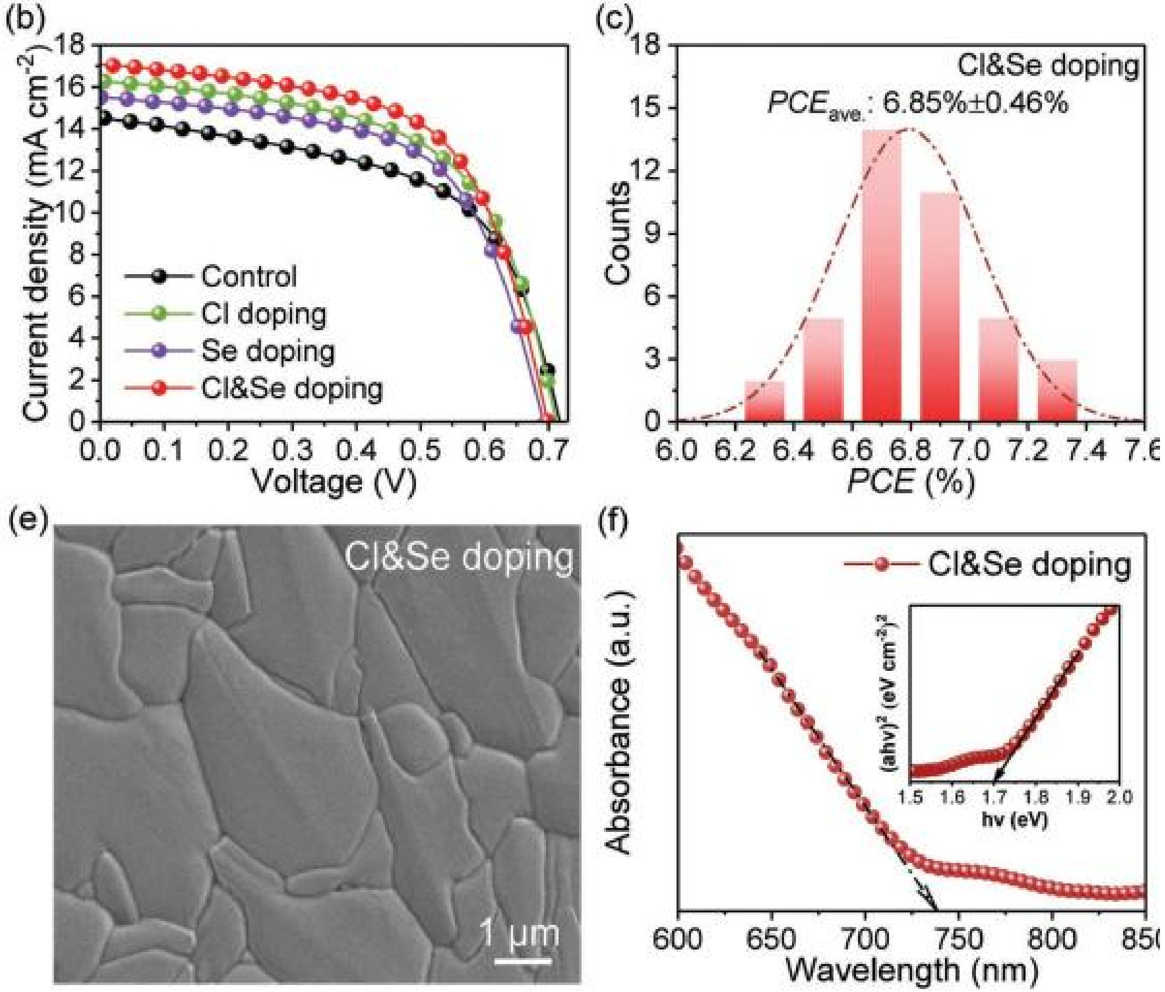

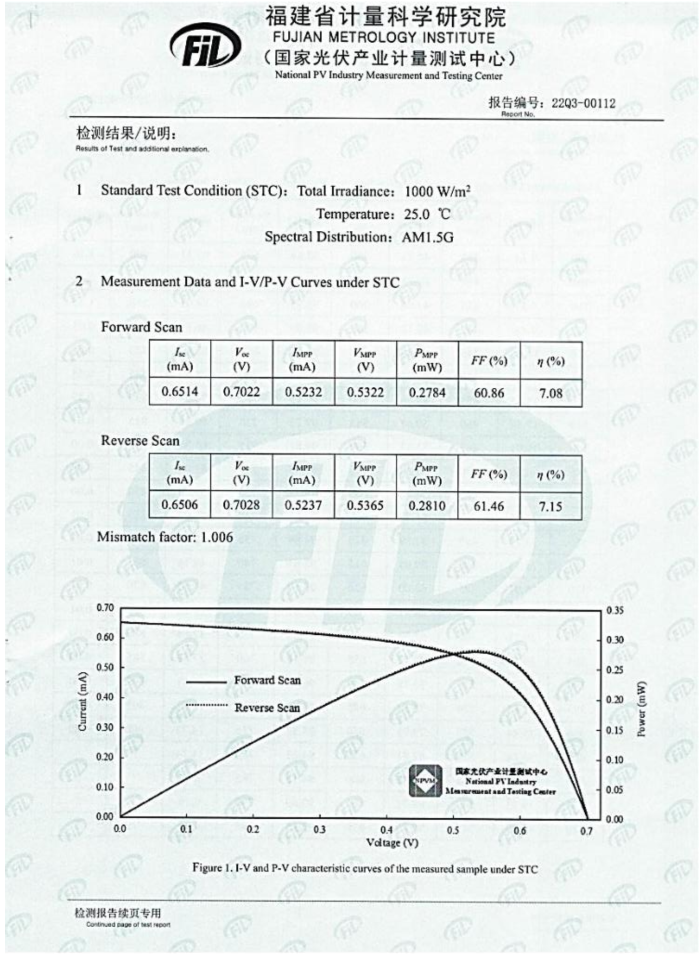

福建省计量科学研究院
FUJIAN METROLOGY INSTITUTE
（国家光伏产业计量测试中心）
National PV Industry Measurement and Testing Center

报告编号：22Q3-00112
Report No.

检测结果/说明：
Results of Test and additional explanation.

1 Standard Test Condition (STC)：Total Irradiance：1000 W/m^2
Temperature：25.0 ℃
Spectral Distribution：AM1.5G

2 Measurement Data and I-V/P-V Curves under STC

Forward Scan

I_{sc} (mA)	V_{oc} (V)	I_{MPP} (mA)	V_{MPP} (V)	P_{MPP} (mW)	FF (%)	η (%)
0.6514	0.7022	0.5232	0.5322	0.2784	60.86	7.08

Reverse Scan

I_{sc} (mA)	V_{oc} (V)	I_{MPP} (mA)	V_{MPP} (V)	P_{MPP} (mW)	FF (%)	η (%)
0.6506	0.7028	0.5237	0.5365	0.2810	61.46	7.15

Mismatch factor: 1.006

Figure 1. I-V and P-V characteristic curves of the measured sample under STC

检测报告续页专用
Continued page of test report

Se doping fill V_S; Cl doping regulate [hk1] orientation；yield a certified PCE of 7.15%

J. Tang, H. Song*, et al. Adv. Energy Mater. 2022, 12, 2202897

Double buffer layer + coordination

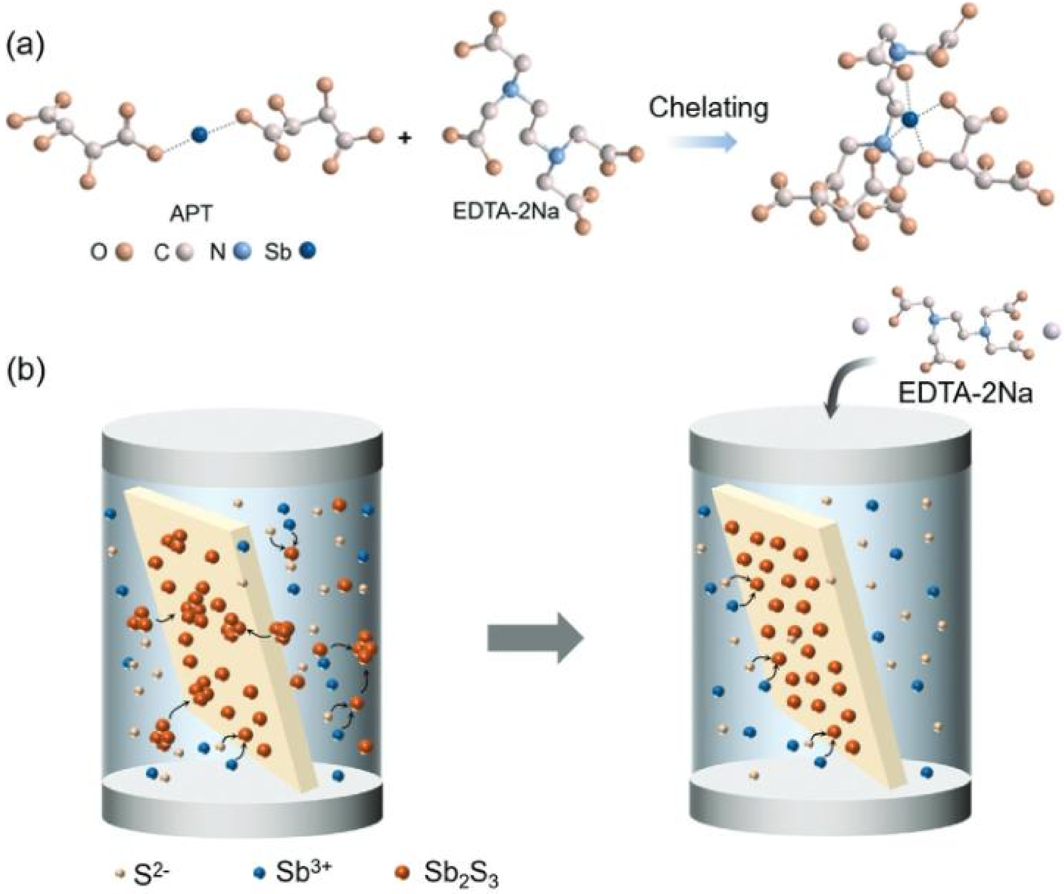

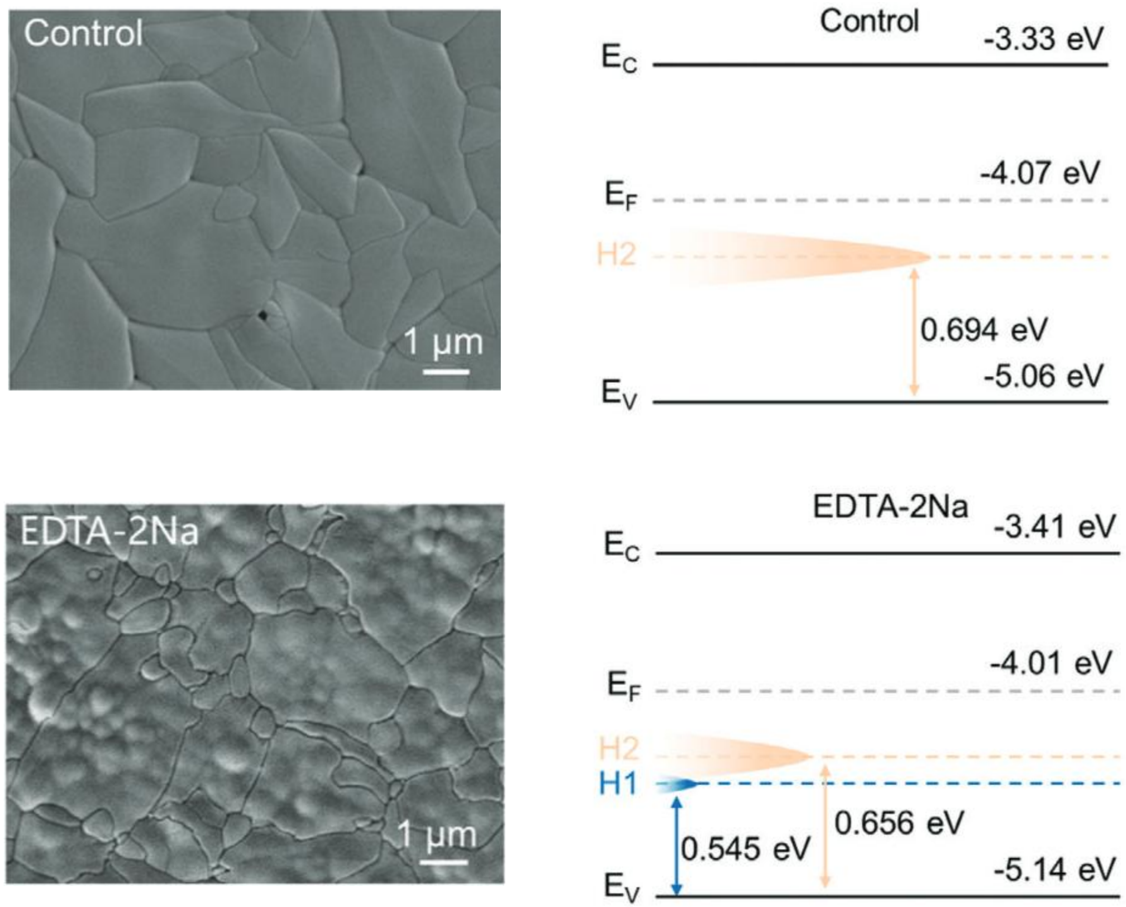

EDTA-2Na restrains homogeneous nucleation and retards deposition rate

Larger grains and less deep defects

H. Song*, J. Tang, et al. Adv. Energy Mater. 2025, DOI: 10.1002/aenm.202406051

Double buffer layer + coordination

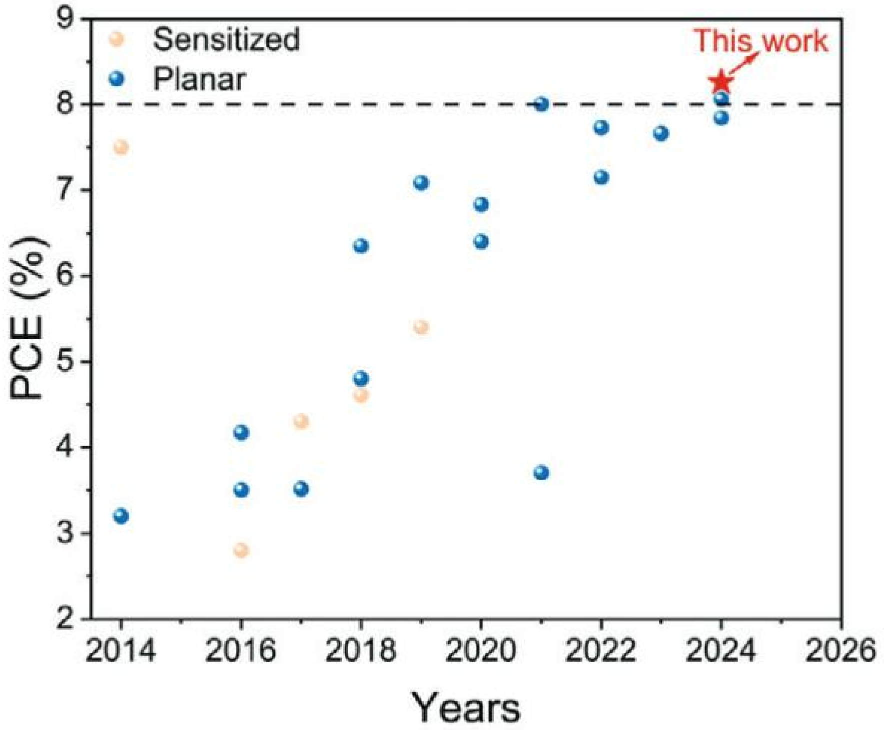

A record PCE of 8.08% (certified)

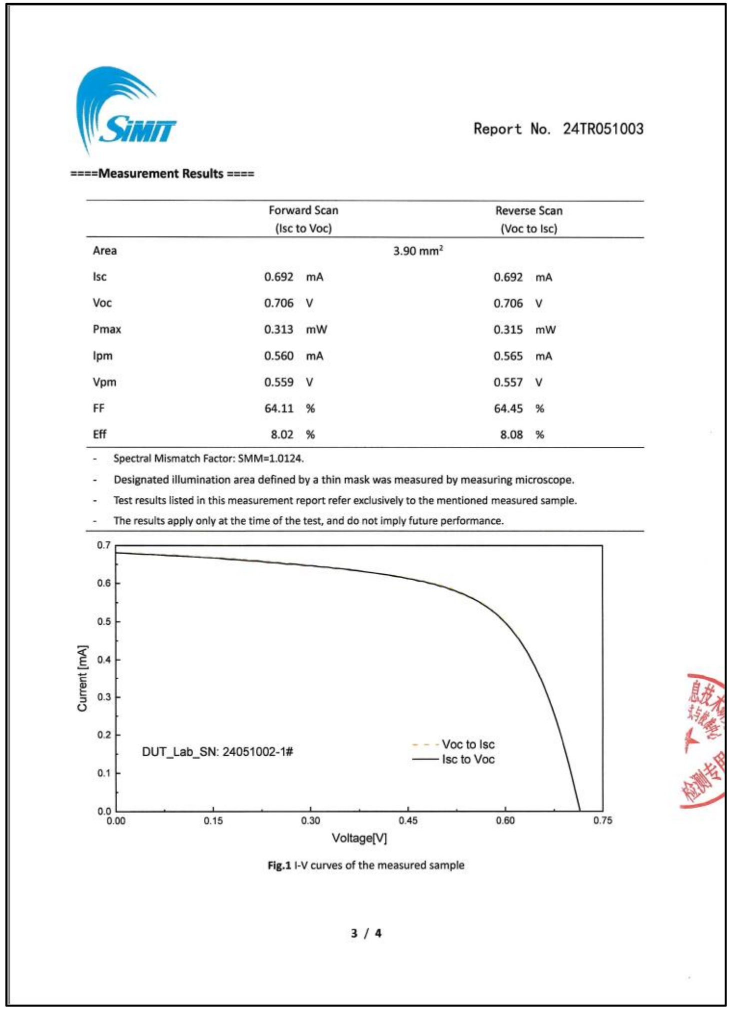

SIMIT

Report No. 24TR051003

====Measurement Results ====

	Forward Scan (Isc to Voc)		Reverse Scan (Voc to Isc)	
Area	3.90 mm²			
Isc	0.692	mA	0.692	mA
Voc	0.706	V	0.706	V
Pmax	0.313	mW	0.315	mW
Ipm	0.560	mA	0.565	mA
Vpm	0.559	V	0.557	V
FF	64.11	%	64.45	%
Eff	8.02	%	8.08	%

- Spectral Mismatch Factor: SMM=1.0124.
- Designated illumination area defined by a thin mask was measured by measuring microscope.
- Test results listed in this measurement report refer exclusively to the mentioned measured sample.
- The results apply only at the time of the test, and do not imply future performance.

Fig.1 I-V curves of the measured sample

3 / 4

H. Song*, J. Tang, et al. Adv. Energy Mater. 2025, DOI: 10.1002/aenm.202406051

Outline

1. Background of tandem solar cells

2. Exploration for Si-based tandem solar cells

   - 1.72 eV CdSe solar cells
   - 1.68 eV Sb_2S_3 solar cells
   - 1.72 eV $CsPbI_3$ solar cell

3. Exploration for all-perovskite tandem solar cells

4. Summary and acknowledgment

Why chose $CsPbI_3$?

E_g~1.68-1.73 eV

✓ suitable for Si-based top sub-cell

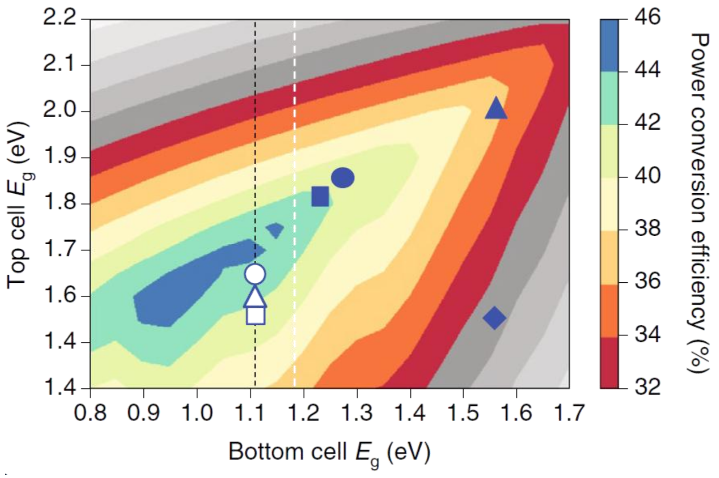

Ref. Nat. Energy **2018**, 3, 828

Inorganic components

✓ good chemical, thermal and light stability

✓ suitable for thermal evaporation

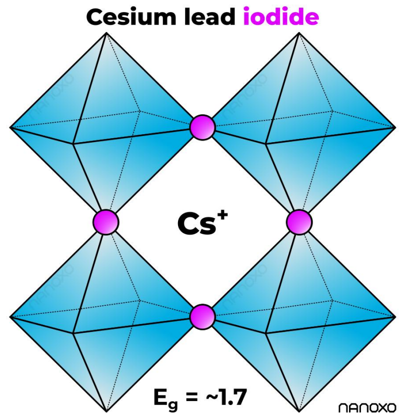

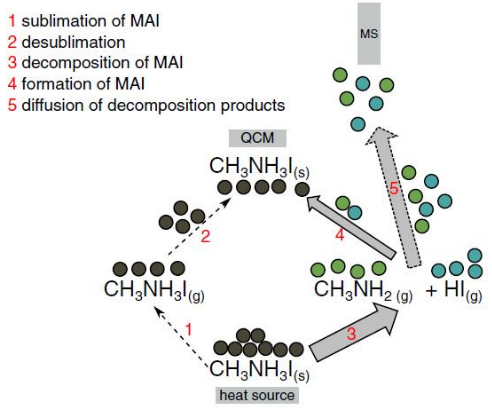

Sol. RRL **2022**, 6, 2200500

Why chose TE to deposition $CsPbI_3$?

Method	Conformal	Large area	Production compatibility	Substrate dependence	Toxic solvent	Environ. sensitivity	Notes
Spinning	×	×	×	strong	DMF/DMSO	H_2O/O_2	Poor uniformity
Blading	×	√	×	strong	DMF/DMSO	H_2O/O_2	Poor reproducibility
Printing	√	√	×	strong	DMF/DMSO	H_2O/O_2	Low performance
TE	√	√	√ (OLED)	weak	no	Vacuum	Low performance

TE= Thermal Evaporation

TE is suitable for large-area conformal deposition on textured surfaces

Status of thermal evaporation $CsPbI_3$ solar cells

	Single source TE	Two source co-TE	Layer-by-layer TE
	$CsPbI_3 \rightarrow CsPbI_3$ (s)	$CsI + PbI_2 \rightarrow CsPbI_3$ (s)	$CsI/PbI_2/../CsI/PbI_2 \rightarrow CsPbI_3$
	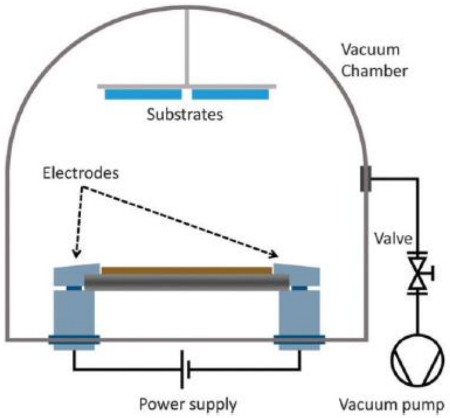	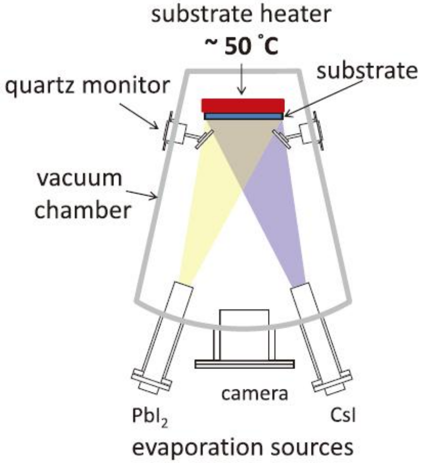	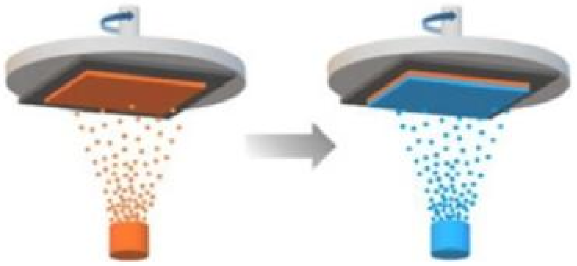
Device structure	Only film, no device	**ITO/PTAA/$CsPbI_3$/C_{60}/BCP/Cu**	ITO/PTAA/$CsPbI_3$/PCBM/Al
Champion PCE		**16.3%**	10.2%
Features	Non-stoichiometric	**Stoichiometric**	Secondary phase

Growth mechanism of TE γ-$CsPbI_3$ film

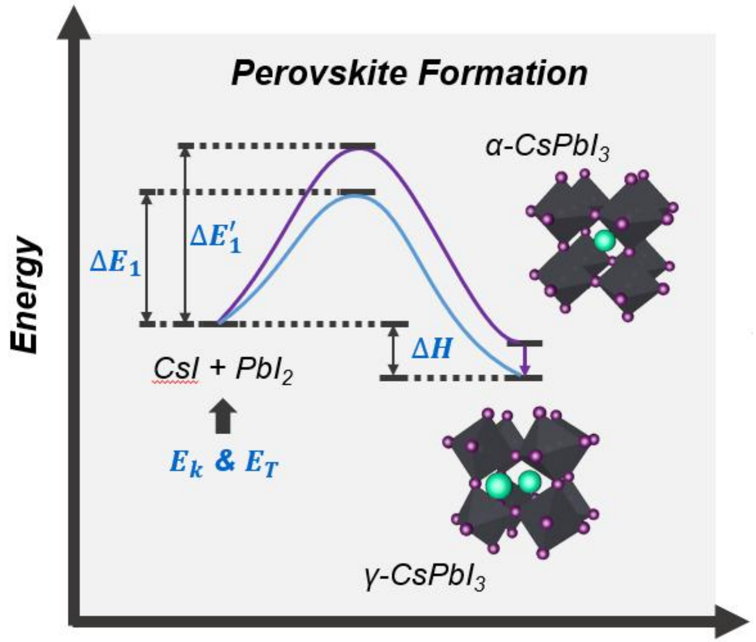

Formation process of TE γ-$CsPbI_3$

CsI+PbI_2 powder reaction:

- At 50℃, no reaction
- At 80℃, reaction (γ)
- At 100℃, fading (γ→δ)

80℃ can overcome reaction barrier

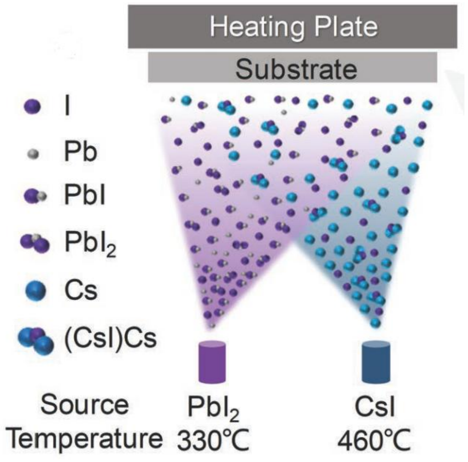

Tem. of vapor molecule is **>300**℃

Kinetic energy of vapor molecule promotes formation of the γ-$CsPbI_3$ phase

C. Chen*, **J. Tang*,** et al. Adv. Function. Mater. 2023, 33, 2214414.

Phase stability mechanism of TE γ-$CsPbI_3$ film

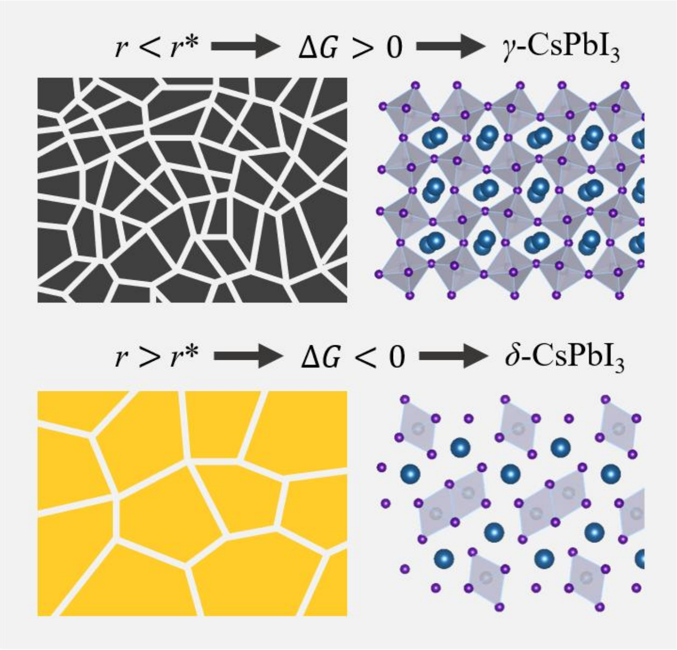

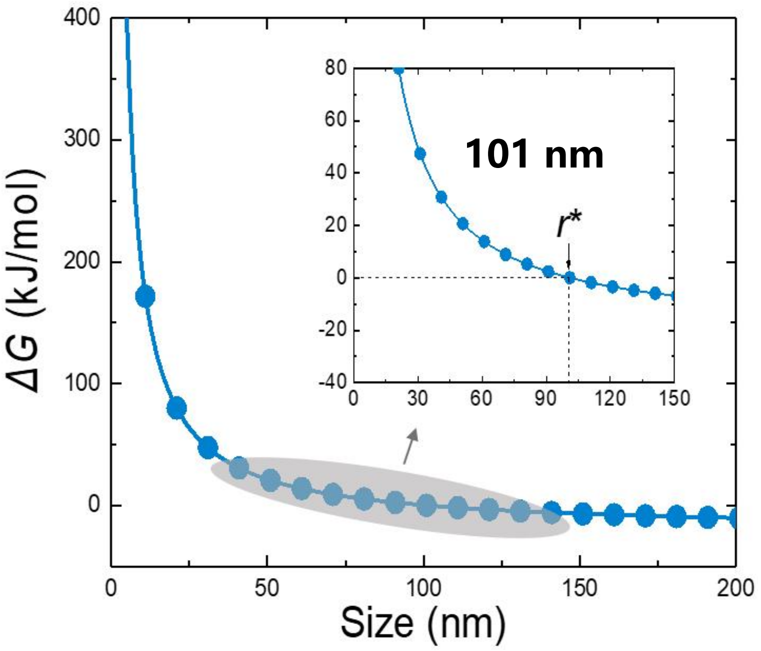

$$\Delta G = \Delta G_b + \Delta G_s$$

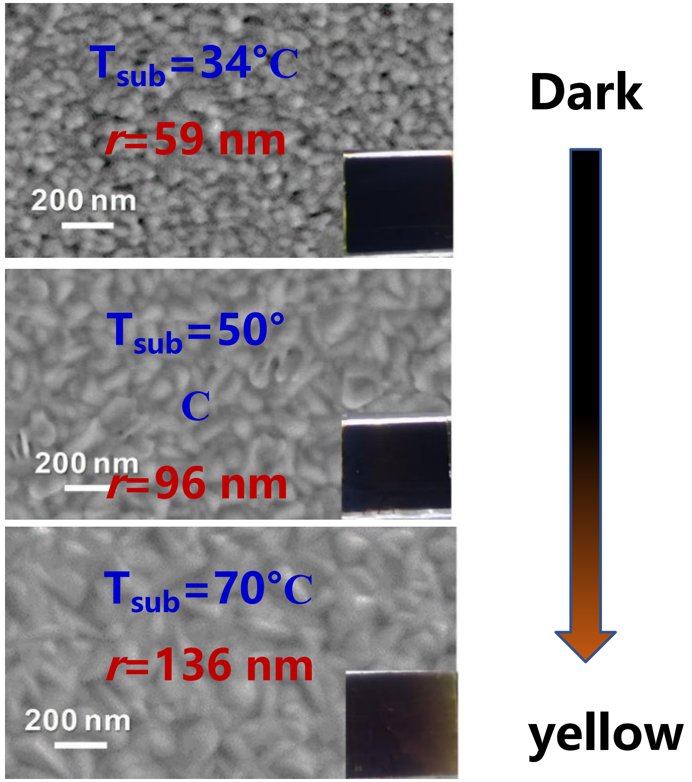

Surface effect of small grain (<101 nm) can stabilize γ-$CsPbI_3$ film

C. Chen*, **J. Tang***, et al. Adv. Function. Mater. 2023, 33, 2214414.

Crystallinity control of TE γ-$CsPbI_3$ film

Small grains Random orientation

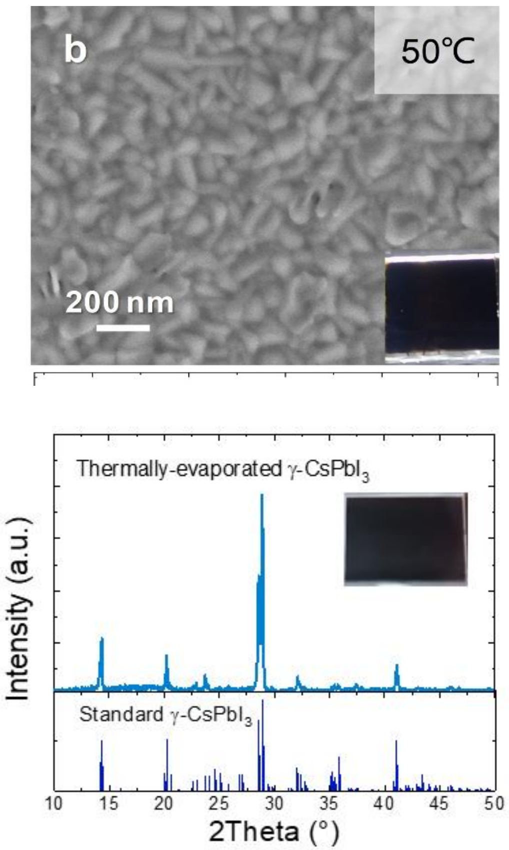

Nucleus Regulation via DMAI

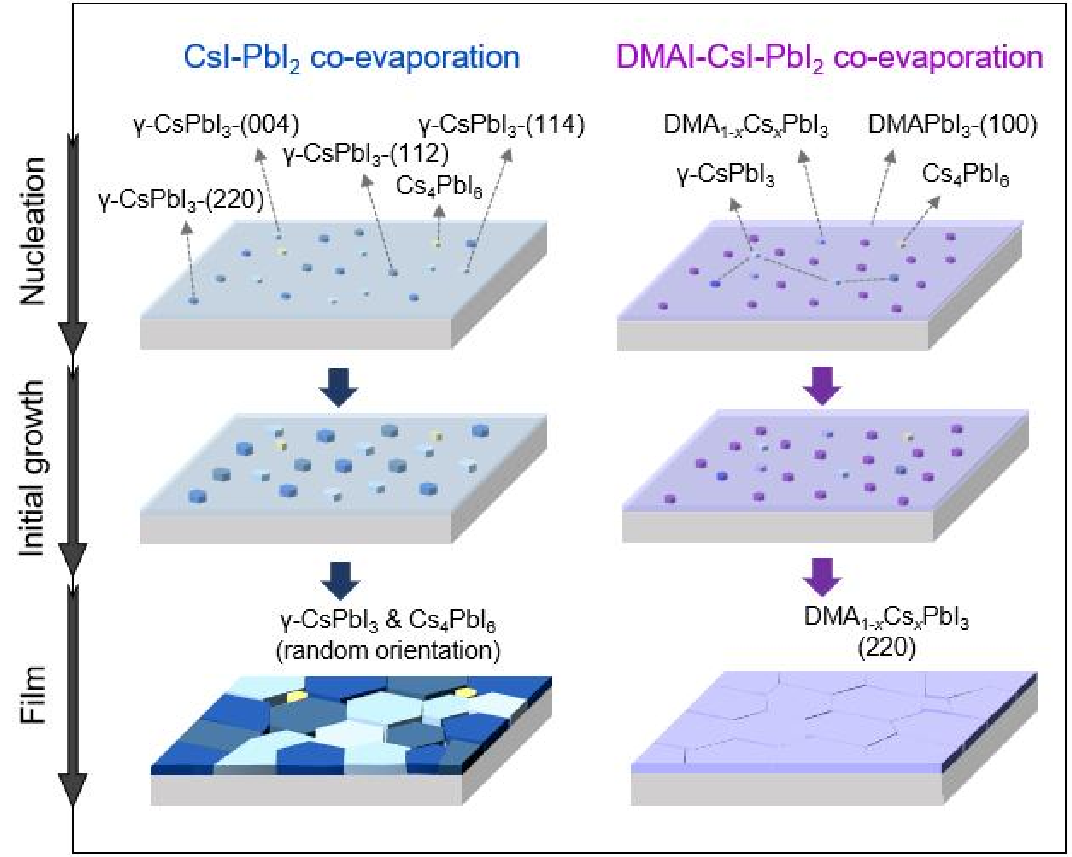

Preferred (100) orientation

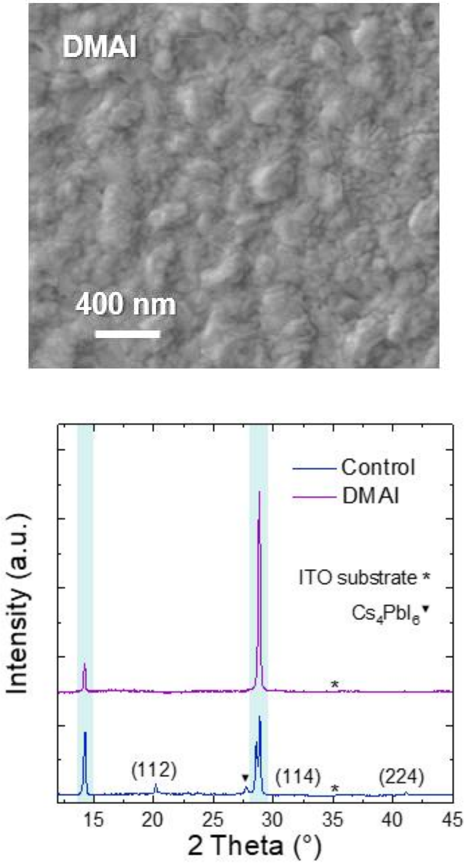

DMAI co-evaporation enable preferred (100) orientation

L. Wang*, C. Chen*, **J. Tang,** et al. Nano Energy 2024, 120, 109159.

Device performance of TE γ-$CsPbI_3$ solar cells

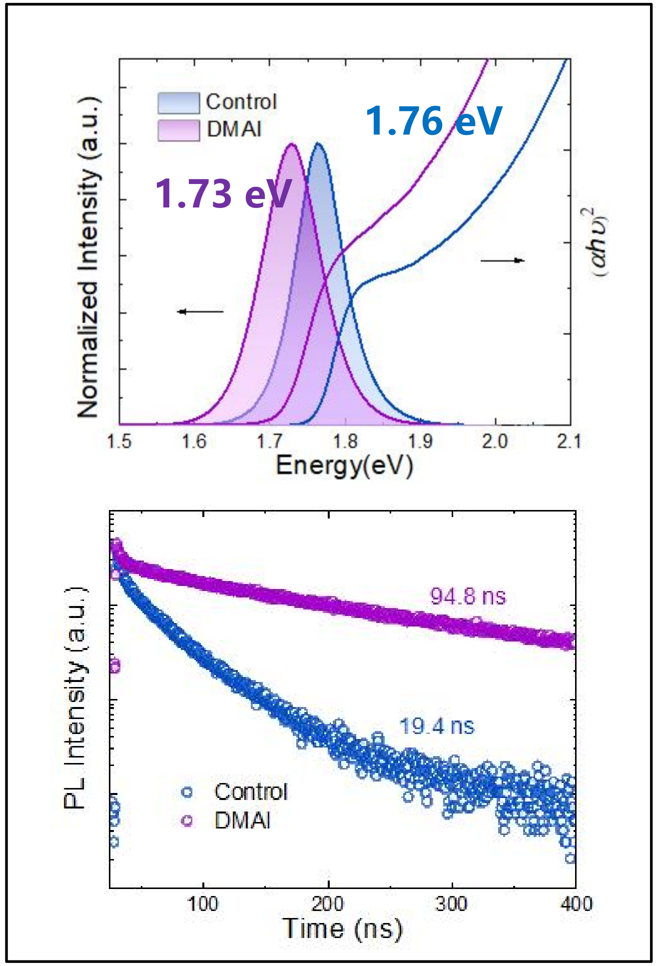

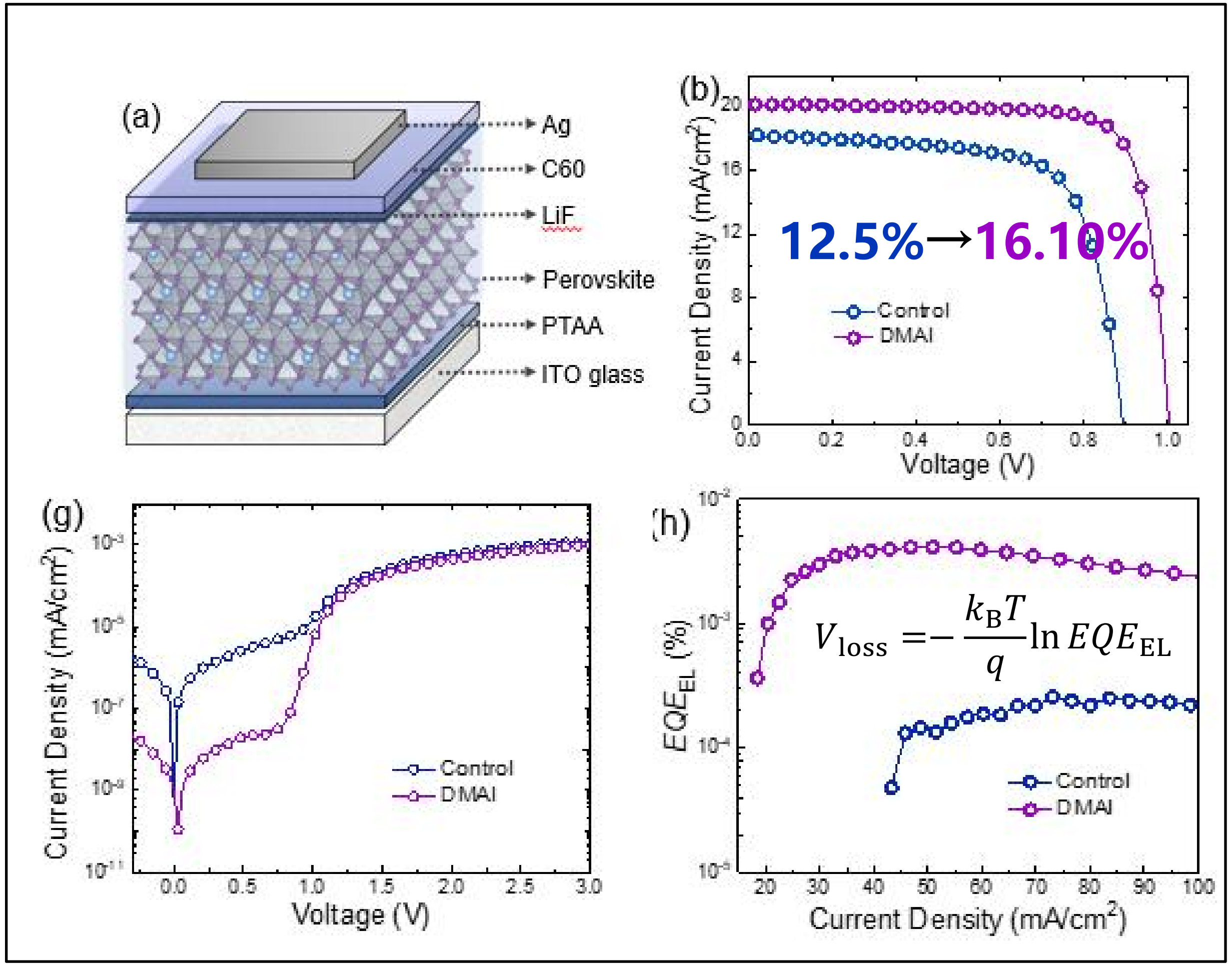

$$V_{\text{loss}} = -\frac{k_B T}{q} \ln EQE_{EL}$$

A record PCE of 16.10% based on annealing-free $CsPbI_3$ film

L. Wang*, C. Chen*, **J. Tang,** et al. Nano Energy 2024, 120, 109159.

Surficial passivation using BaI$_2$ vapor

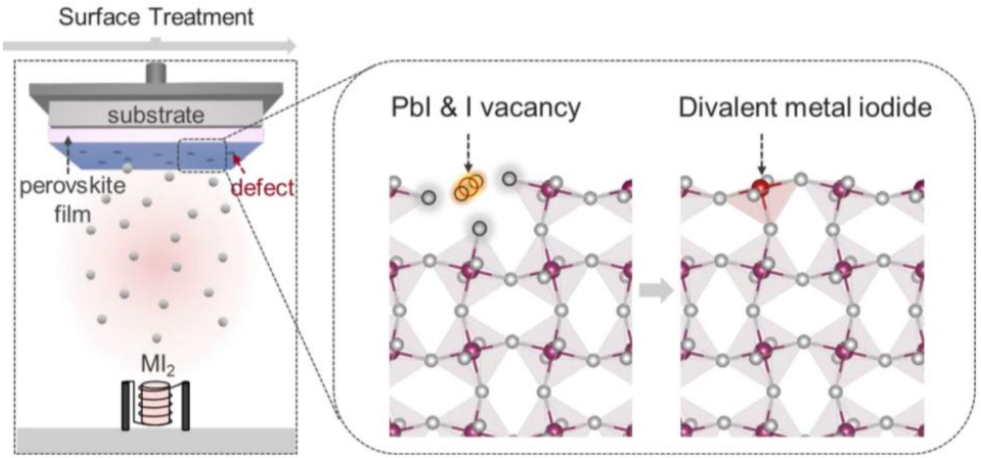

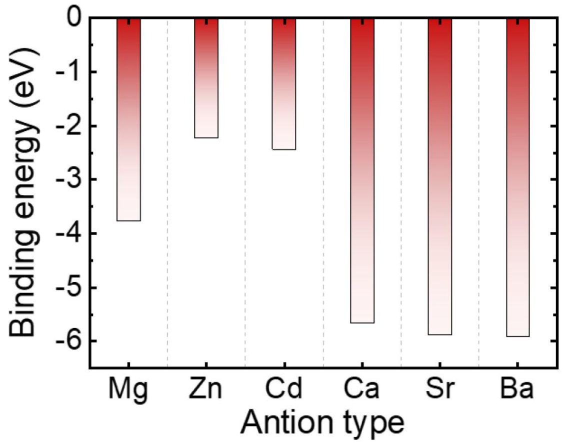

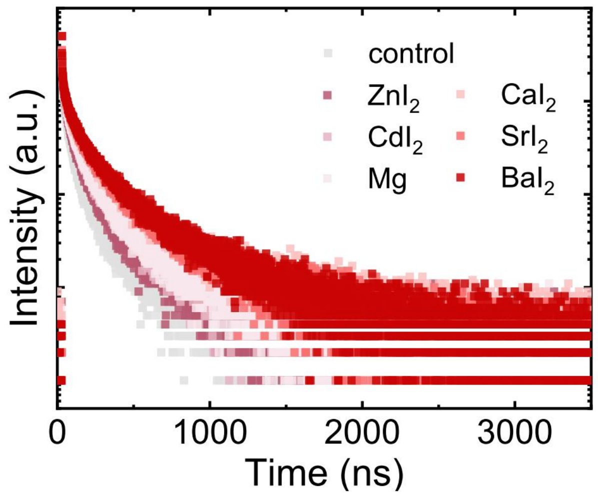

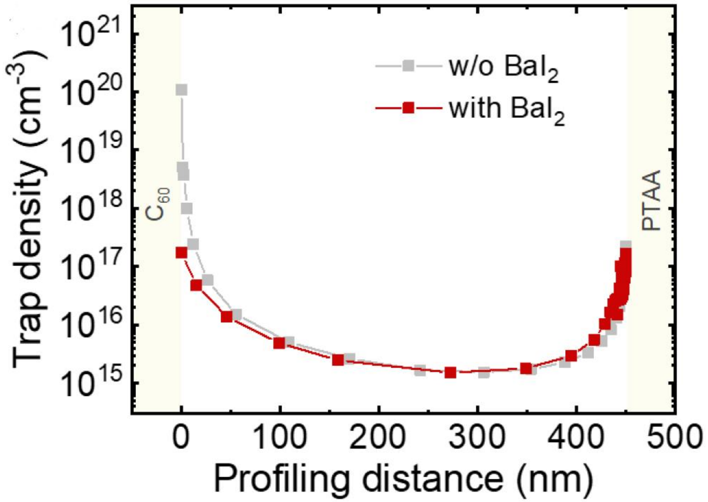

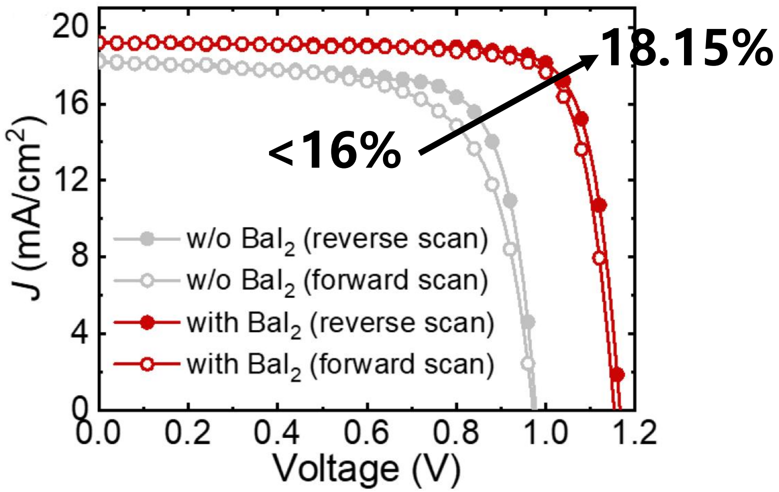

Record PCE of 18.15% among all thermal-evaporation $CsPbI_3$–based solar cells

Exploration of $CsPbI_3$ growth on textured Si

textured surface

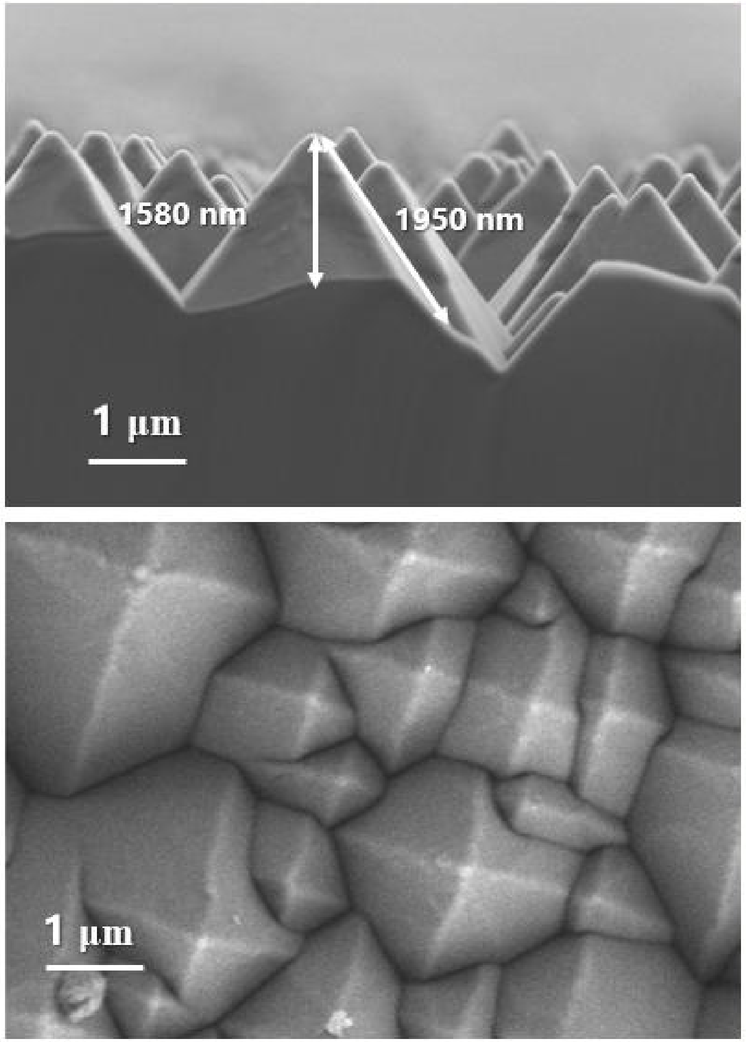

TE $CsPbI_3$ on textured surface

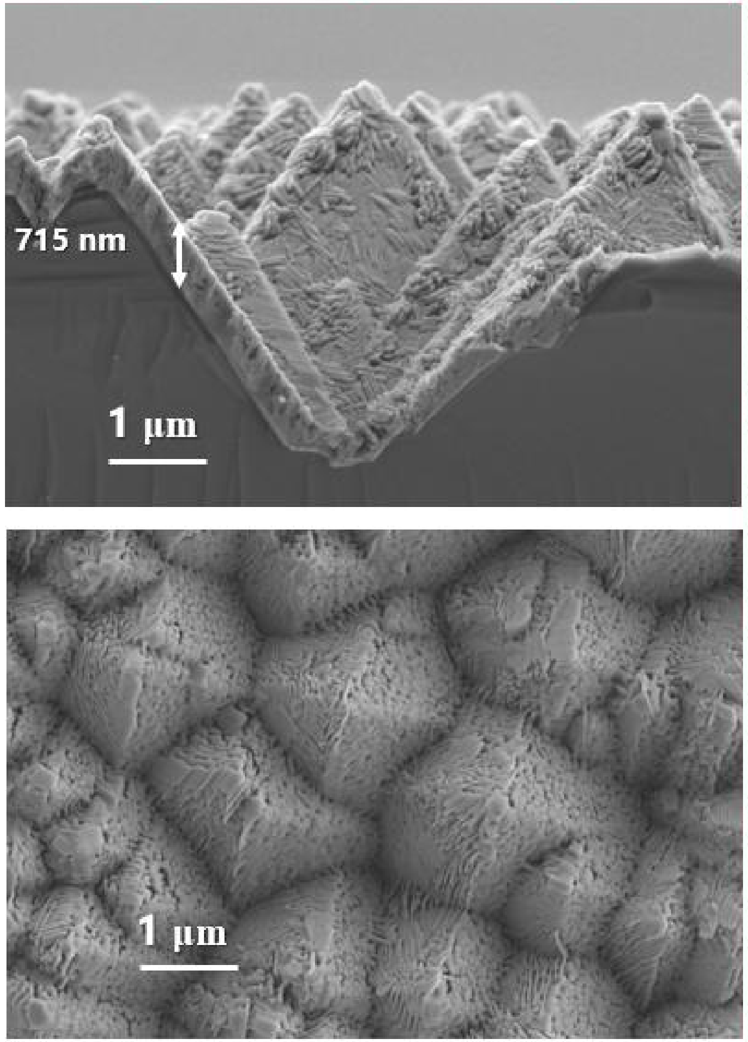

Outline

Excellent photovoltaic properties

ABX$_3$ perovskite

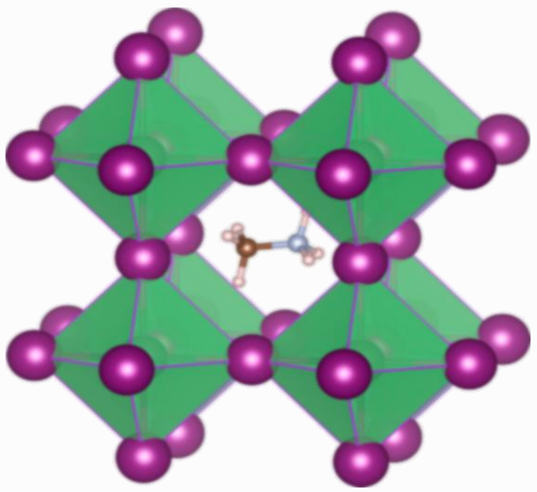

Highly symmetrical structure

Tunable bandgap

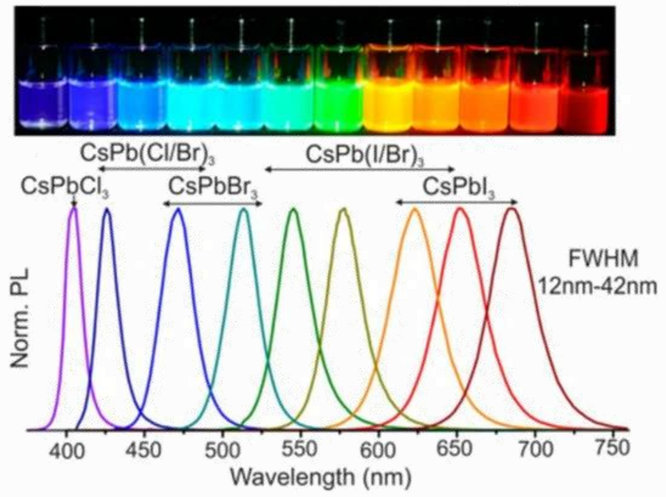

Tunableness from 1.2 to 3.1 eV

Defect tolerance

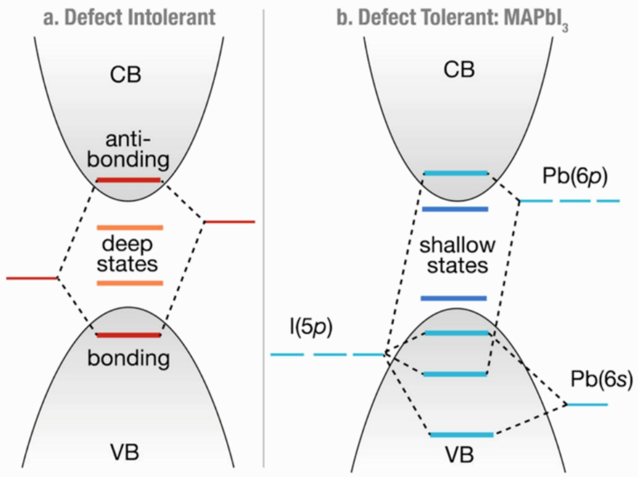

Valence band top formed by the antibonding orbitals

Excellent photovoltaic properties, highly suitalble for tandem PSCs

Vacuum-assisted crystallization for tandem cells

Anti-Solvent Method for Tandem All-Perovskite Solar Cells

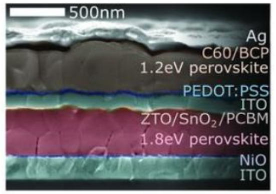

First TPSCs
PCE: 17.0%
(*Science*, 2016)

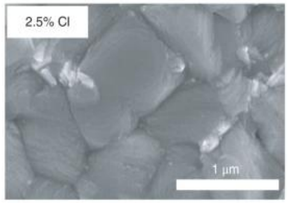

Crystallization control
PCE >20%
(*Nat. Energy*, 2018)

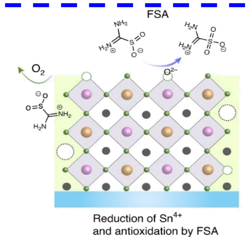

Multifunctional reducing agent
PCE: 25.6%
(*Nat. Energy*, 2020)

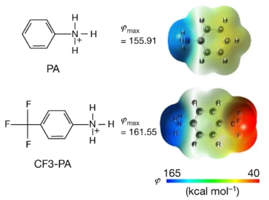

Interface passivation
PCE: 26.4%
(*Nature*, 2022)

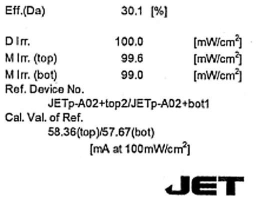

Suzhou Renshuo Optoelectronics
PCE: 30.1%
(2024)

2016 2018 2020 2022 2024

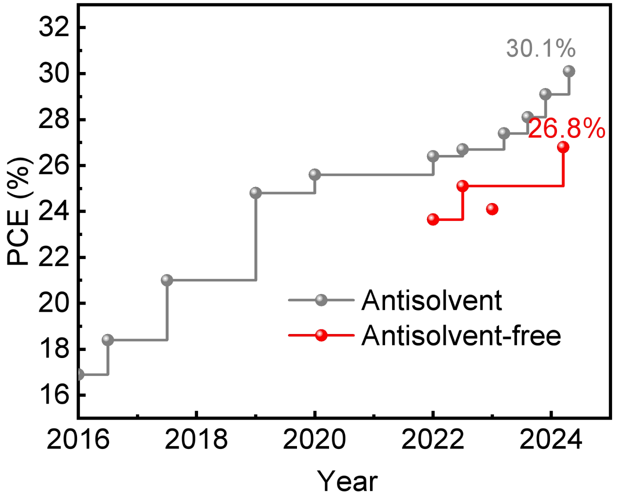

Vacuum-Assisted Crystallization

First time
PCE: 23.5% (*Nat. Energy*, 2022)

Bulk passivation
PCE: 23.65%
(*ACS Energy Lett.*, 2022)

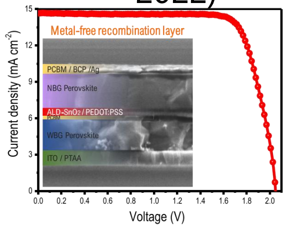

Hot air assisted
PCE: 23.0%
(*Nat. Energy*, 2022)

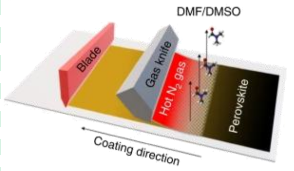

Additive engineering
PCE: 26.8%
(*Science*, 2024)

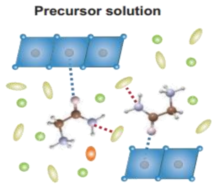

Gas-Assisted Crystallization

TPSCs based on vacuum-assisted methods remain far lower PCE than antisolvent method.

Industrial preparation methods for tandem cells

Anti-Solvent Method

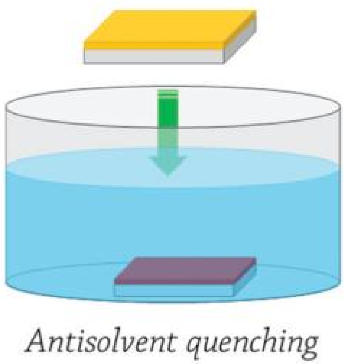

Characteristics:

- High film quality
- Simple process
- Non-continuous
- Environmental concerns
- High solvent cost

Vacuum-Assisted Crystallization Method

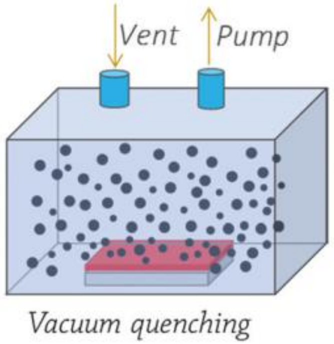

Characteristics:

- Large-area compatibility
- High material utilization
- Good reproducibility
- Low cost
- wide compatibility

Antisolvent-free method is most competitive for industrial production

Inconsistent crystallization in Sn–Pb perovskite

An uneven composition

Surface defects and band fluctuation

low solvent quenching rate amplifies above effects.

$MAPbI_3$: slow crystallization kinetics

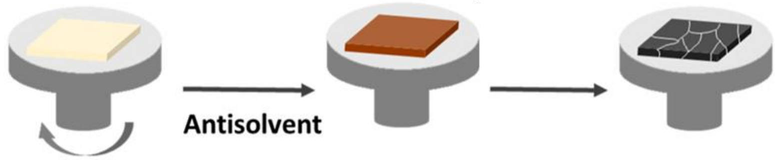

$MASnI_3$: fast crystallization kinetics

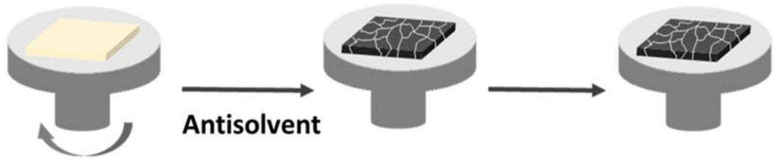

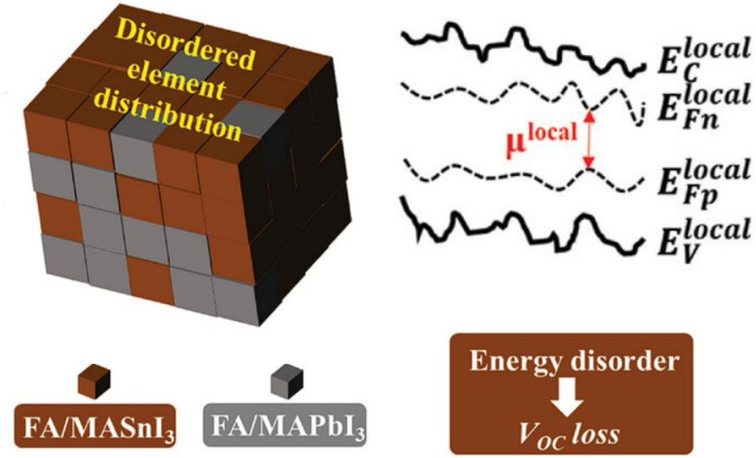

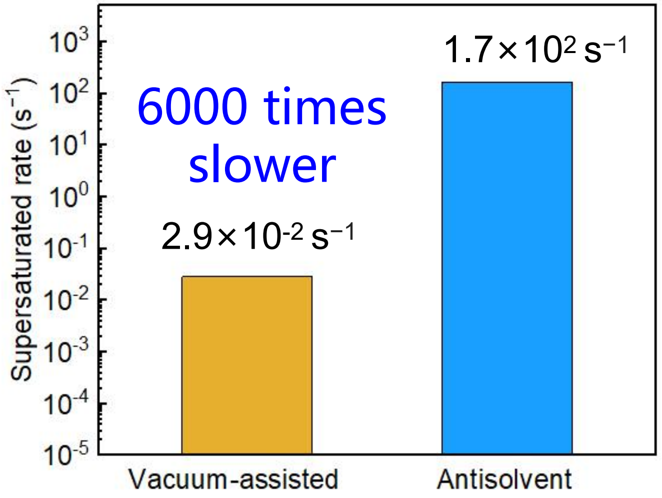

Large difference in crystallization rate leads to severe component segregation

Ref: Junfeng Fang, et al. Advanced Materials 2023, 35, 2303674.

Crystallization mechanism in Sn–Pb NBG PVSK

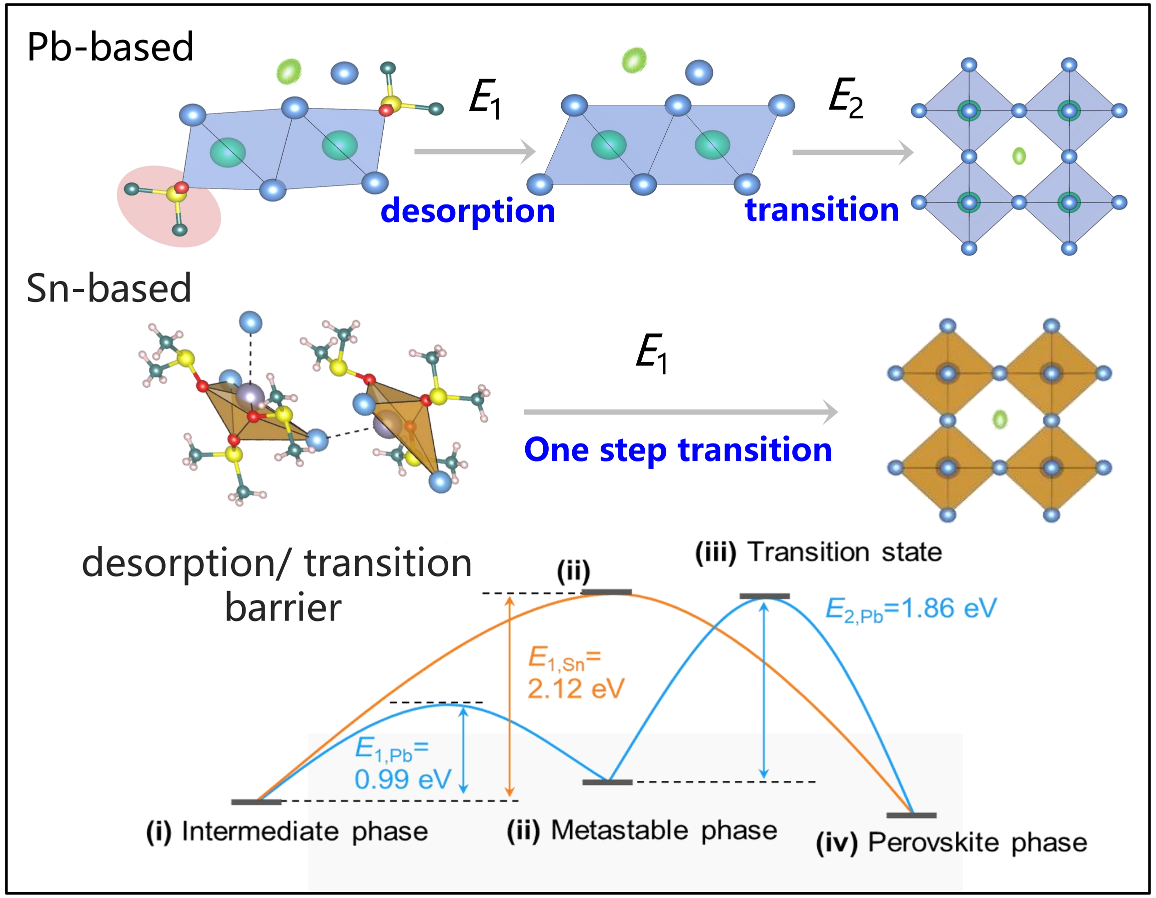

$$R = A_{tot} \exp\left(-E/k_B T\right)$$

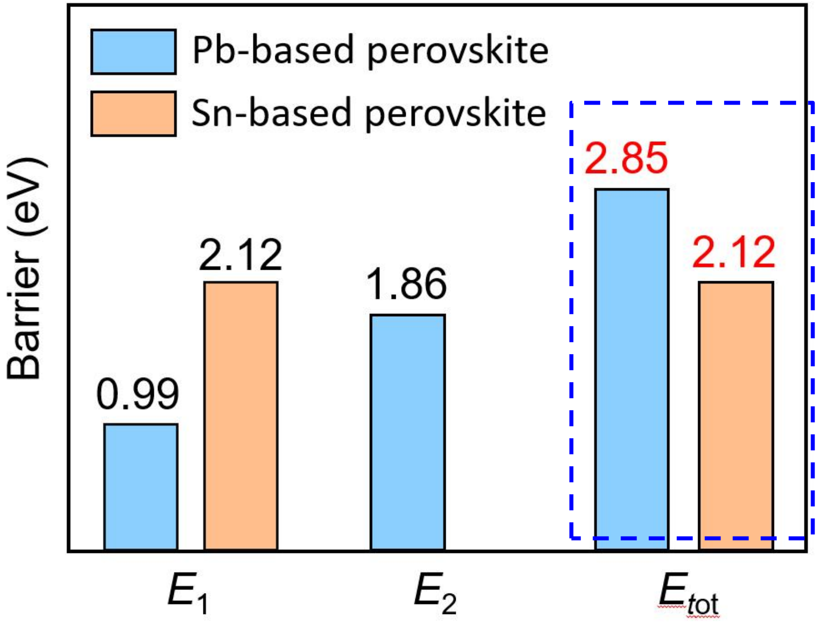

$E_{Sn} < E_{Pb}$

- ☐ **Pb perovskite: solvent desorption and phase transition → slow nucleation**
- ☐ **Sn perovskite: only solvent desorption → rapid nucleation**

C. Chen*, H. Song*, J. Tang*, et al. *Nat. Photonics* 2025, 19, 426.

Crystallization regulation for Sn–Pb NBG films

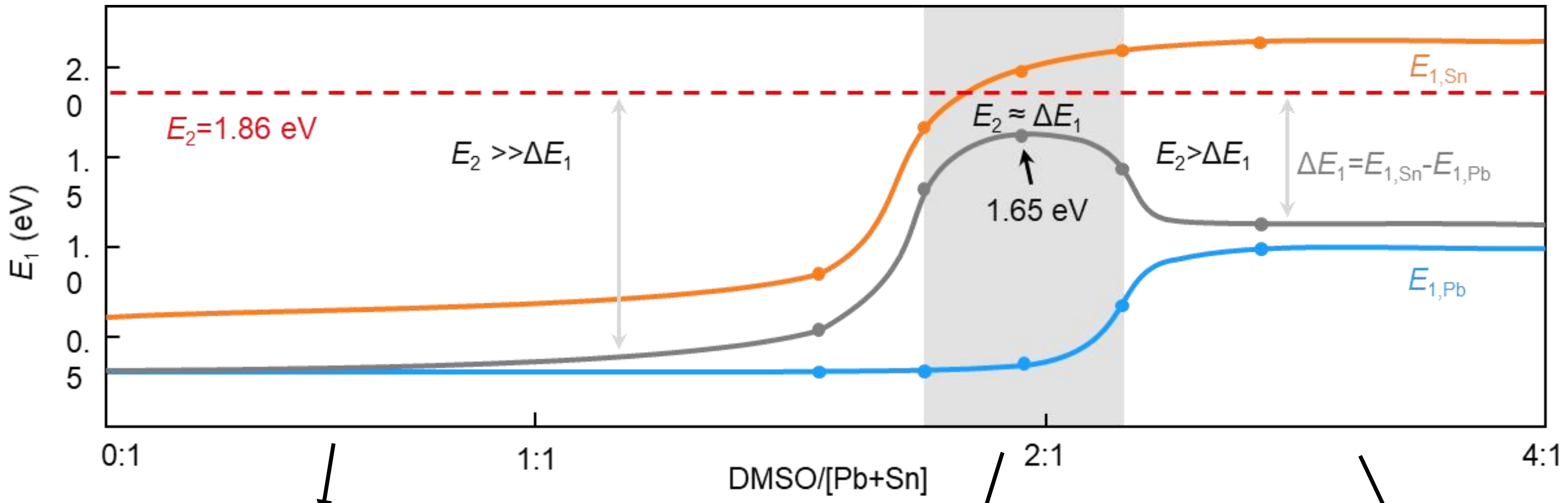

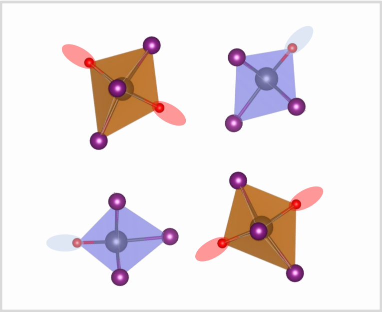

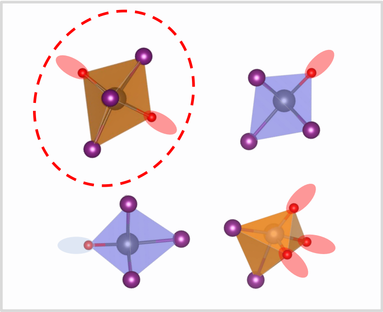

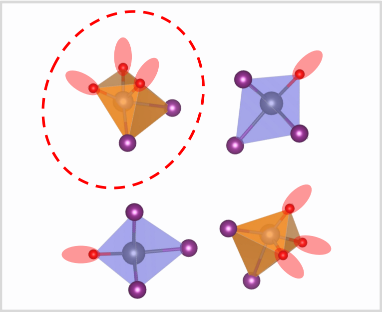

All SnI_2 coordinated with < 3 DMSO
All PbI_2 coordinated with DMF

Part SnI_2 coordinated with < 3 DMSO
Part PbI_2 coordinated with DMF

All SnI_2 coordinated with 3 DMSO
All PbI_2 coordinated with 1 DMSO

Selective complexation to adjust solvent desorption of Pb and Sn perovskites

C. Chen*, H. Song*, J. Tang* et al. ***Nat. Photonics*** 2025, 19, 426.

High-quality Pb-Sn film preparation

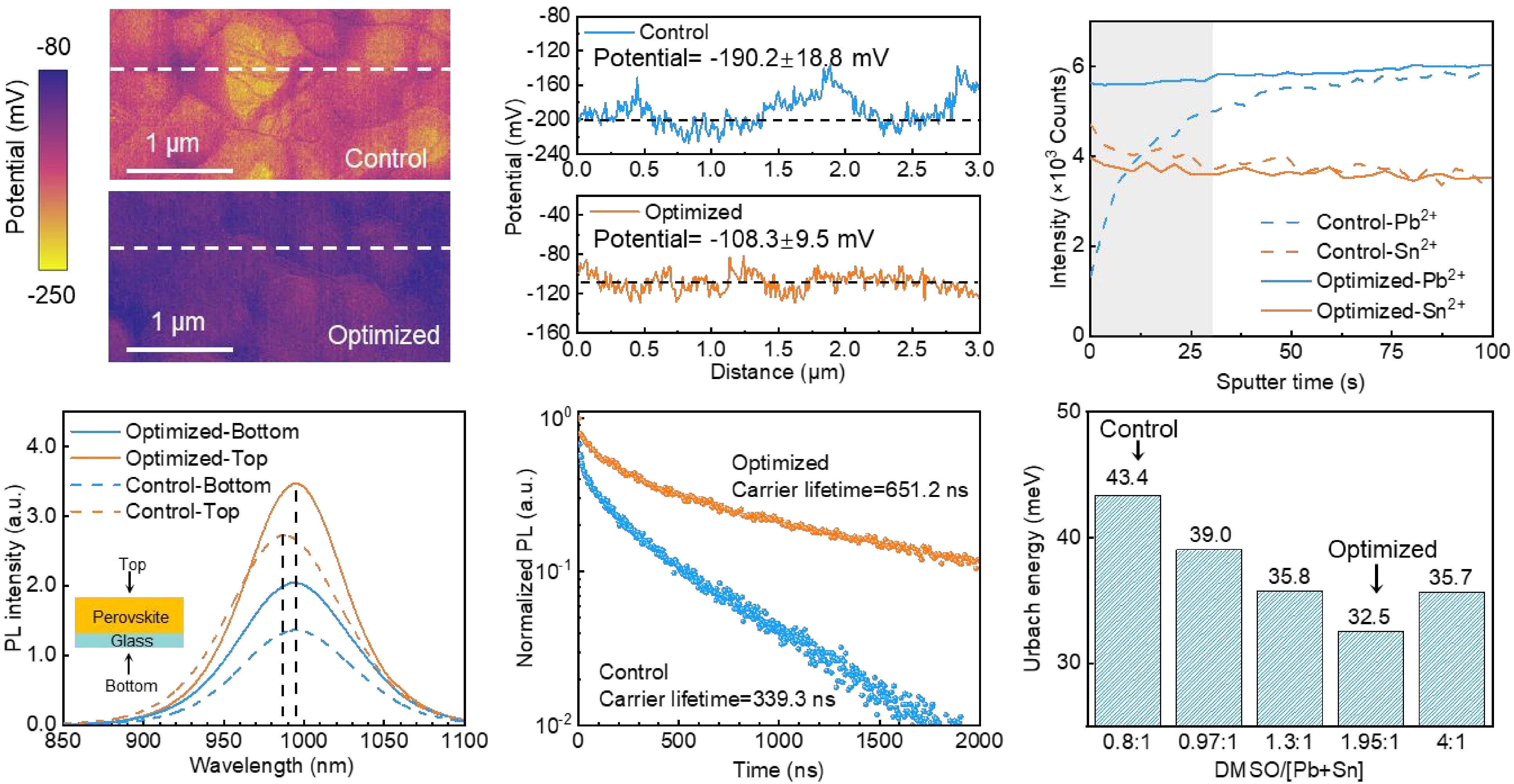

Homogeneous composition and high-quality NBG films

C. Chen*, H. Song*, J. Tang* et al. ***Nat. Photonics*** 2025, 19, 426.

High-efficiency Pb-Sn solar cell

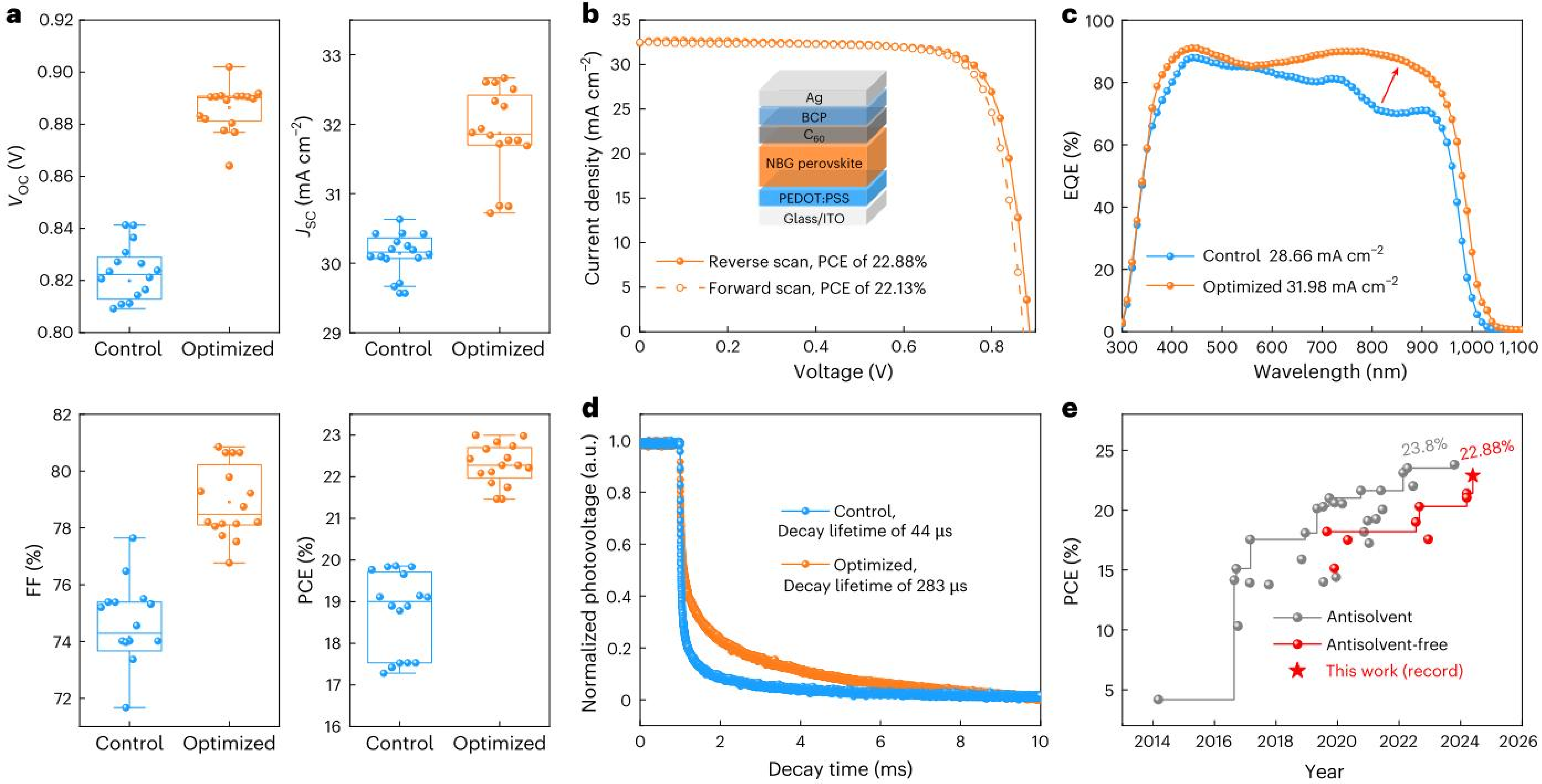

Record PCE of 22.88% for NBG device based on antisolvent-free method

C. Chen*, H. Song*, J. Tang* et al. ***Nat. Photonics*** 2025, 19, 426.

High-efficiency Pb-Sn solar cell

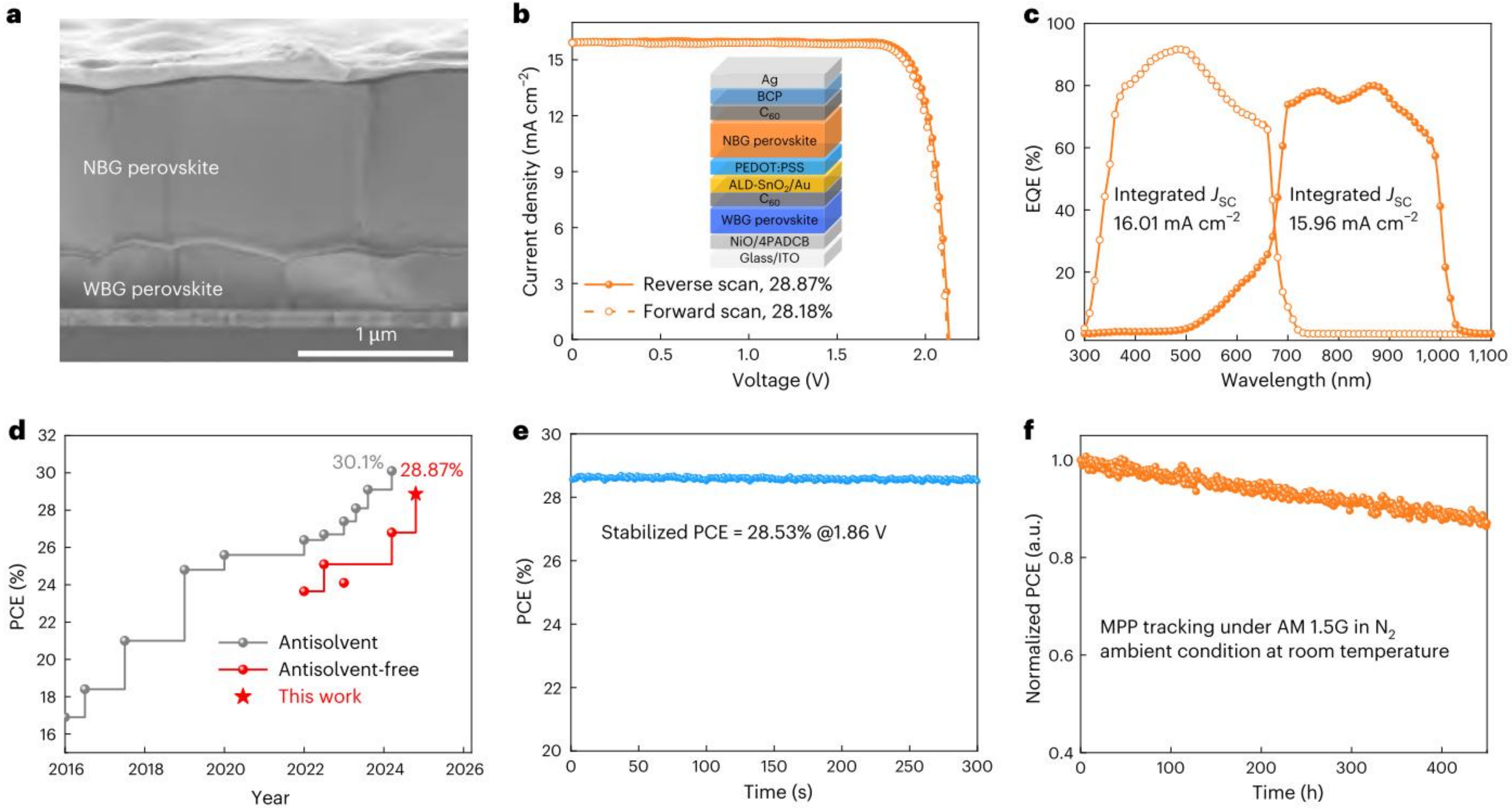

Record PCE of 28.87% for tandem device based on antisolvent-free method

C. Chen*, H. Song*, J. Tang* et al. ***Nat. Photonics*** 2025, 19, 426.

Voids and stratification in thick Sn-Pb films

- **Buried voids:** thick Sn–Pb film shows buried voids caused by residual solvents
- **Film stratification:** Upper layer nucleates preferentially, resulting in film stratification

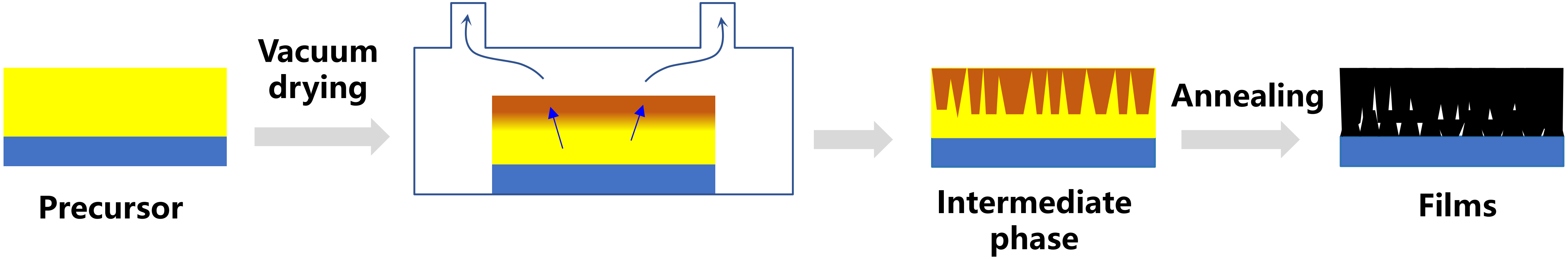

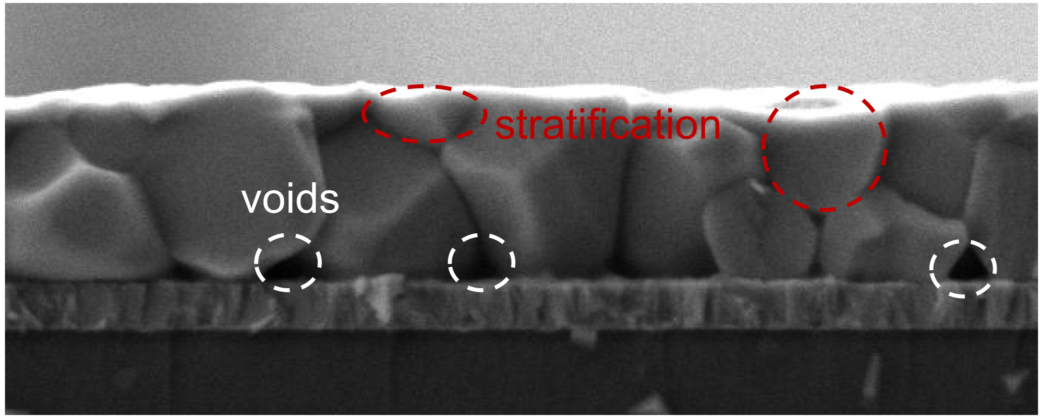

Light radiation annealing enables throughout grain

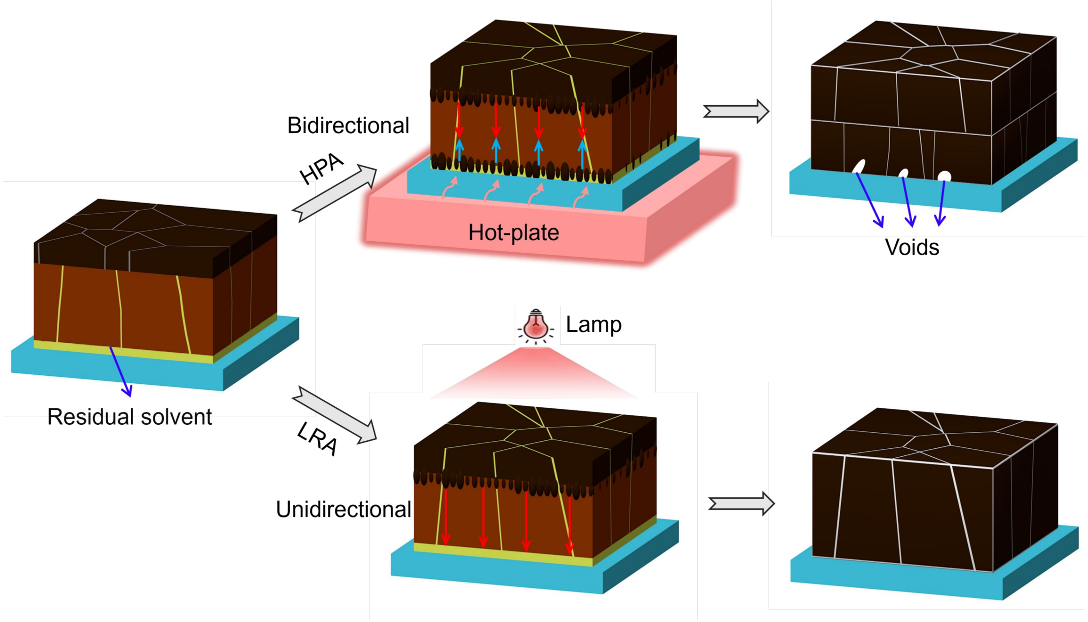

- ☐ uniform heating
- ☐ rapid solvent removal

Hot-plate: first glass, then films

$$q = -\lambda A \frac{dT}{dx}$$ λ~1 W/(m·K)

Light radiation: directly on perovskite

$$q = \epsilon\sigma(T_1^4 - T_2^4)$$

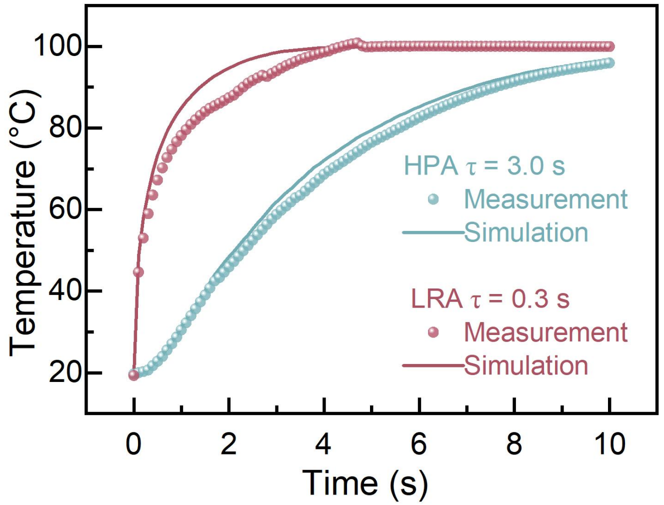

Light radiation annealing can reduce solvent residual

C. Chen*, J. Tang*, et al. *Energy Environ. Sci.* 2025, 18, 430

Light radiation annealing enables throughout grain

Vertical grains → **No voids** → **Less defects** → **Higher device PCE**

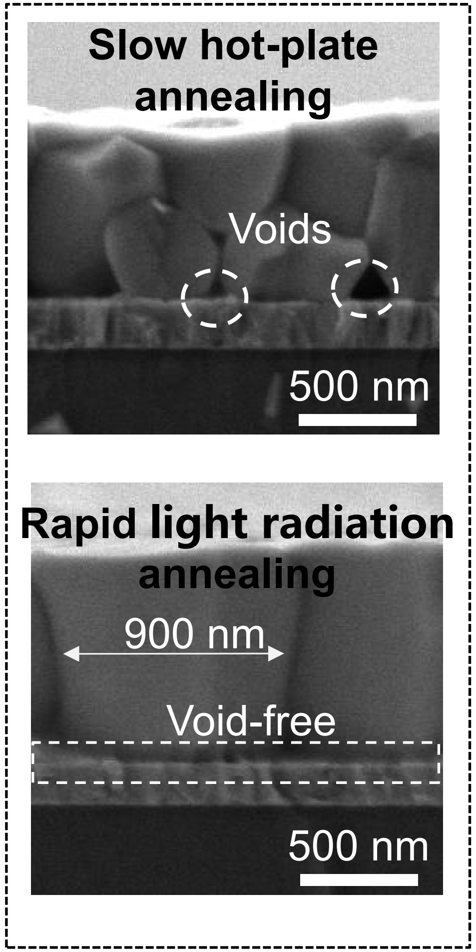

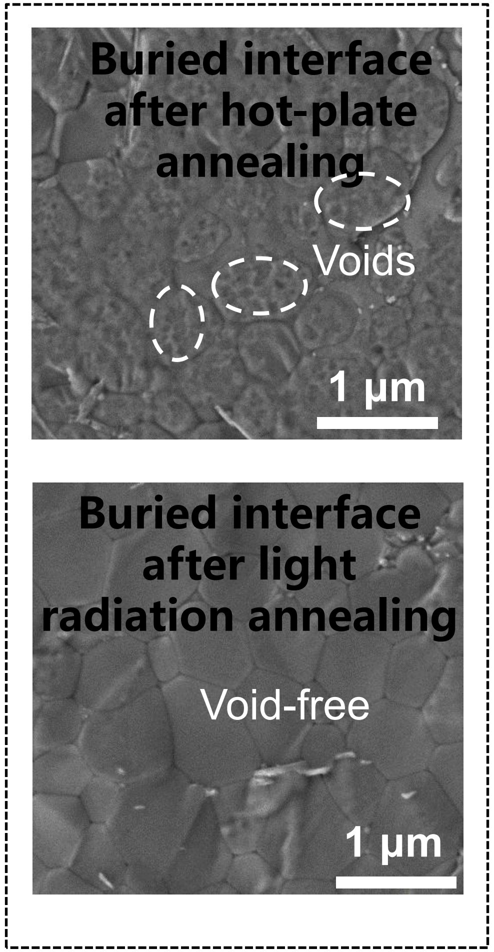

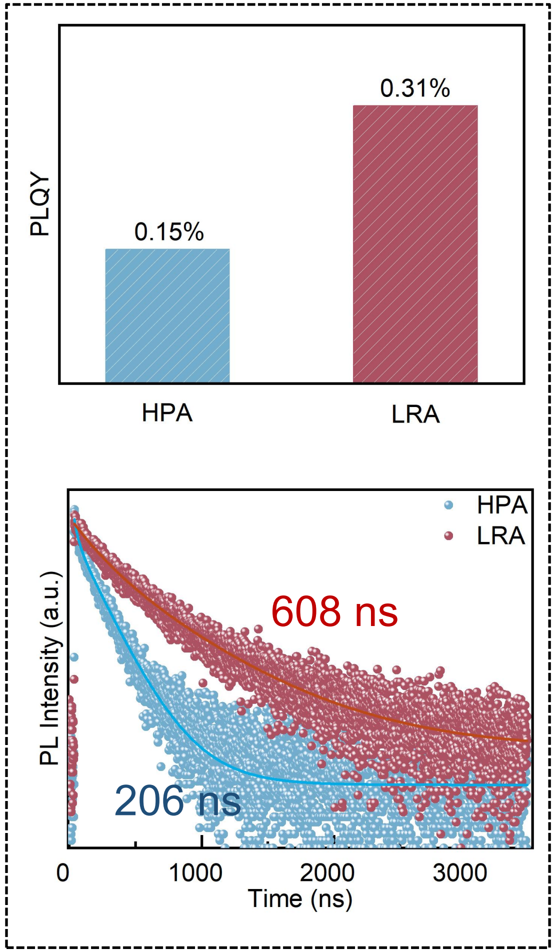

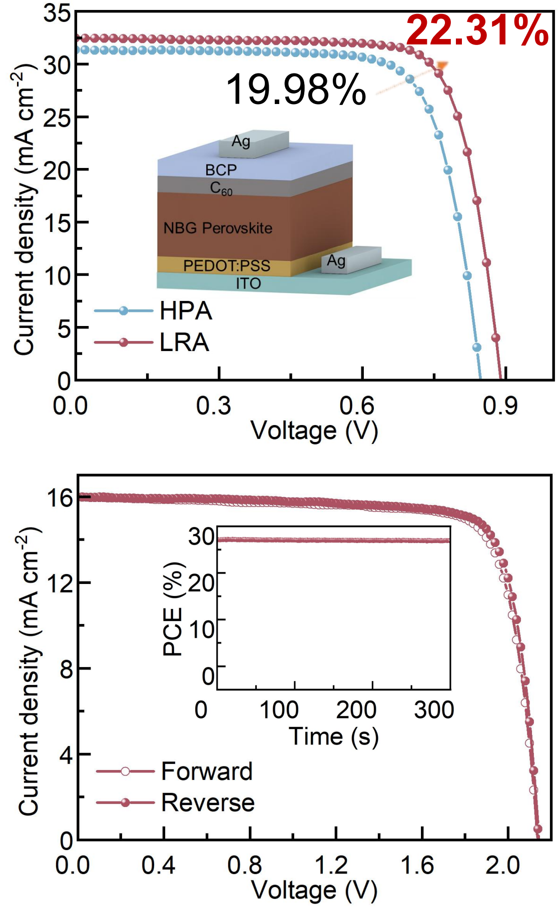

Single-junction devices 22.3%

Tandem devices 27.6%

Optimized NBG film yields a high PCE of 22.3% for single-junction and 27.6% for tandem devices

C. Chen*, J. Tang*, et al. ***Energy Environ. Sci.*** 2025, 18, 430

Deep defects introduced by Sn^{2+} oxidation

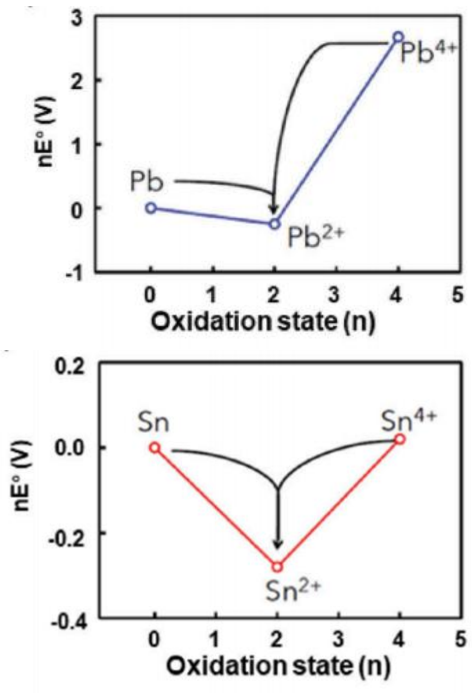

Sn^{2+} is easily oxidized

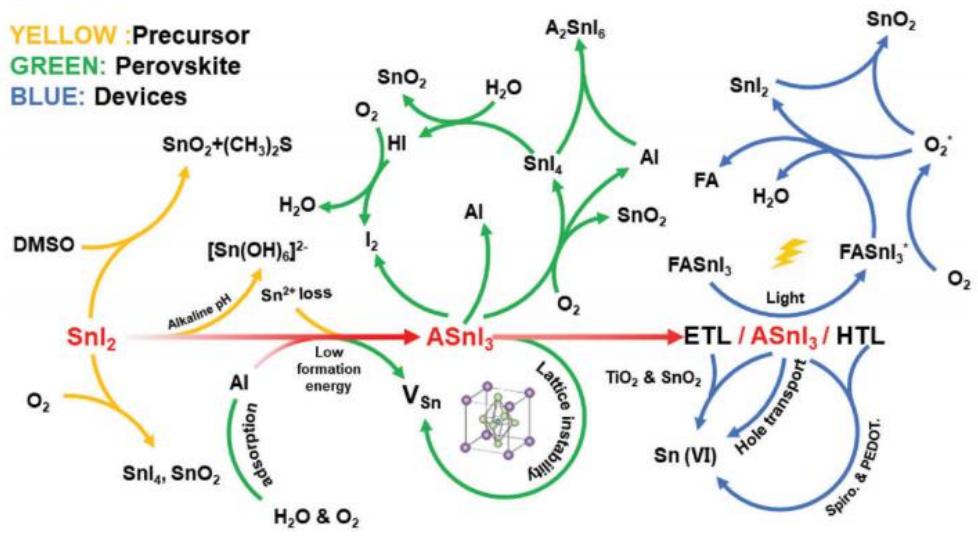

Multiple oxidation pathways
for Sn–Pb perovskites

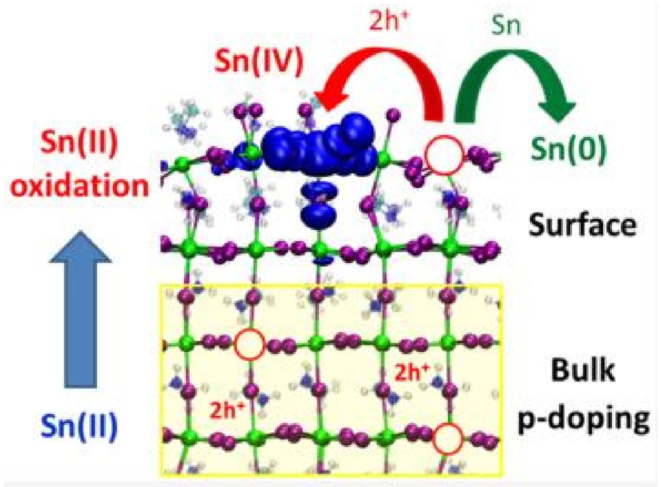

Sn^{4+} leads to harmful V_{Sn} deep defects

Sn^{2+} are prone to be oxidated into Sn^{4+}, and leads to V_{Sn} defect.

DMPU solvent for efficient NBG solar cells

Oxidation sources in precursors

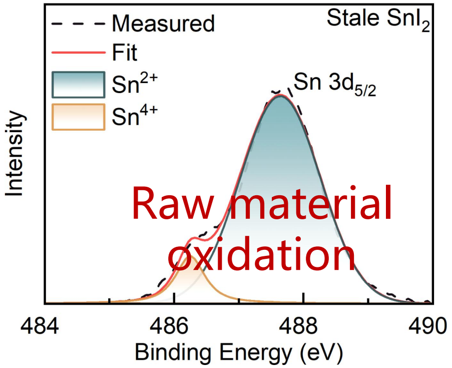

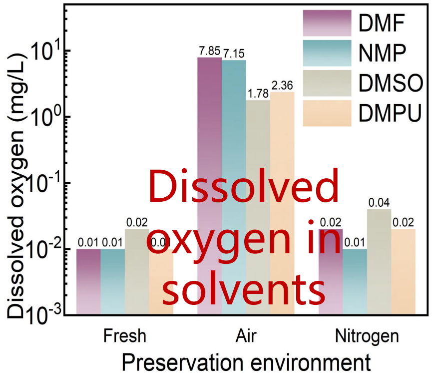

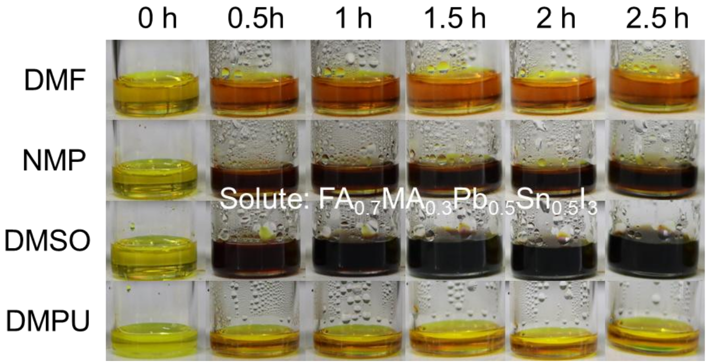

Oxidizing nature of solvents

Solvent screening

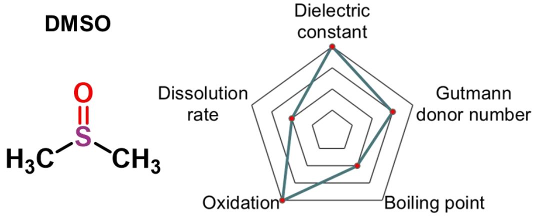

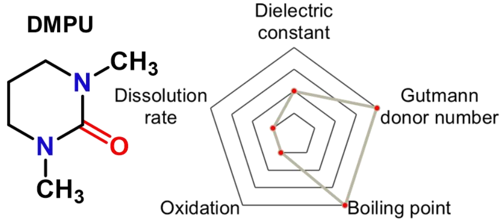

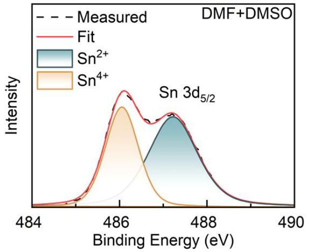

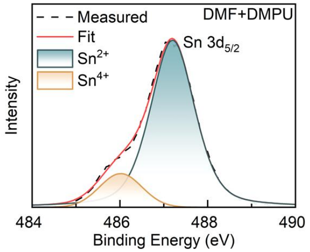

Device performance

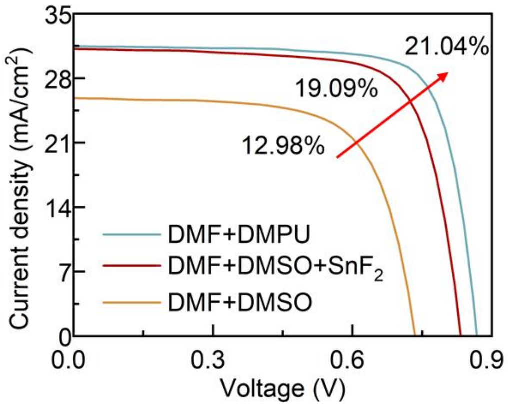

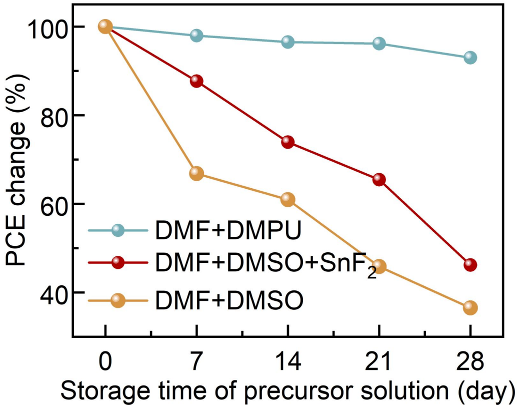

- Develop DMPU solvent (high-donor-number solvent with weak oxidizing ability)
- High efficiency of 21.04% using additive-free NBG precursor

C. Chen*, J. Tang*, et al. ***Adv. Funct. Mater.*** 2024, 2400075.

High-coordination $SnI_2 \cdot x$DMSO precursors

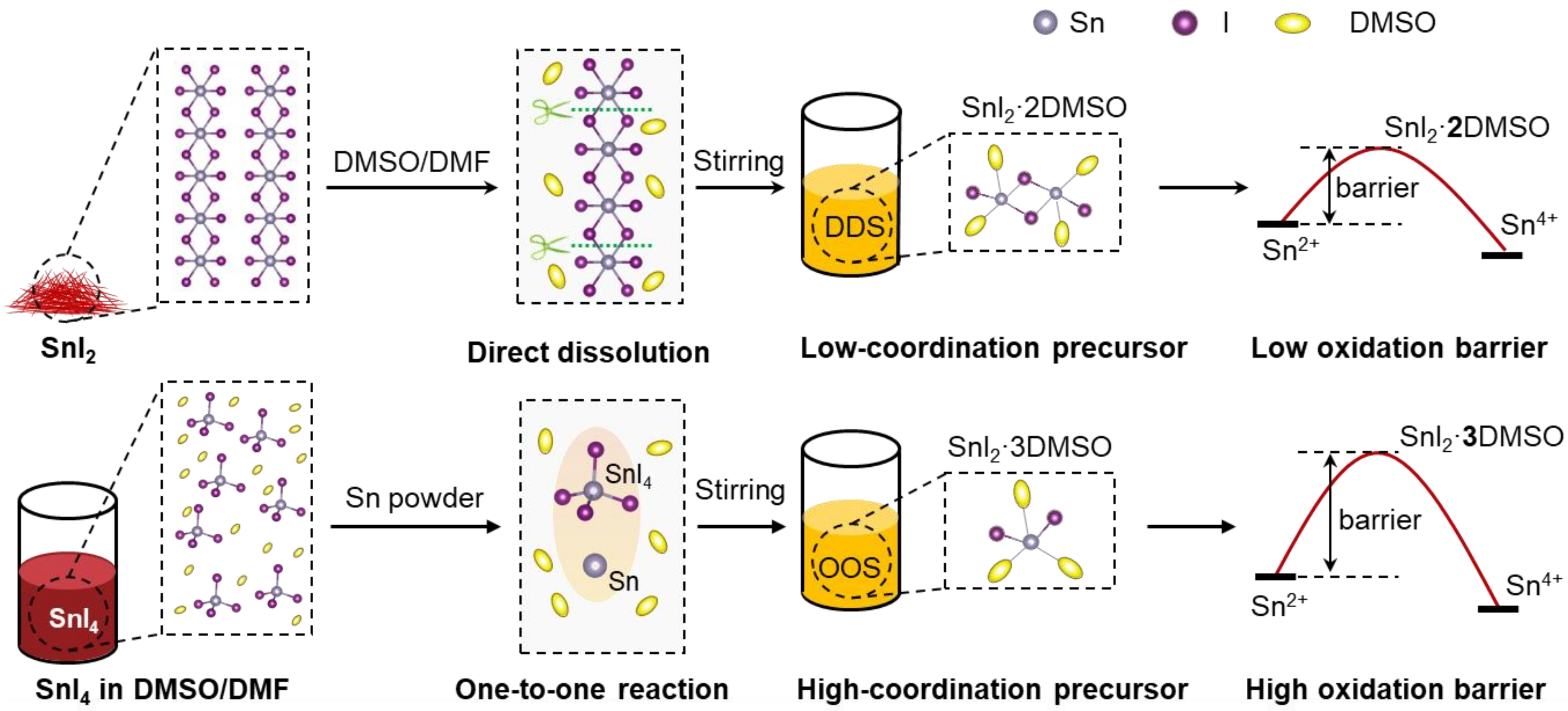

SnI_4+Sn redox reaction produces high-coordination $SnI_2 \cdot 3DMSO$, improving precursor dispersion and oxidation barrier

C. Chen*, J. Tang*, et al. ***JACS*** 2025 https://doi.org/10.1021/jacs.5c05430

High-coordination SnI_2•*x*DMSO precursors

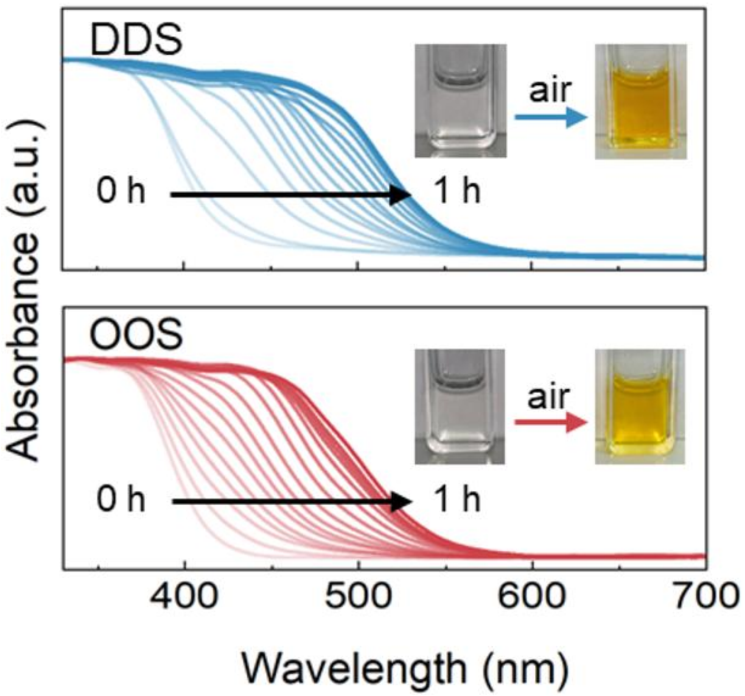

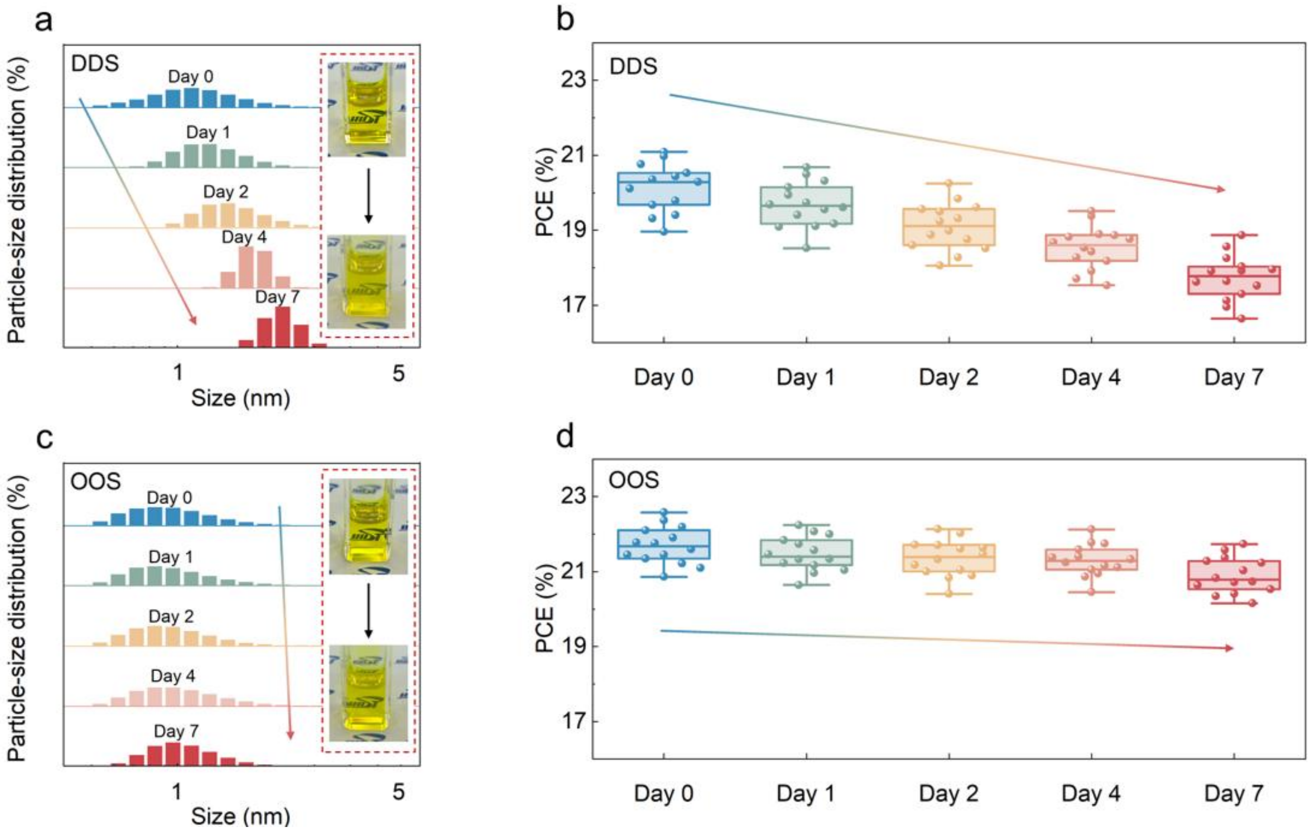

Significant improvement in precursor stability

C. Chen*, J. Tang*, et al. ***JACS*** 2025 https://doi.org/10.1021/jacs.5c05430

High-coordination $SnI_2 \cdot x$DMSO precursors

Reduced film defects

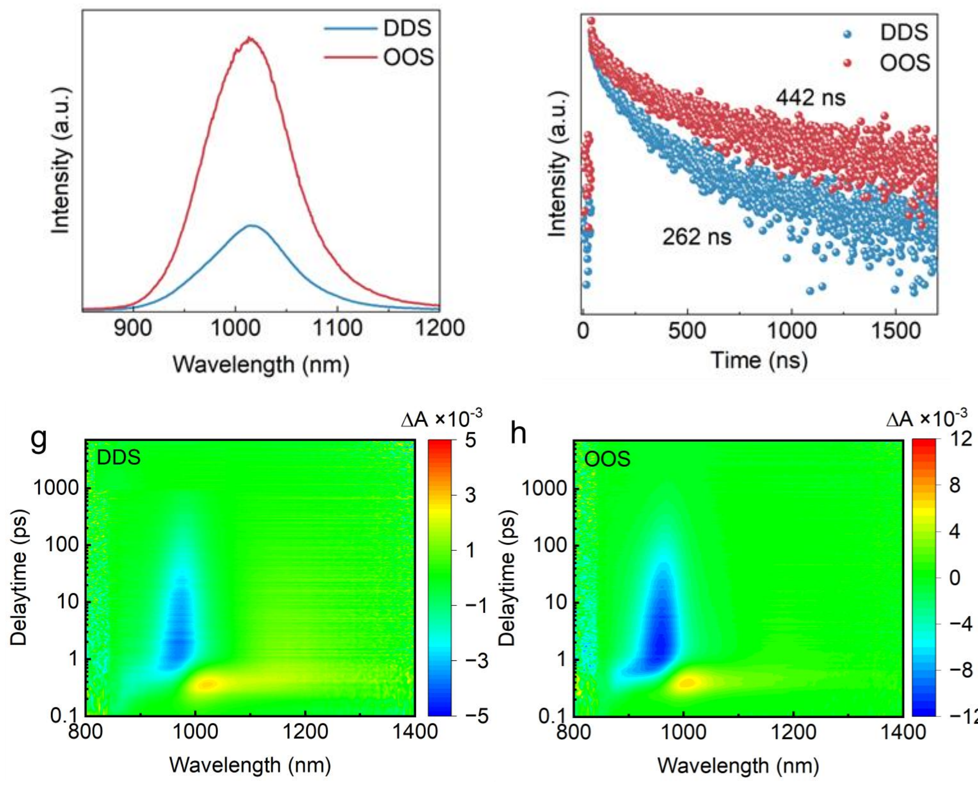

Enhanced device efficiency and stability

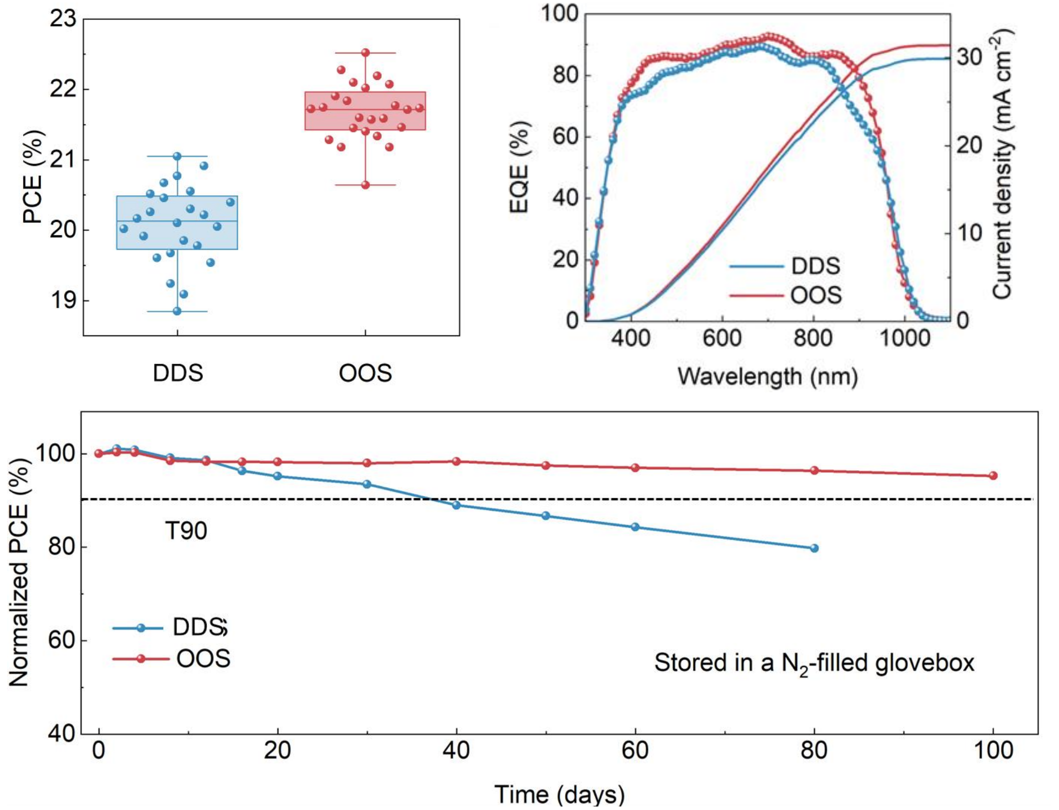

High-quality film with less defects and longer lifetime yield higher PCE and longer stability

C. Chen*, J. Tang*, et al. ***JACS*** 2025 https://doi.org/10.1021/jacs.5c05430

Multidentate additive for NBG perovskite

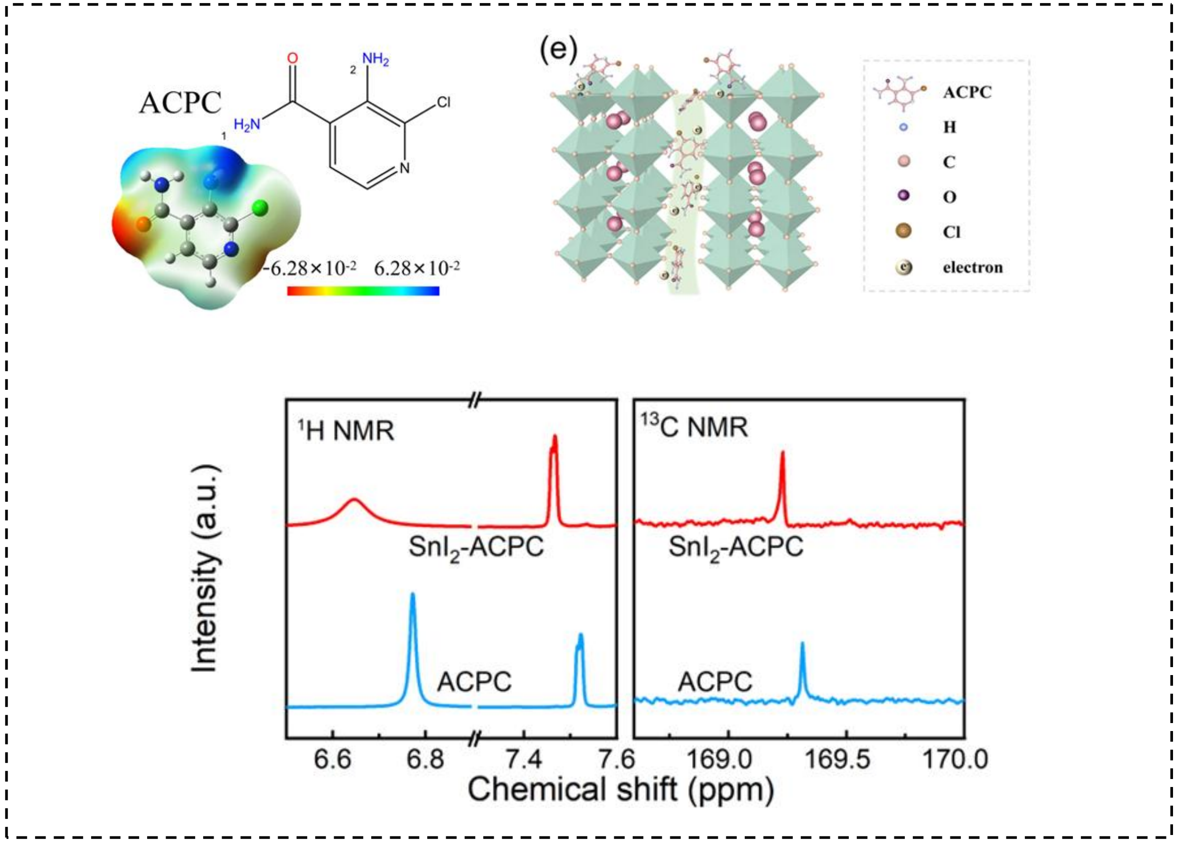

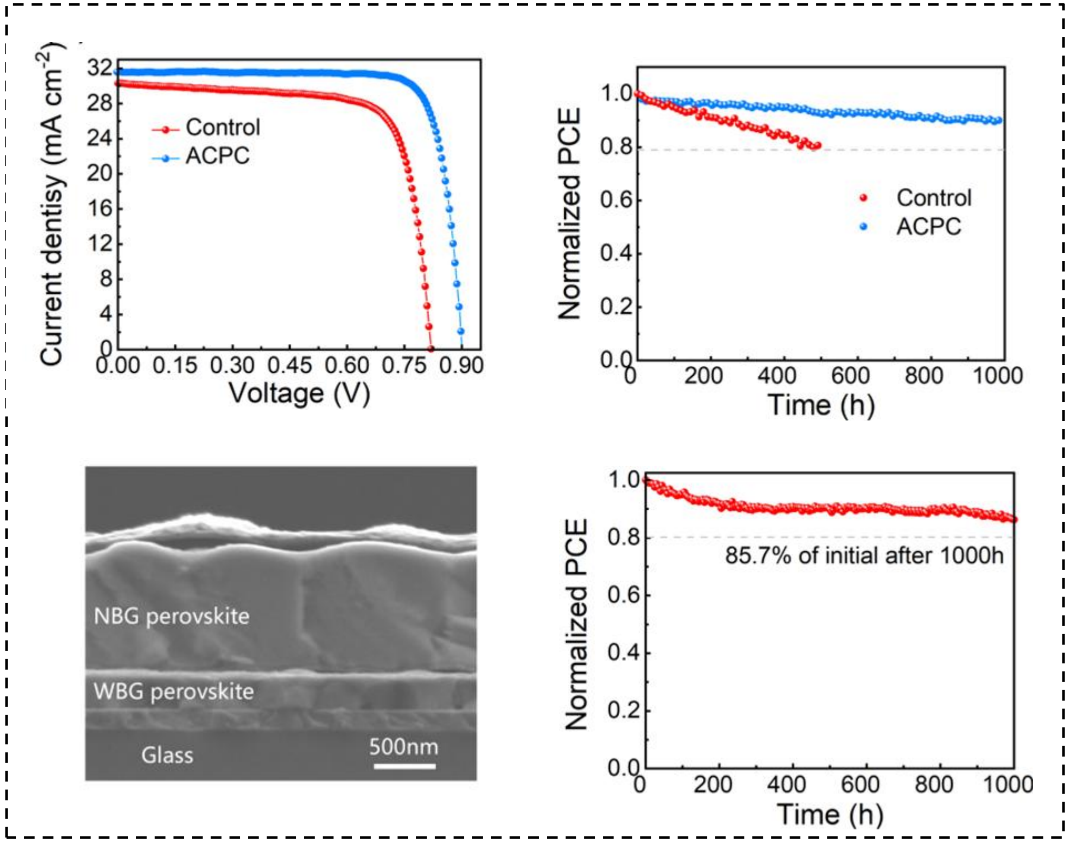

ACPC multidentate chelating molecule:

- C=O coordinate with Sn^{2+} to prevent oxidation
- $-NH_2$ coordinate with I^- to suppress migration

- Reduced defect density
- improved V_{OC} and stability

C. Chen*, H. Song*, J. Tang*, et al. *Adv. Funct. Mater.* 2025, 2412216

Two-step passivation strategy for Sn–Pb film

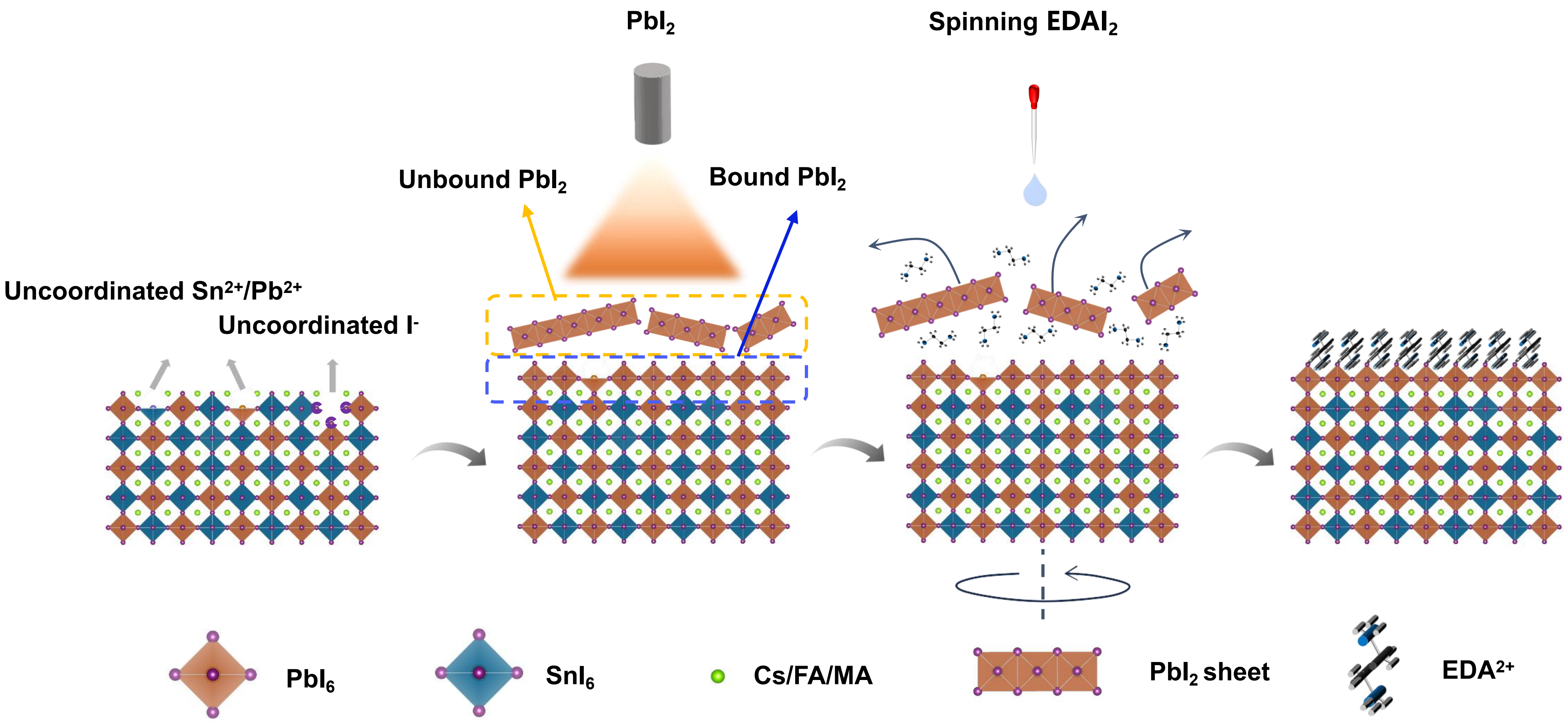

- Complex surface defects make effective passivation difficult;
- Reconstruct Sn–Pb perovskite surfaces into pure-Pb termination, simplifying defect types

C. Chen*, J. Tang*, et al. ***Nano Energy*** 2025, 139, 110927

Two-step passivation strategy for Sn–Pb film

Defect suppression

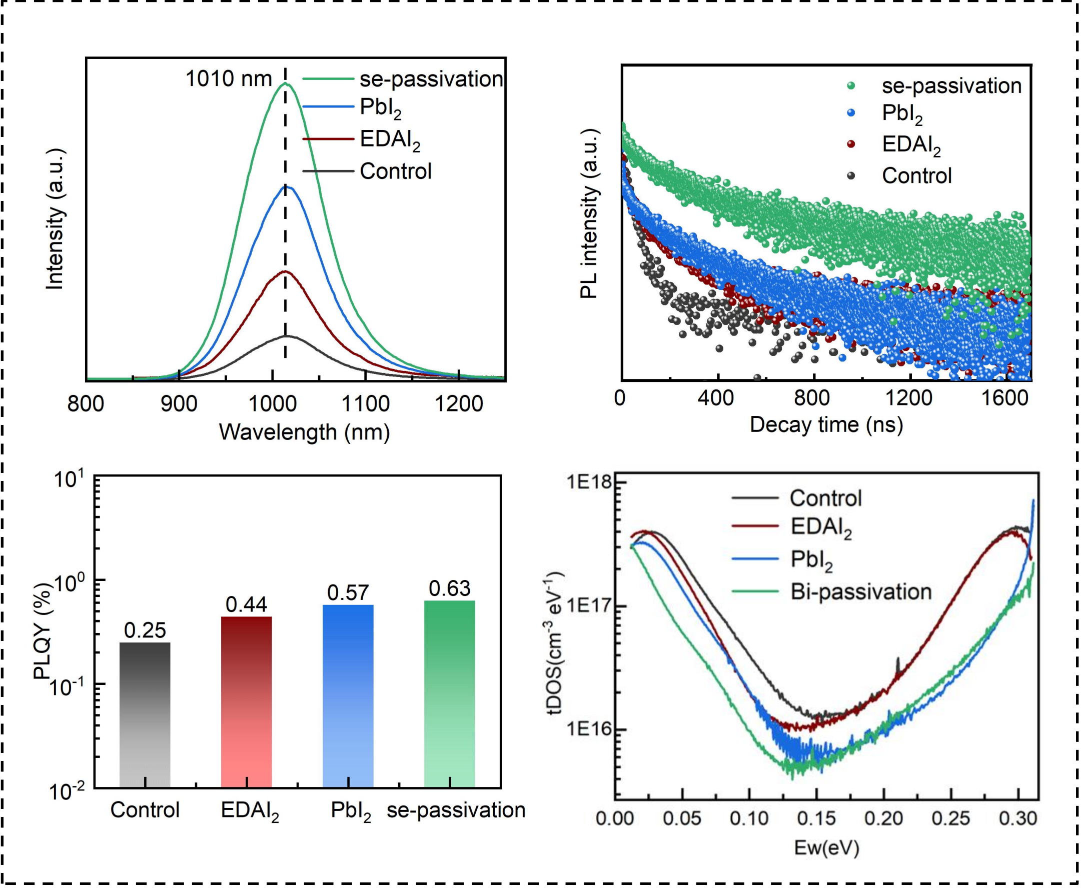

Device performance

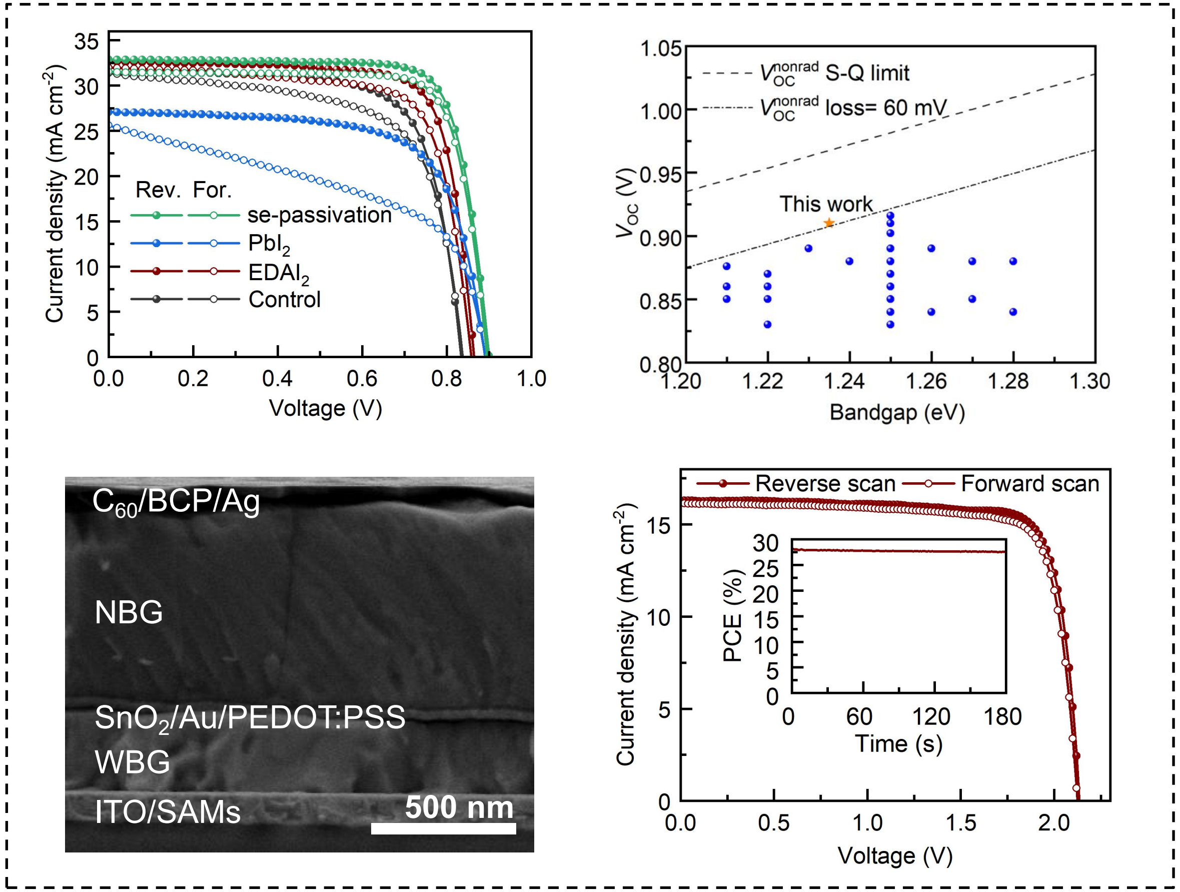

- NBG single-junction V_{OC}=0.91 V, PCE=23.31%
- All-perovskite tandem PCE=28.16%

C. Chen*, J. Tang*, et al. *Nano Energy* 2025, 139, 110927

Outline

Photo-induced phase separation in WBG PVKS

photo-induced reversible phase segregation

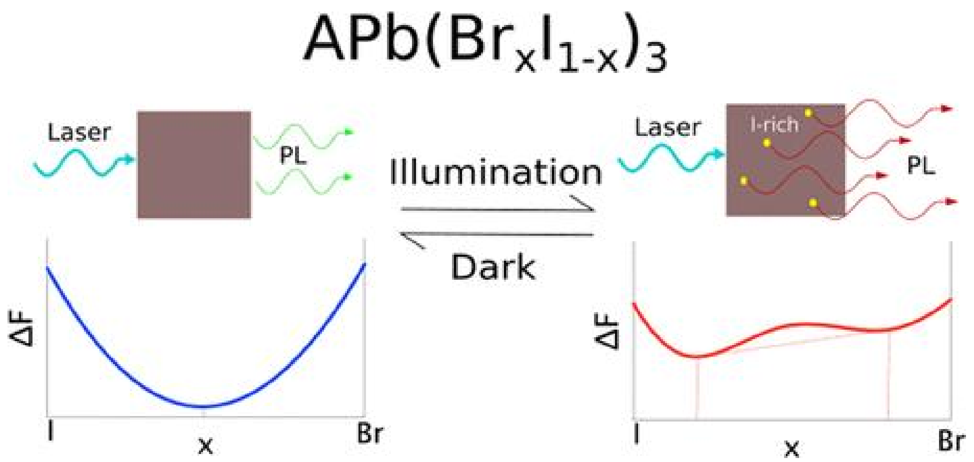

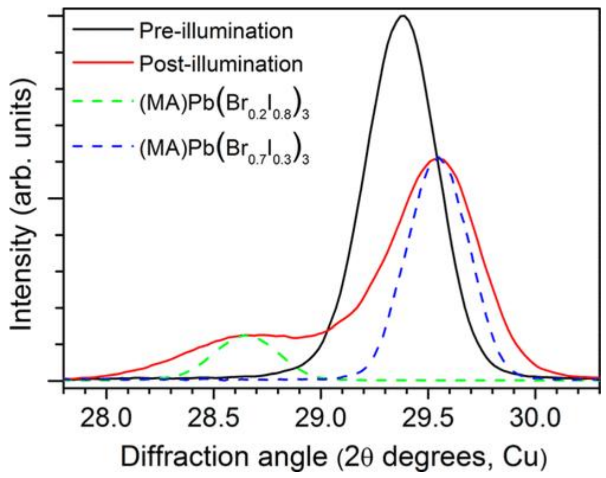

photo-induced I-rich region

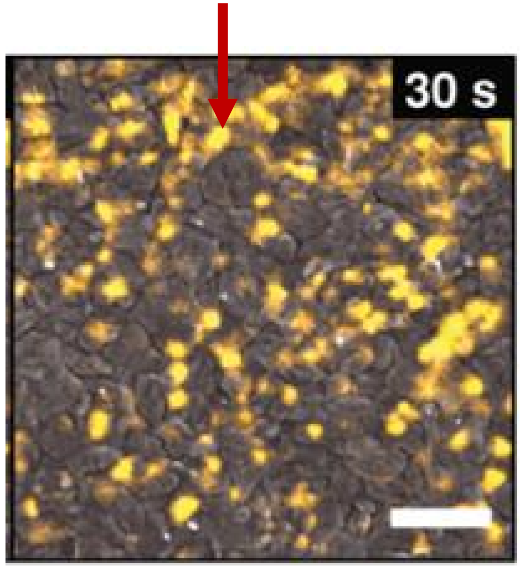

phase segregation leads to charge carrier trapping and poor device performance

Ref. *ACS Energy Lett.* 2016, 1, 1199
Ref. *Nano Lett.* 2017, 17, 1028

Photo-induced phase separation in WBG PVKS

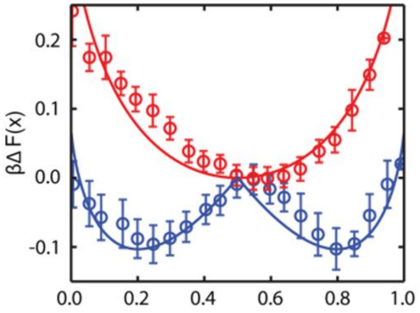

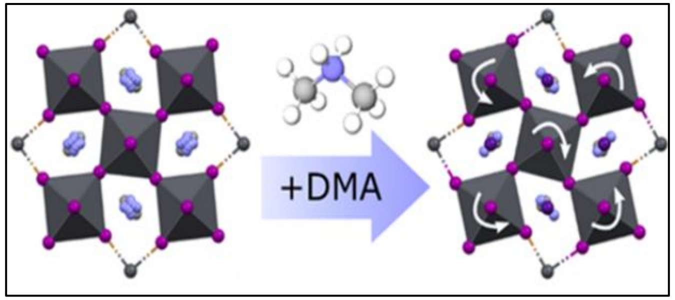

- **increasing lattice distortion** via DMA^+
- **reducing Br content** from 40% to 25%

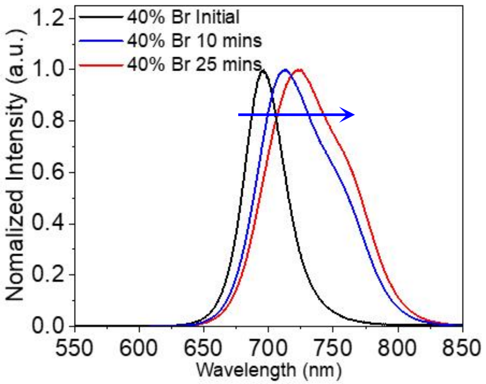

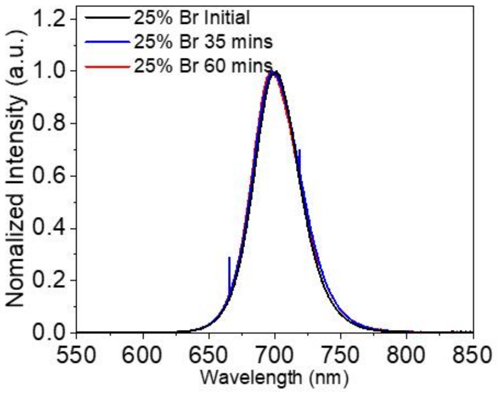

- **Improved stability under AM1.5G**

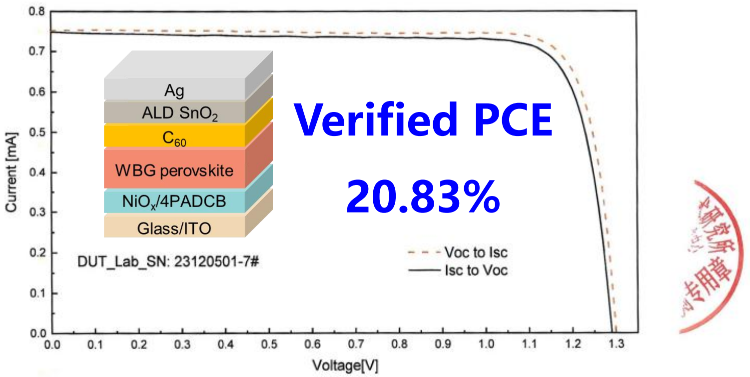

Fig.1 I-V curves of the measured sample

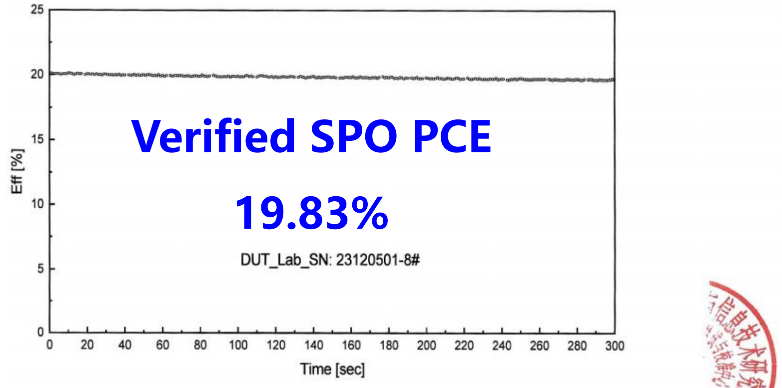

Fig.1 Steady-state maximum power output of the measured sample

By component engineering, a certified PCE of 20.83% was achieved in WBG solar cell

Role of NiO for SAM

SAM on ITO

SAM on ITO/NiO

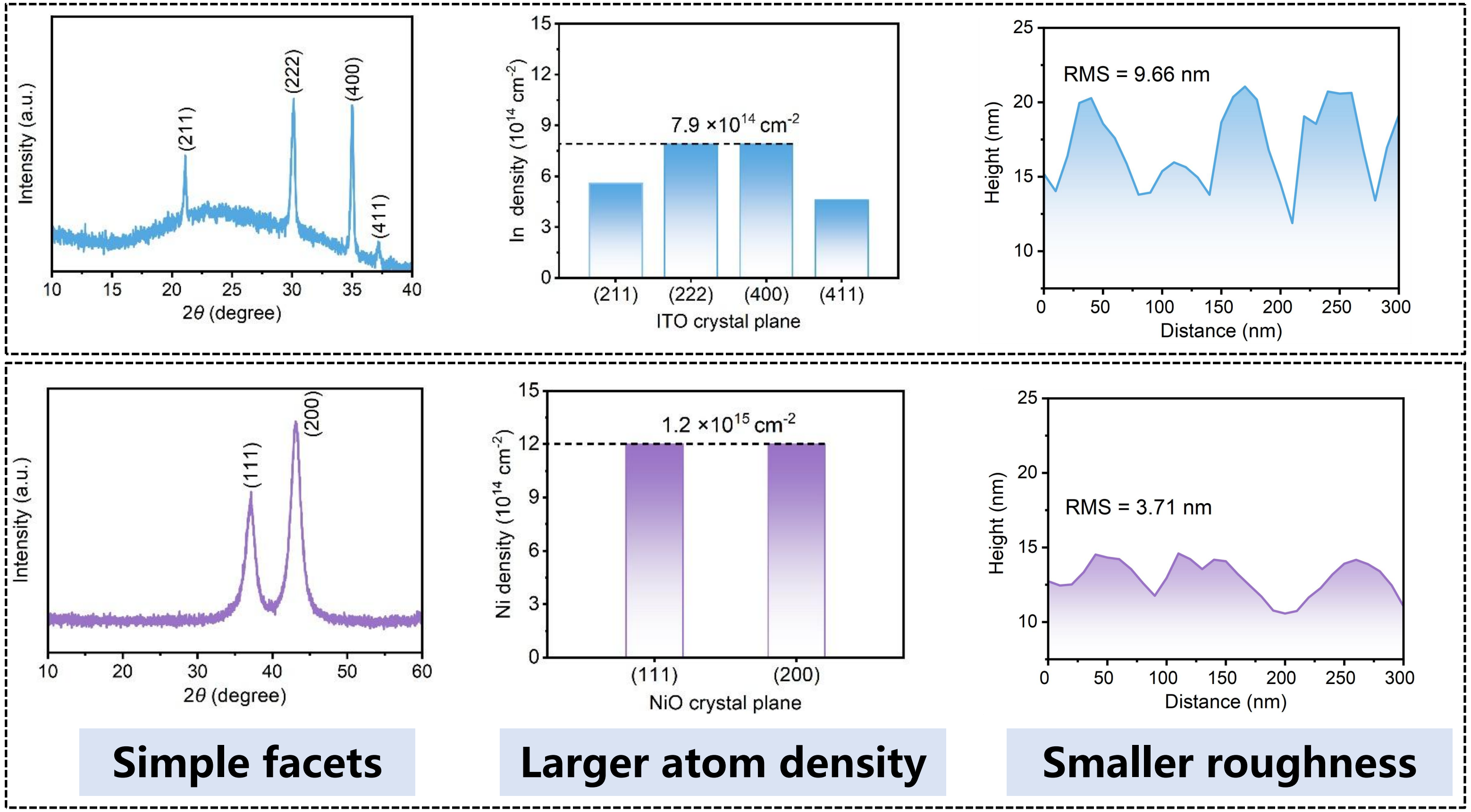

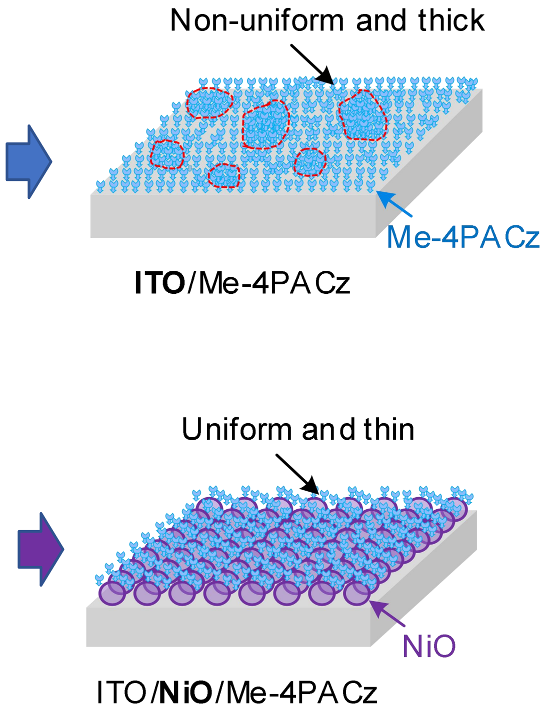

NiO nanoparticle modified ITO substrate is beneficial to SAM assemble

H. Song*, C. Chen*, Jiang Tang*, et al. Chem. Eng. J. 2024, 494, 153253

Role of NiO for SAM

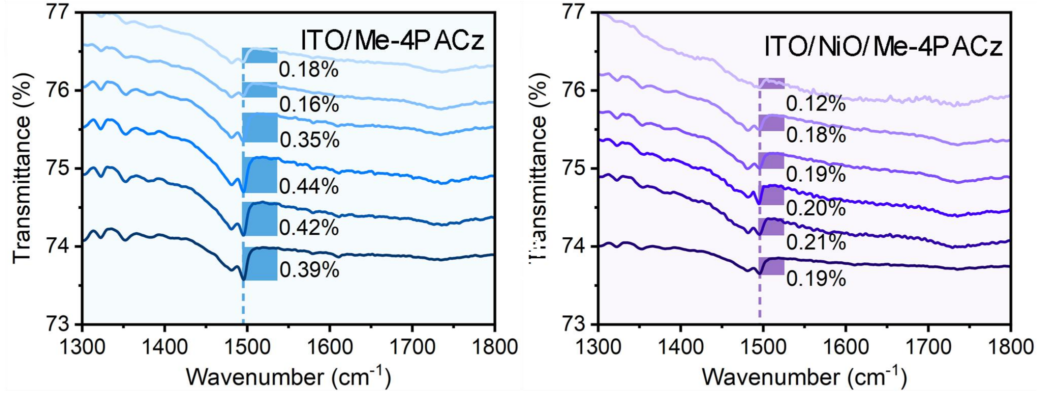

Thinner SAM on NiO/ITO substrate

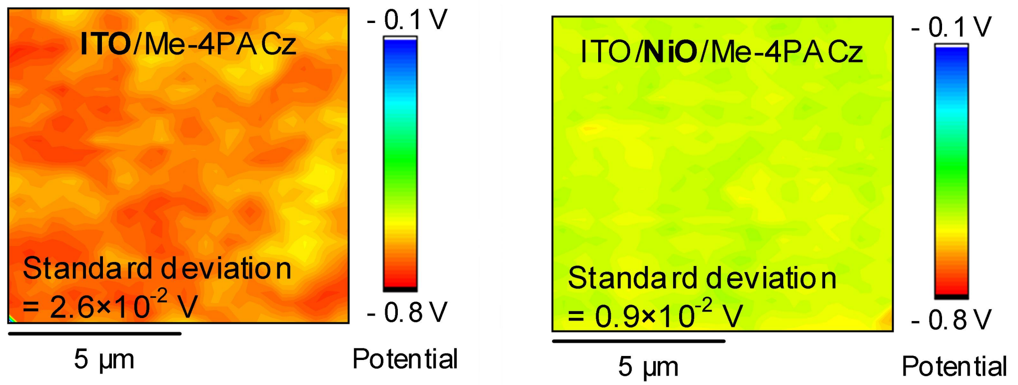

More uniform SAM on NiO/ITO substrate

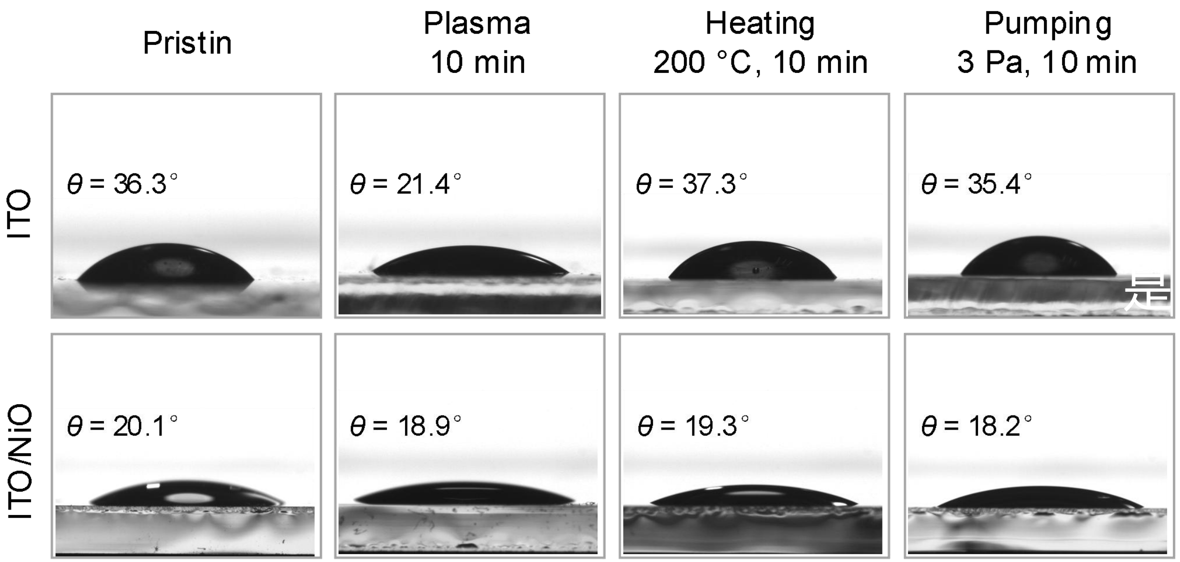

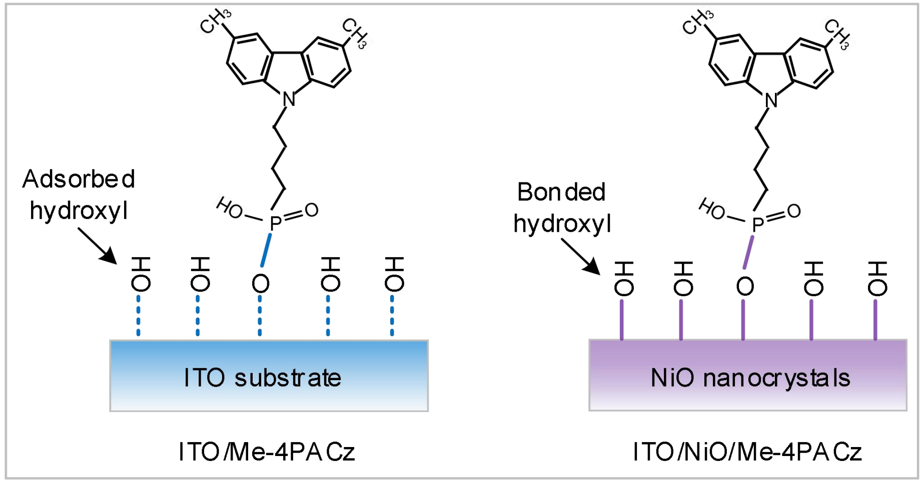

More stable SAM on NiO/ITO substrate

H. Song*, C. Chen*, Jiang Tang*, et al. Chem. Eng. J. 2024, 494, 153253

Role of NiO for SAM

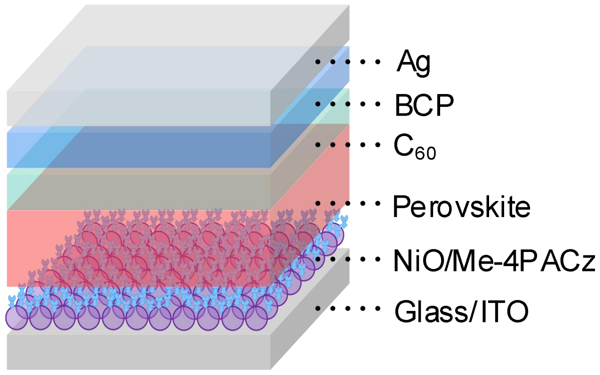

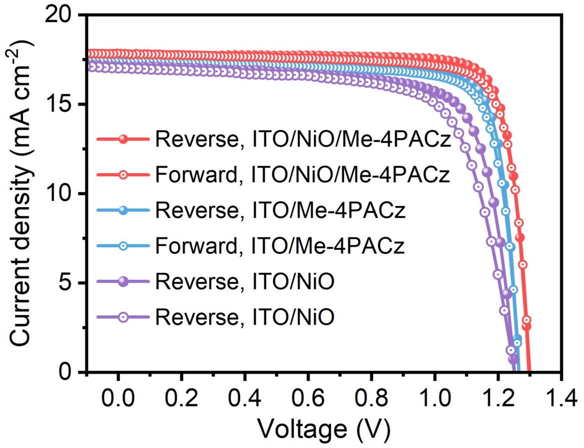

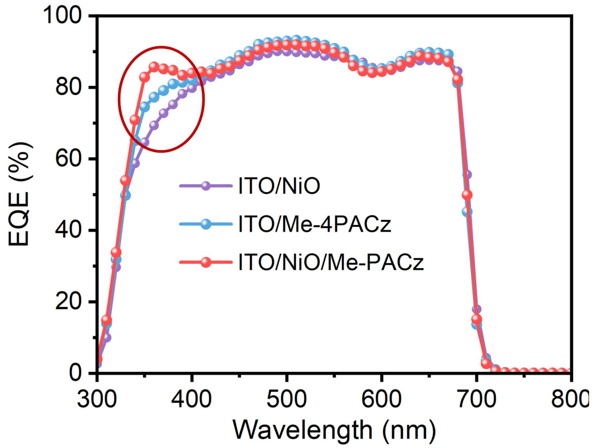

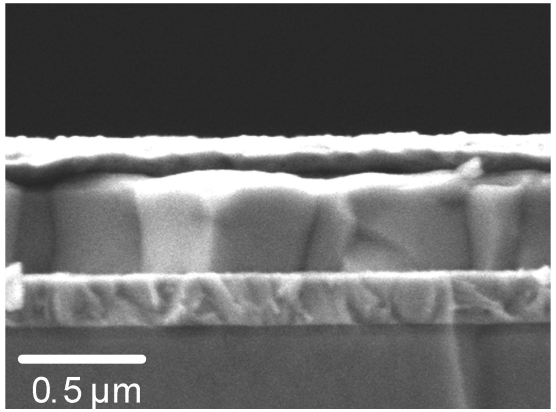

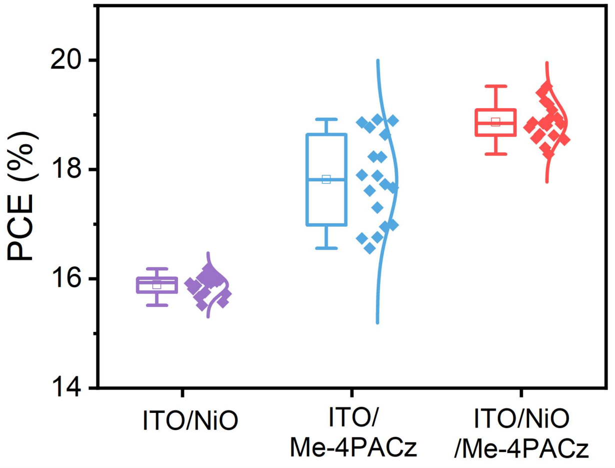

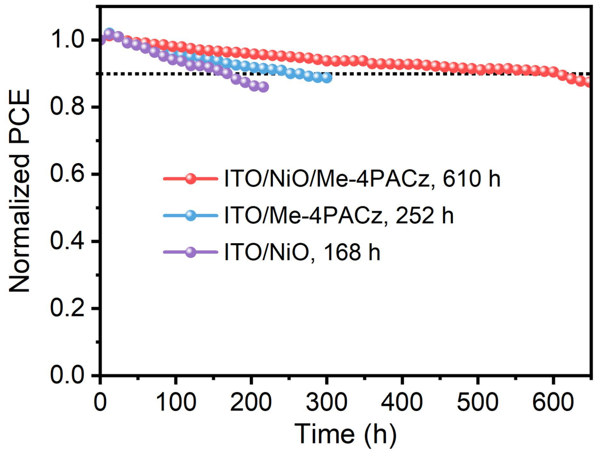

NiO can improve SAM quality, and improve WBG PCE from 18.74% to 19.55%

H. Song*, C. Chen*, Jiang Tang*, et al. Chem. Eng. J. 2024, 494, 153253

Outline

1. Background of tandem solar cells
2. Exploration for Si-based tandem solar cells
3. Exploration for all-perovskite tandem solar cells
   - ◆NBG single-junction and tandem device
   - ◆ WBG single-junction and tandem device
   - ◆ 1-cm^2 device and 20-cm^2 module
4. Summary and acknowledgment

Vacuum-driven pre-crystallization for 1 cm² tandem device

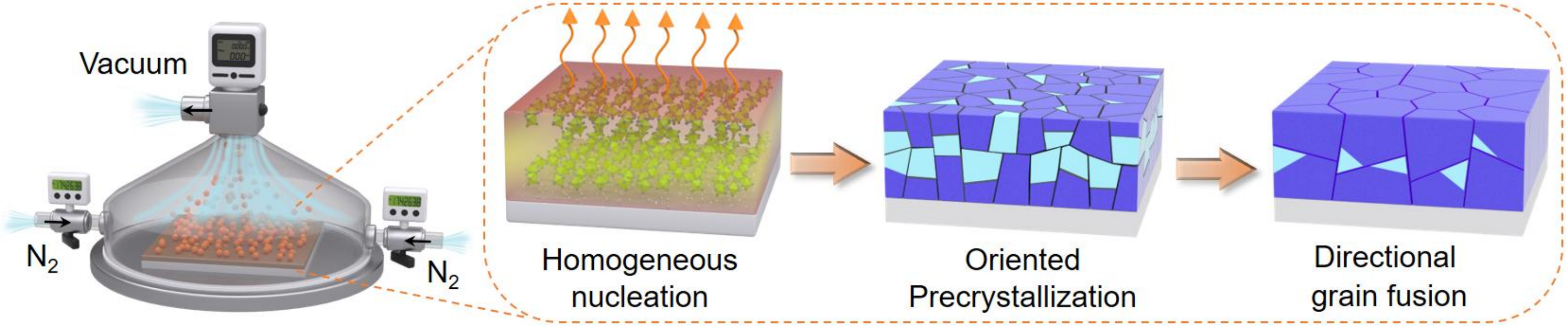

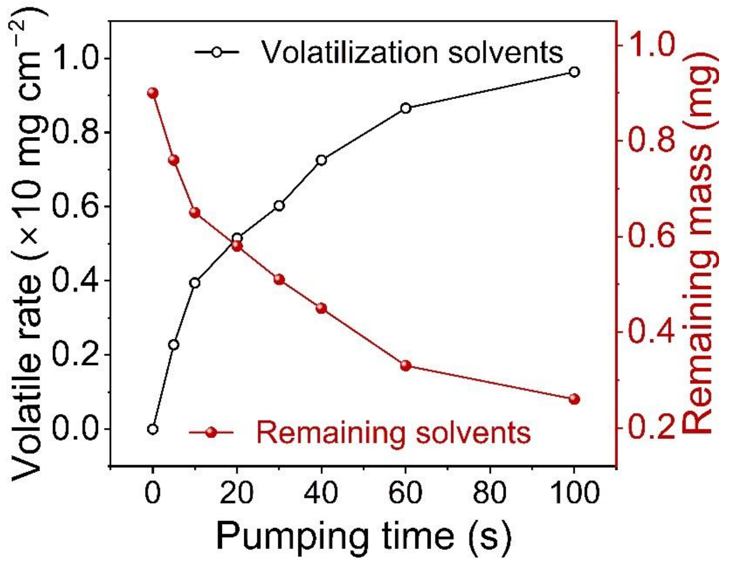

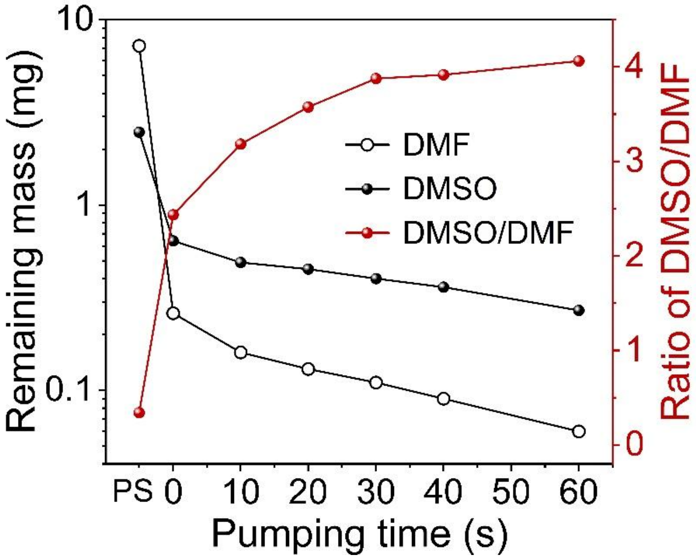

There is an optimal DMF/DMSO window for crystal growth.

C. Chen*, H. Song*, J. Tang, et al. Joule 2025, 9, 101825.

Vacuum-driven pre-crystallization for 1 cm^2 tandem device

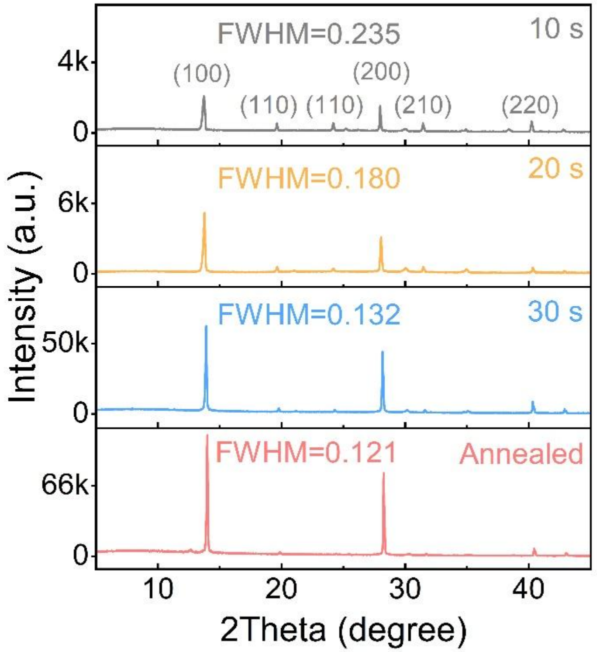

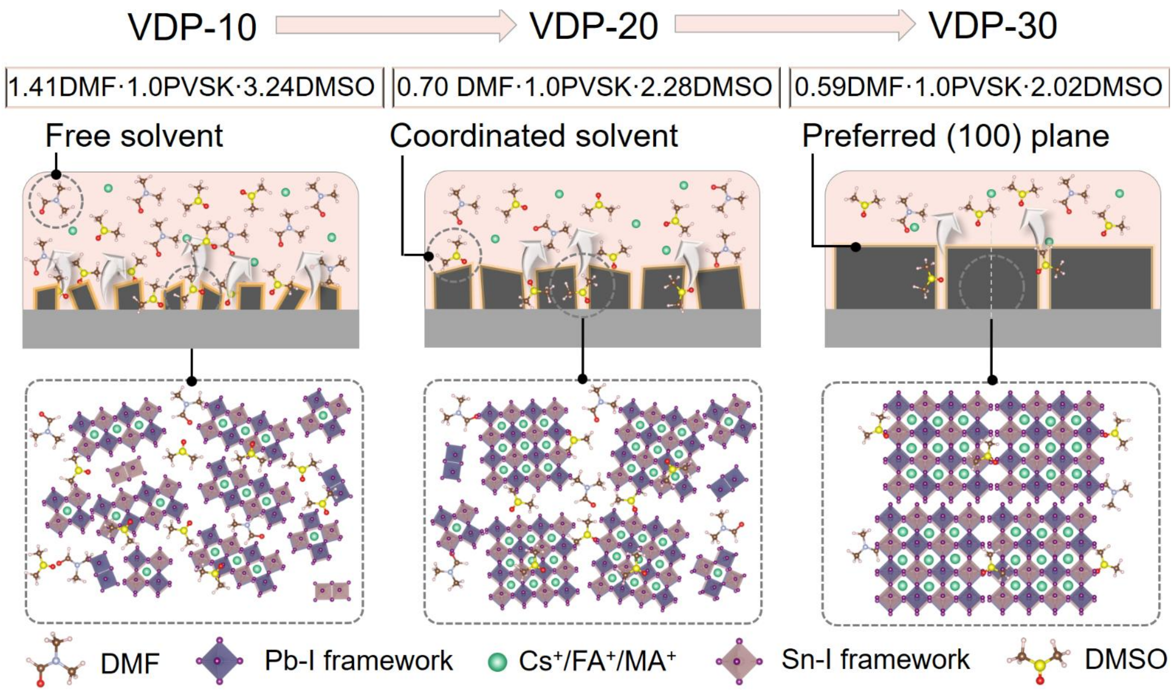

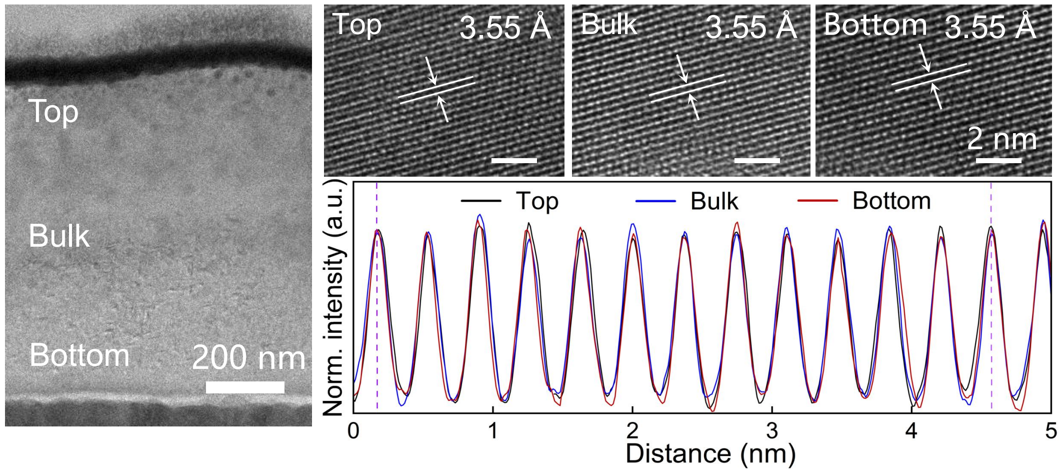

- Vacuum slow quenching rate help the growth of (100) low-energy surface;
- DMSO promote grain fusion, yielding columnar large crystals.

C. Chen*, H. Song*, J. Tang, et al. Joule 2025, 9, 101825.

Vacuum-driven pre-crystallization for 1 cm² tandem device

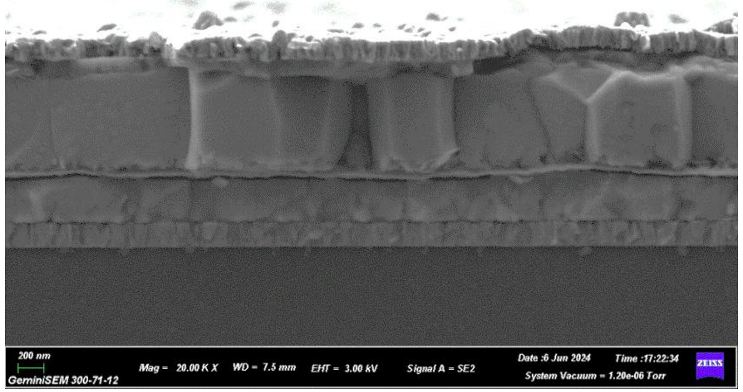

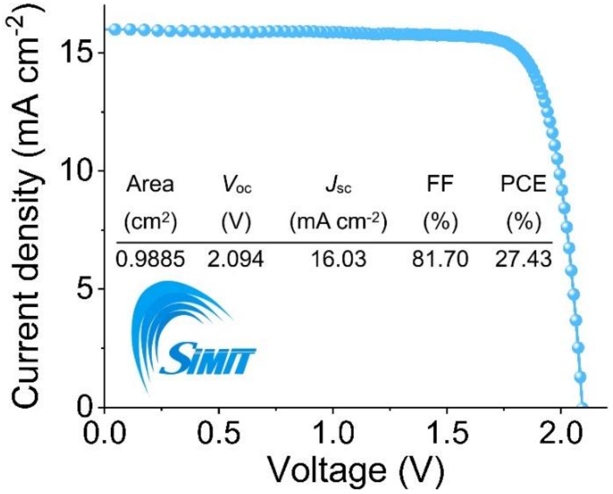

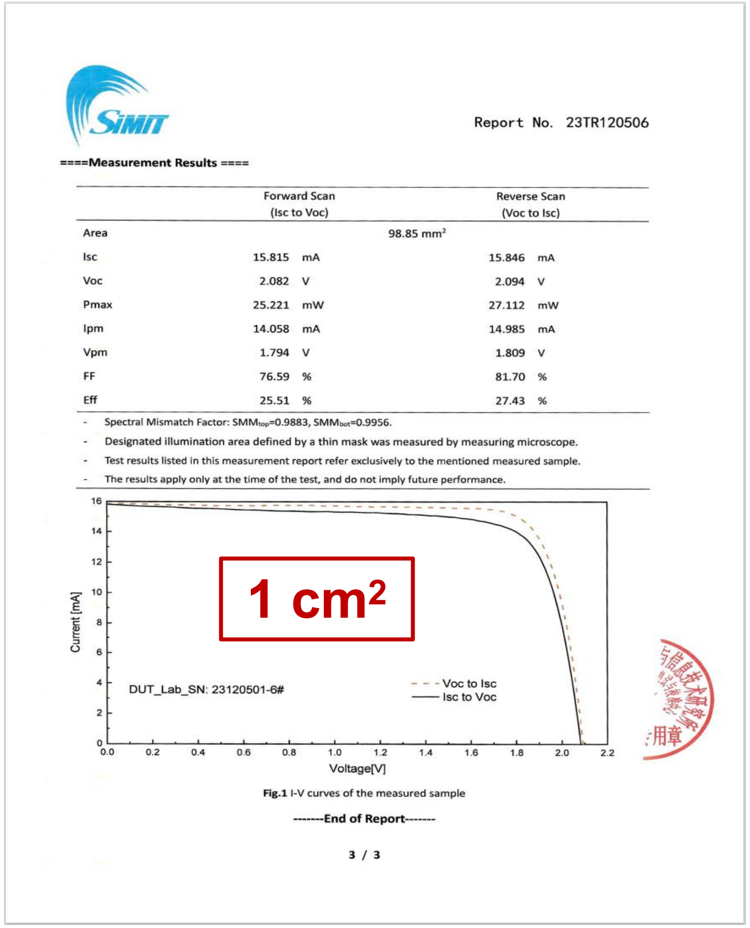
SIMIT

Report No. 23TR120506

====Measurement Results ====

	Forward Scan (Isc to Voc)		Reverse Scan (Voc to Isc)	
Area	98.85 mm²			
Isc	15.815	mA	15.846	mA
Voc	2.082	V	2.094	V
Pmax	25.221	mW	27.112	mW
Ipm	14.058	mA	14.985	mA
Vpm	1.794	V	1.809	V
FF	76.59	%	81.70	%
Eff	25.51	%	27.43	%

- Spectral Mismatch Factor: SMM_{top}=0.9883, SMM_{bot}=0.9956.
- Designated illumination area defined by a thin mask was measured by measuring microscope.
- Test results listed in this measurement report refer exclusively to the mentioned measured sample.
- The results apply only at the time of the test, and do not imply future performance.

Fig.1 I-V curves of the measured sample

-------End of Report-------

3 / 3

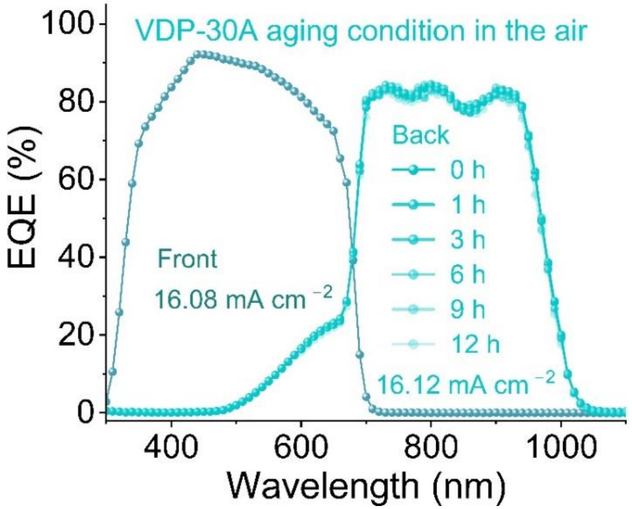

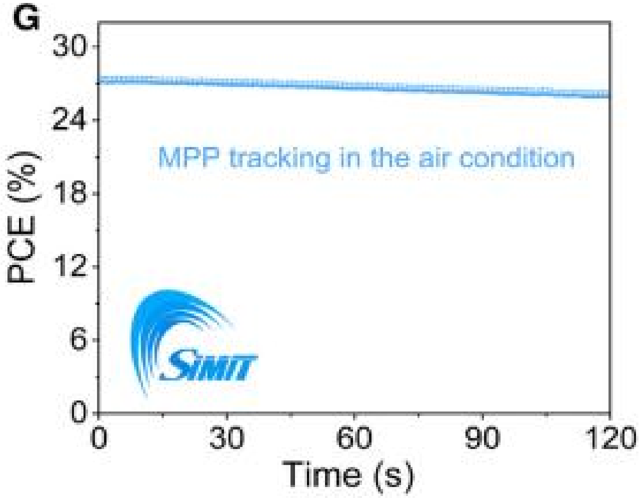

Certified PCE of 27.43%@1cm² based on antisolvent-free method

C. Chen*, H. Song*, J. Tang, et al. Joule 2025, 9, 101825.

1 cm² all-perovskite tandem solar cells

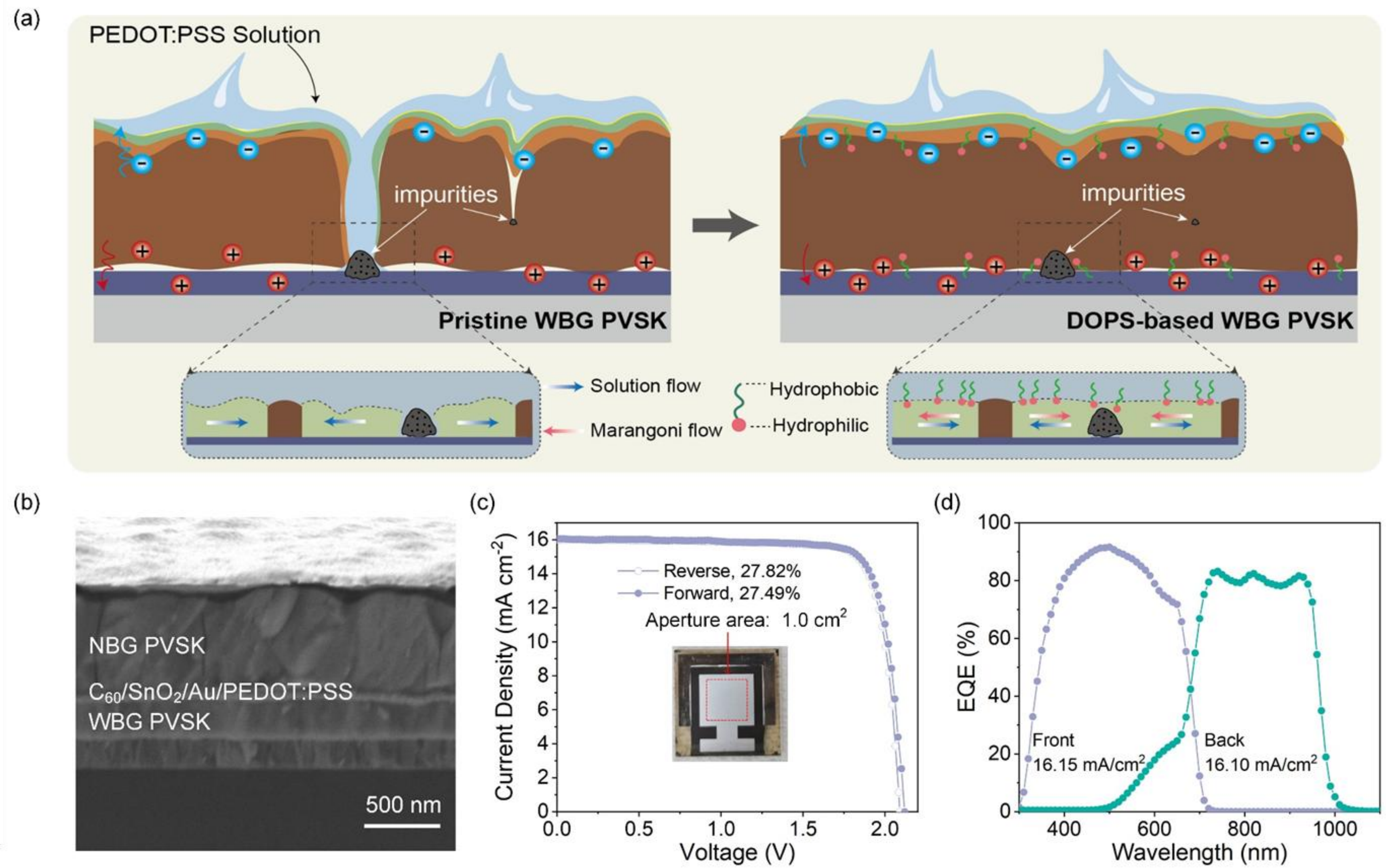

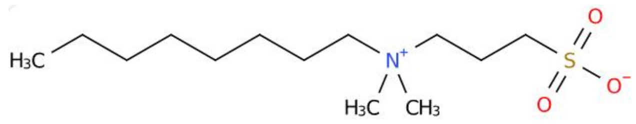

Surfactant additive: DOPS

DOPS surfactant improve film uniformity, yielding a high PCE of 27.82%@1cm²

All-perovskite tandem mini module

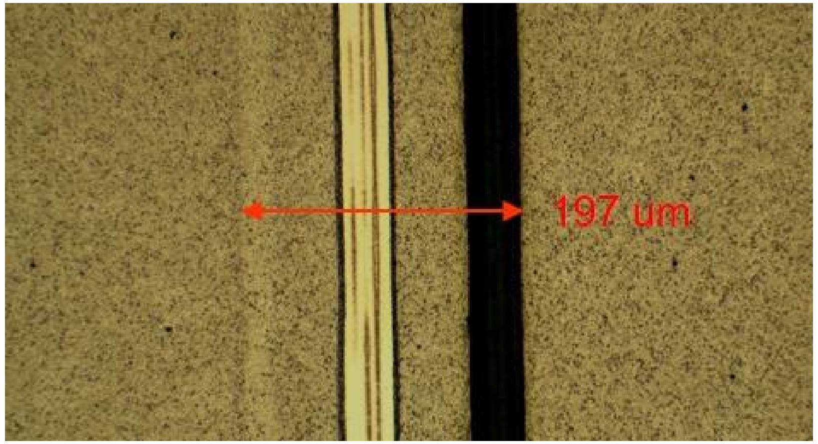

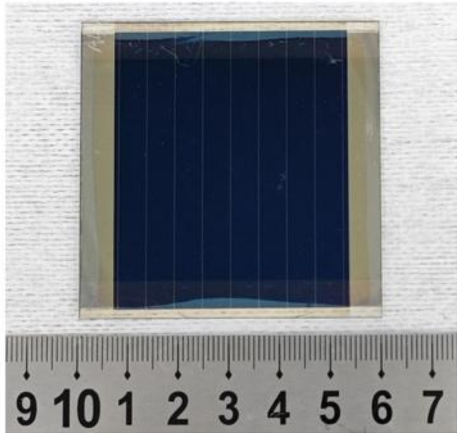

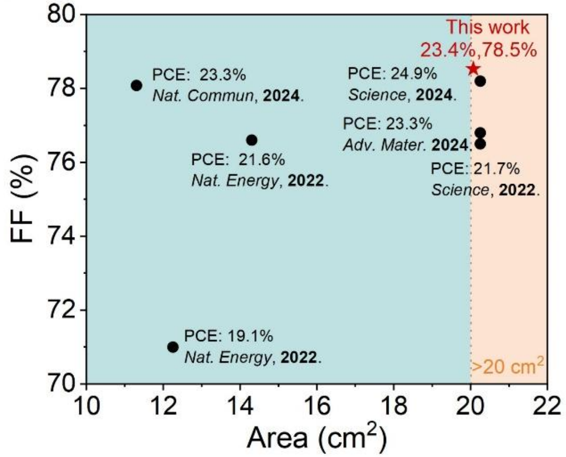

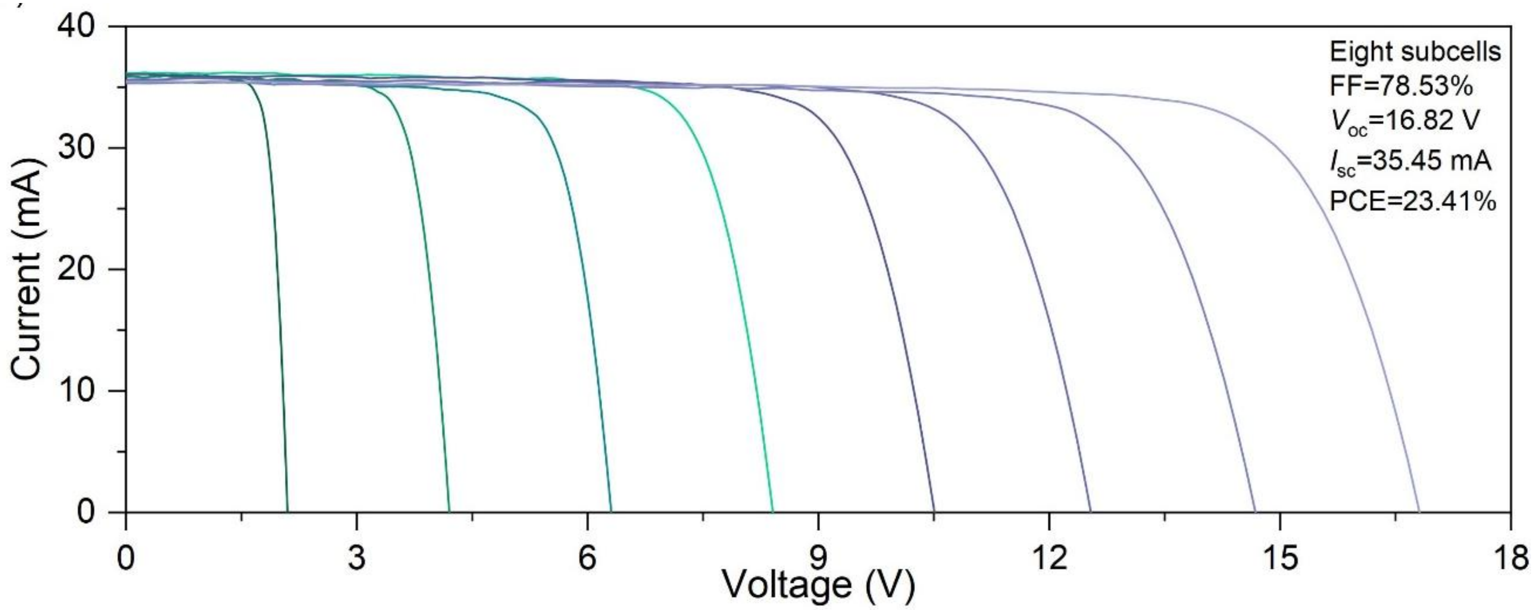

A high PCE of 23.4%@20.25cm^2

Main conclusion

Exploration for Si-based tandem solar cells

- ◆ **CdSe solar cells**: good material properties, low PCE of ~6%, but hold great promise
- ◆ **Sb_2S_3 solar cells**: 1D structure, low-toxicity, <10% PCE, and attract wide attentions
- ◆ **$CsPbI_3$ solar cells**: good material properties, ~18% PCE, but weak stability

Exploration for all-perovskite tandem solar cells

- ◆ **NBG**: high PCE beyond 23%; more attentions on PEDOT:PSS, stability, large area
- ◆ **WBG**: High PCE of 20.8%; photo-induced phase stability, large area
- ◆ **Tandem**: high PCE of ~29%; more attentions on tunneling-junction, stability

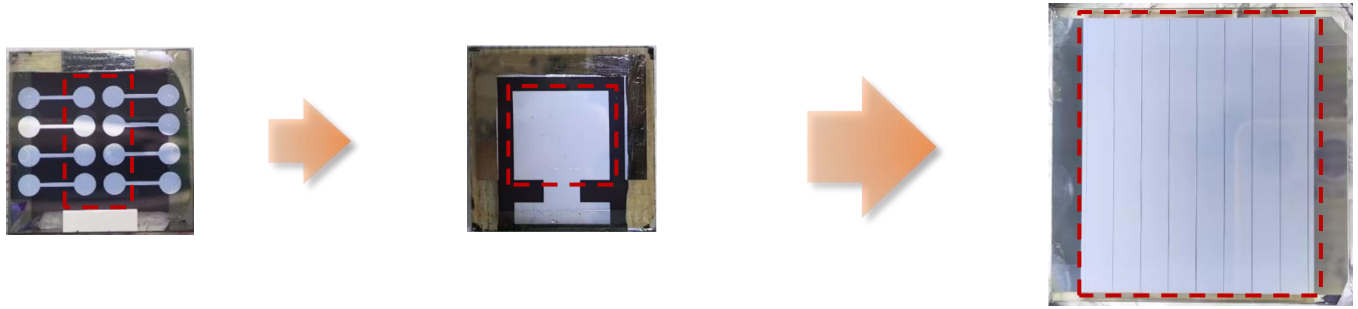

~29%@0.0768 cm² **27.8%@1 cm²** **23.4%@20 cm²**

Acknowledgement

Current group members

Assoc. Prof. Chao Chen
Prof. Haisheng Song
Prof. Ying Zhou
Prof. Guangda Niu
Prof. Junjia Luo

Dr. Xuke Yang	Dr. Ciyu Ge
Dr. Chong Dong	Dr. Mingyu Li
Dr. Tianjun Ma	Dr. Haojun Hu
Dr. Xin Li	Dr. Qi Xu
Dr. Dayu Liu	
M.S. Zhenkai Zhu	M.S. Peiyan Zhang
M.S. Zifan Lin	M.S Haoyang Song

Cooperators

Prof. Edward Sargent, University of Toronto
Prof. Yanfa Yan, University of Toledo
Prof. Hairen Tan, Nanjing University
Prof. Weijun Ke, Wuan University
Prof. Jiakuan Yang, HUST
Prof. Shiyou Chen, East China Normal U.
Prof. Xiaoxing Ke, BJUT

Funds

NSFC
National Natural Science Foundation of China

中华人民共和国科学技术部
Ministry of Science and Technology of the People's Republic of China

WNLO

华中科技大学
HUAZHONG UNIVERSITY OF SCIENCE AND TECHNOLOGY

深圳市科技创新委员会
深圳市高新技术产业园区管理委员会

973 CHINA

Thank you for your attention!

包 SOL mat ZnTe文章

薛 ACS AMI Te掺杂CdSe

李康华 FOE CdSe

Se电池

Rokas JOS

NE综述

AEM 中间层综述

π–π Stacking small

肖奇 Solar RRL